MINISTRY OF SCIENCE AND HIGH EDUCATION OF RUSSIAN FEDERATION

INSTITUTE OF VOLCANOLOGY AND SEISMOLOGY

FAR EASTERN BRANCH OF RUSSIAN ACADEMY OF SCIENCE

8th International MAAR Conference

Petropavlovsk-Kamchatsky, Russia, August 24-30, 2020

Abstract volume

Petropavlovsk-Kamchatsky
2020

UDC 551.21+552+550. 4

Scientific edition
Abstract volume of the 8th International Maar Conference – Petropavlovsk-Kamchatsky: IVS FEB RAS, 2020. – 84 p.

ISBN 978-5-902424-31-4

Materials submitted to the 8th International Maar Conference are presented in this abstract volume, including results of the geophysical, petrological, geochemical, geomorphological studies and modeling of the phreato-magmatic processes.

Approved for publishing by the
Scientific committee of the conference and IVS Academic council

Chief editor:
Dr. Alexei Ozerov

Executive secretary:
Anna Volynets

Editorial team:
Elena Kalacheva, Alexander Belousov, Marina Belousova

Cover image:

Dal'nee lake maar, Uzon caldera
Photo courtesy Marina Belousova

ISBN 978-5-902424-31-4

Preface

Since the first "International Maar Conference" (IMC), these meetings became among the most successful discussion forums in volcanology, mainly because they provide a unique opportunity to bring together people from many different volcanological fields (geologists, physical volcanologists, sedimentologists, modellers, geophysicists, petrologists, etc.) with researchers from environmental and post-volcanic subjects. Previous IMC meetings have been held in volcanic areas that present different problems in terms of eruption dynamics, products, and landforms. The venue of the 8 IMC must have been Kamchatka – one of the most volcanically and seismically active regions on Earth. Besides 30 active volcanoes, Kamchatka hosts more than 20 monogenetic volcanic fields located both in frontal and back-arc settings. This volcanic region provides a unique place for holding this multidisciplinary volcanological forum due to its highly active nature. Unfortunately due to the dramatically fast developing situation with coronavirus in Europe and other parts of the world the Organizing Committee was forced to make a decision to cancel the 8th International Maar Conference. Nevertheless, it was decided to publish this abstract volume in gratitude to all researchers who expressed their willingness to come to this remote part of the world to share their ideas with others. We do it with a great hope for better future safe for travels and meetings again.

Scientific Committee members (in alphabetical order)

Alexander BELOUSOV / Institute of Volcanology and Seismology FEB RAS (Russian Federation)
Xavier BOLÓS / Institute of Geophysics - Campus Morelia - UNAM
Tatiana CHURIKOVA / Institute of Volcanology and Seismology FEB RAS (Russian Federation)
Alison GRAETTINGER / University of Missouri (USA)
Elena KALACHEVA / Institute of Volcanology and Seismology FEB RAS (Russian Federation)
Gabor KERESZTURI / Massey University (New Zealand)
Mitsuhiro NAKAGAWA / Hokkaido University (Japan)
Károly NÉMETH / Massey University (New Zealand)
Alexei OZEROV / Institute of Volcanology and Seismology FEB RAS (Russian Federation)
Vera PONOMAREVA / Institute of Volcanology and Seismology FEB RAS (Russian Federation)
Dmitri ROUWET / Instituto Nazionale di Geofisica e Vulkanologia, Sezione di Bologna (Italy)
Anna VOLYNETS / Institute of Volcanology and Seismology FEB RAS (Russian Federation)

Table of contents

Session 1. Morphology and structure of maars and monogenetic volcanoes

Monogenetic volcanic landforms preserve evidence of the construction, modification and preservation of volcanic deposits from small volume eruptions. This session invited contributions about the morphology, architecture, and distribution of explosive and effusive small volume eruptions including subsurface structures as in maar-diatremes. The morphology of individual landforms and comparisons of size and shape across groups of landforms can be used to help reconstruct eruption history, associated hazards, and interactions with surrounding geology. This session encouraged contributions on the full spectrum of monogenetic volcanic features including maar-diatremes, scoria cones, spatter ramparts, and lava flows; contributions from field studies, numerical and analog modelling, remote sensing, geophysical techniques, and spatial analyses.

The first morphological analysis of scoria cones in the Negros de Aras monogenetic volcanic field, northern of Chile

Mauricio Aguilera[1,4], Gabriel Ureta[2,3,4], Felipe Aguilera[1,2,4], Károly Németh[5] and Matías Vilches[1,4]

[1] *Departamento en Ciencias Geológicas, Facultad de Ingeniería y Ciencias Geológicas, Universidad Católica del Norte, Av. Angamos 0610, Antofagasta, Chile.*
mag040@alumnos.ucn.cl
[2] *Centro Nacional de Investigación para la Gestión Integrada del Riesgo de Desastres (CIGIDEN), Av. Vicuña Mackenna 4860, Santiago, Chile.*
[3] *Programa de Doctorado en Ciencias Mención Geología, Universidad Católica del Norte, Av. Angamos 0610, Antofagasta, Chile.*
[4] *Núcleo de Investigación en Riesgo Volcánico - CKELAR volcanes, Universidad Católica del Norte, Av. Angamos 0610, Antofagasta, Chile.*
[5] *Volcanic Risk Solutions, School of Agriculture and Environment, Massey University, Palmerston North, New Zealand.*

Keywords: Morphometry, monogenetic volcanism, scoria cone.

Monogenetic volcanism represents the type of volcanism more widespread on the Earth, which corresponds to small volume volcanism (< 1km^3), with an eruption duration range between hours to years (Kereszturi and Németh, 2012). It is also characterized to display a wide range of eruptive styles generating different morphologies, which can be classified such as spatter cones, scoria or cinder cones, tuff rings, maars and tuff cones. This classification is based in the magma/water ratio, dominant eruptive style and typical volcano architecture (Németh and Kereszturi, 2015). Scoria cone presents a determined size and shape that is the result of a complex evolution involving the interaction of aggradation and degradation processes (Grosse et al., 2012). They can be classified on the basis of their cone shape such as ideal, gully, horseshoe, tilted, crater row, parasitic and amorphous cone (Bemis and Ferencz, 2017). Studying the morphometric parameters of scoria cones permits to know the formation processes and evolution stage of a scoria cone, allowing for predicting how it would be affected by a future reactivation or eruption.

Negros de Aras (also called as El Negrillar) is a monogenetic volcanic field located in the Central Andean Volcanic Zone, northern Chile. Specifically, at the south of the Salar de Atacama on the Monturaqui-Negrillar-Tilopozo (MNT) aquifer, which is limited to the south by the Socompa debris avalanche at 30 km from the Socompa border crossing (Chile-Argentina). This monogenetic volcanic field hosts at least 20 vents with evidences of strombolian and phreatomagmatic style eruptions, forming scoria cones and lava flows of basaltic andesite and andesite composition that display olivine and pyroxene crystals (Hoffman, 2011). In this work, we have considered 10 scoria cones located at the southern area of Negros de Aras monogenetic volcanic field (Fig. 1), which we have identified with the letters from A to J, respectively (Fig. 1, Fig.3).

Fig. 1 – Negros de Aras monogenetic volcanic field, the scoria cones used in this study are identified with letter from A to J, respectively.

Understanding the magmatic processes associated with their formation and estimating their degree of erosion we aimed to provide an estimate for their relative age and cone growth processes to be able to define the volcanic evolution of the monogenetic volcanic field as a whole. A pristine scoria cone, slope angle ranges between 30° and 33°, the cone base width/max height ratio of 0.18 and the width summit/cone base of 0.4 were determined on the basis of young scoria cones (Wood, 1980). Any deviations from these parameters inferred to be associated with either a change in the eruptive styles through the growth of the cone and/or degradational processes. Thus, we have calculated the morphometric parameters of the scoria cones before mentioned using a digital elevation model image of 12 m (TanDEM-X 12m).

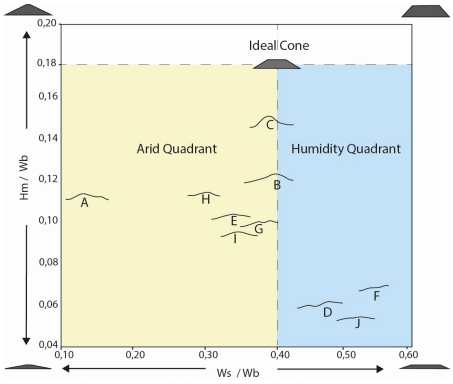

Fig. 2 – Degradation model modified of Forniciai et al. (2012) and Grosse et al. (2012) for the ten-scoria cones of Negros de Aras.

The morphometric parameters calculated for each scoria cone were volume (V), max. height (Hm), width base (Wb), width summit (Ws), ellipticity, elongation and slope angle.

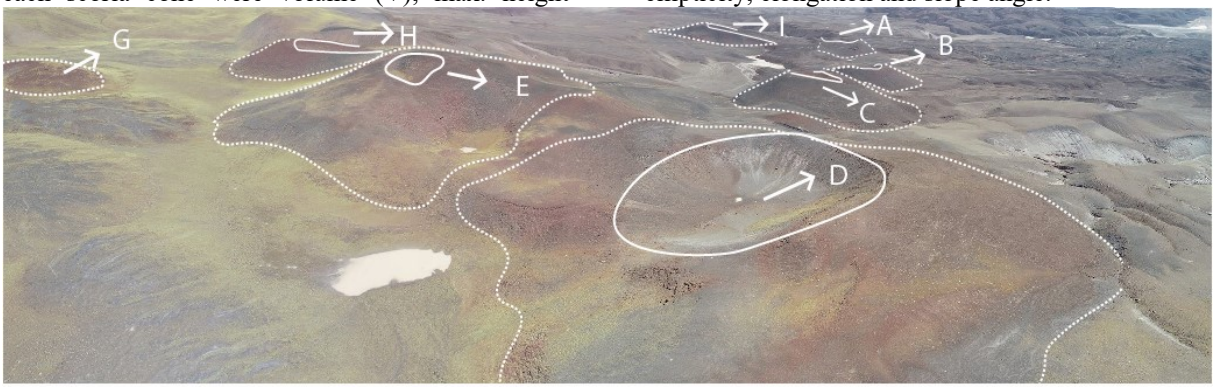

Fig. 3 – Western view of A,B,C,D,E,G,H and I scoria cones, Negros de Aras monogenetic volcanic field.

The first six parameters were estimated by the MORVOLC algorithm (Grosse et al., 2012), while the last parameter was estimated from a slope map generated through of an Arc Toolbox catalog tool (ArcGIS™ software).

According to Bemis and Ferencz (2017), we identified three types of scoria cone morphology such as amorphous, horseshoe and gully. Whereas the result obtained for the Hm/Wb and Ws/Wb ratios are plotted in the Fig. 2. According to our results obtained in the A, B, C, E, G, Hand I cones are associated with magmatic processes without the presence of water (arid quadrant; Fig. 2) these cones can be associated with a strombolian eruptive style. For the D, F and J cones degradational events can be interpreted. These cones show a crater with wide dimensions or highly eroded (humidity quadrant; Fig. 2) that could be explained by explosive eruptions of magma-water interaction (phreatomagmatism). Phreatomagmatic eruptions can be suggested due to the presence of the MNT aquifer and the evidences of rocks with cauliflower textures, cooling cracks and high contents of lithic fragments found around of the crater surface. Specifically, the scoria cone J is the most eroded cone, which could be interpreted as the older cone and for that could displays these values. On the other hand, the A, B, C and D cones and the E, F, G, H, I and J cones (Fig. 1) show a preferential orientation of their vents to NE-SW, respectively, which suggest a structural control in the volcanic activity of this area. Despite of Negros de Aras monogenetic volcanic field is not located so close of a village or city (~44 km to Tilomonte and ~57 km to Peine). It is important to understand and to know the magmatic, syn-eruptive and post-eruptive processes of this monogenetic volcanic field. This is because an eruptive event would affect the Zaldivar and Escondida mines and their water well located just about ~5 km away. In addition, an eruption would also affect the Socompa border crossing (Chile-Argentina) and the power lines that connect Chile-Argentina generating a great impact in the Chilean and Argentinian economy.

Acknowledgements

To Pablo Grosse, CONICET researcher and Fundación Miguel Lillo academic, for facilitating and allowing to use of TanDEM-X 12m.

References

Bemis, K.G., Ferencz, M., 2017. Morphometric analysis of scoria cones: the potential for inferring process from shape. Geol. Soc. Lond., Spec. Publ. 446 (1), 61–100.

Fornaciai, A., Favalli, M., Karátson, D., Tarquini, S., Boschi, E., 2012. Morphometry of scoria cones, and their relation to geodynamic setting: a DEM-based analysis. J. Volcanol.Geotherm. Res. 217, 56–72.

Grosse P, vanWyk de Vries B, Euillades PA, Kervyn M, Petrinovic IA, 2012., Systematic morphometric characterization of volcanic edifices using digital elevation models . Geomorphology 136:114 13.

Hoffman, C., 2011. Petrografía y geoquimíca de los conos del campo de lavas negros de aras (23º57´- 24º26´ lat. s. y 67º57´- 68º42´ long. o.) al norte del volcán Socompa, II Region de Antofagasta, Chile. Undergraduate thesis, Universidad de Concepción, Chile.

Kereszturi, G., Nemeth, K., 2012. Structural and morphometric irregularities of eroded Pliocene scoria cones at the Bakony-Balaton Highland Volcanic Field, Hungary. Geomorphology. 136. 45-58.

Németh, K., Kereszturi, G., 2015. Monogenetic volcanism: personal views and discussion. Int J Earth Sci (GeolRundsch) 104, 2131–2146

Wood, C.A., 1980. Morphometric analysis of cinder cone degradation. J. Volcanol.Geotherm. Res. 8, 137–160.

An explosive volcanism on the eve of the Cambrian "explosion" (~540 My ago) in the northeast of Siberia

Ivan Chayka[1], Dmitriy Grazhdankin[2,3], Vladimir Rogov[2], and Andrey Izokh[1,3]

[1] *Sobolev Institute of Geology and Mineralogy (IGM SB RAS), Novosibirsk, 630090, Russia,ivanlab211@gmail.com*
[2]*Trofimuk Insitute of Petroleum Geology and Geophysics (IPGG SB RAS), Novosibirsk, 630090, Russia*
[3]*Novosibirsk State University, Novosibirsk, 630090, Russia*

Keywords: volcanic complex, maar, Olenek Uplift, Ediacaran

Terminal Ediacaran and Terreneuvian strata cropping out along the northwestern slope of the Olenek Uplift, NE Siberia provide an exceptionally informative record of the Cambrian "explosion" of metazoan ecological and morphological complexity. The succession hosts laterally discontinuous stratiform tuff breccia and tuffites, occasionally basaltic flows, and is penetrated by numerous diatremes composed of tuff breccia and basalts, which are considered to be feeders for the stratified bodies. A U–Pb zircon date of 543.9 ± 0.24 Ma for a diatrem tuff breccia (Bowring et al., 1993) has long been used to constrain the age of the Ediacaran/Cambrian boundary in Siberia; however, the origin of the zircons remains ambiguous (Kiselev et al., 2016; Rogov et al., 2015; Vishnevskaya et al., 2017) and is in need of revision. A comprehensive field study conducted in 2018 allowed us to re-examine and re-sample a wide range of magmatic and volcanic formations cropping out in the middle reaches of the Khorbusuonka River, Olenek Uplift.

The following main types of magmatic formations have been recognized in the field (Fig.1):

1. Discordant bodies (diatremes) composed of tuff breccia, with variable amounts of tuff, lava-like and lithoclastic compounds, and often cross-cut by dolerite dykes. The bodies are several meters to ~200 m across; however, their exact size was difficult to resolve because of intricate shape and relationships with the host rocks. The diatremes penetrate the Khatyspyt, Turkut and lowermost Syhargalakh formations (Fig. 2A, 2B).
2. Stratiform tuff breccia sheets comprising heavily weathered outcrops as part of the Syhargalakh Formation.
3. Basalt flows interstratified with tuff breccia sheets cropping out on the northern slope of the Tas-Neleger Hill.
4. A volcanic plug composed of basalts and dolerites located in close proximity to the Tas-Neleger basalt flows.
5. Ubiquitous dolerite dykes occurring within large diatremes and as isolated intrusions cross-cutting the Khatyspyt, Turkut and lowermost Syhargalakh formations.
6. Dolerite sills varying in thickness on scale from from tens of cms to tens of meters emplaced in the Khatyspyt Formation.

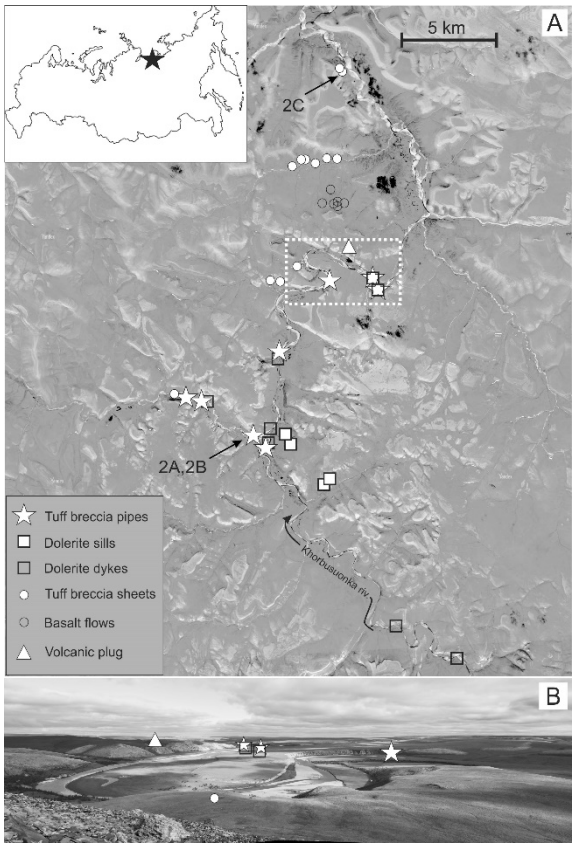

Fig. 1 – (A) The examined outcrops on a satellite photograph. (B) Locations of the outcrops in the landscape of the area outlined on (A).

Based on the field observations and preliminary laboratory examination the following genetic relationships can be inferred:

- Given the apparent textural, geochemical and mineralogical similarity we assume that the basalts, diatreme-hosted dolerite intrusions, and dolerite sills correspond to the same magmatic event. Although the magmatic compound of the breccia has been completely modified precluding chemical comparison with the basalts, the textural evidence and stratigraphic relationships suggest that it is basaltic in composition and the tuff breccia is co-magmatic with the basalts.
- The mingling structure of sandstone xenoliths in the tuff breccia, as well as the "infiltration" of the sandstone xenoliths with tuff matrix (Fig. 2C) provide further evidence that the eruptions are coeval with deposition of the Syhargalakh sandstones.
- Interstratification of the amygdaloidal basalt flows with the tuff breccia sheets in the Tas-

Neleger, along with the intricate relationship between the tuff breccia and the dolerite cross-cutting each other within the large diatremes imply an ambivalent style of eruptions. The basalts are thought to have poured out during "calm" eruptions, whereas the tuff breccia is most likely to have an explosive origin.

- Given that the diatreme-hosting magma contains xenoliths derived exclusively from the Khatyspyt, Turkut and Syhargalakh formations, the diatreme must have exploded at shallow (<200 m) depths, which is a characteristic of phreatomagmatic eruptions (Valentine et al., 2014). Since both surface and underground waters can act as coolant in phreatomagmatic eruptions, it is hard to distinguish whether the eruptions occurred overland or in underwater conditions. However, lithofacial constraints provided by Syhargalakh Formation, favor underwater regime of the eruptions.

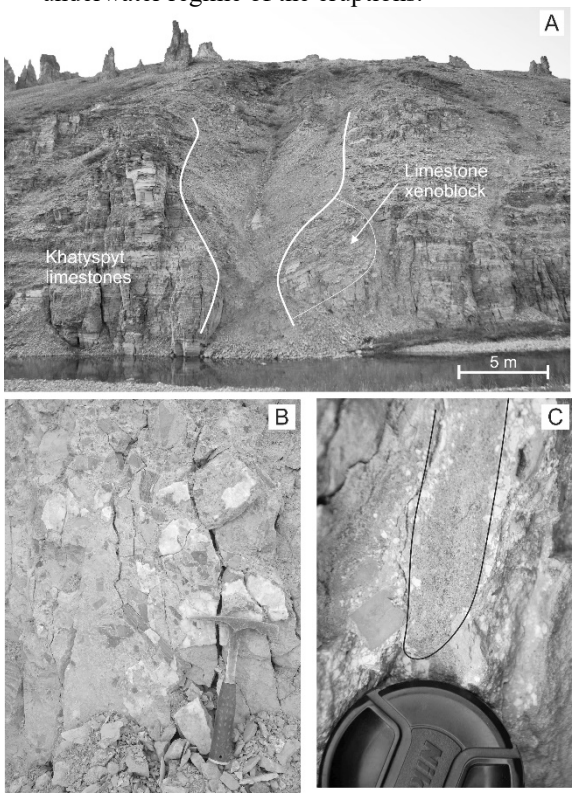

Fig. 2 – (A) Tuff breccia pipe emplaced within Khatyspyt formation. (B) Textures of the breccia within the outcrop. (C) Sandstone mingling (outlined) in the base contact of tuff breccia and Syhargalakh formation (photo rotated 90°).

This study provides a robust field and laboratory evidence for recognizing the Tas-Yuryakh volcano-magmatic complex comprising shallow-level chambers (sills), lava feeders, dome structures, solitary explosion pipes and sheets of basalts and tuff breccia. Insofar as the style of submarine eruptions is thought to be sensitive to water depth (Wohletz and Heiken, 1992), the observed alteration of explosive and effusive eruptions could have resulted from periodic sea-level oscillations in a relatively shallow-water setting, a conclusion that is consistent with lithofacies interpretation for the Syhargalakh Formation. Finally, assuming that the sills are coeval with the volcanic rocks, the U–Pb dating should be performed on baddeleyite from coarse-grained gabbro composing the sills, in order to better constrain the age of Ediacaran/Cambrian boundary in the Siberia.

Acknowledgements

The study was conducted at IGM SB RAS and IPGG SB RAS under Government Contracts and supported by the Russian Foundation for Basic Research grant 18-05-70110.

References

Bowring, S.A., Grotzinger, J.P., Isachsen, C.E., Knoll, A.H., Pelenchaty, S.M., Kolosov P. 1993. Calibrating rates of Early Cambrian evolution. Science 261: 1293-1298

Kiselev, A.I., Kochnev, B.B., Yarmolyuk, V.V., Rogov, V.I and Egorov, K.N. 2016. The Early Paleozoic basite magmatism in the northeastern Siberian Craton. Geodynamics and Tectonophysics 7: 233-250.

Rogov, V.I., Karlova, G.A., Marusin, V.V., Kochnev, B.B., Nagovitsyn, K.E., Grazhdankin, D.V. 2015 Duration of the first biozone in the Siberian hypostratotypepf the Vendian. Russian Geology and Geophysics 56: 573-583.

Valentine, A.G., Graettinger, A.H., Sonder, I. 2014. Explosion depths for phreatomagmatic eruptions. Geophysical Research Letters 41: 3045-3051.

Vishnevskaya, I.A., Letnikova, E.F., Vetrova., N.I., Kochnev, B.B., Drill., S.I., 2017 Chemostratigraphy and detrital zircon geochronology of the Neoproterozoic Khorbusuonka group, Olenek uplift, Notrheastern Siberia. Gondwana Research 51: 255-271

Wohletz, K.H. and Heiken, G. 1992. Volcanology and Geothermal energy. In: Los Alamos Series in Basic and Applied Sciences. Univ. California Press, Berkeley, CA, 432 pp.

Migrating hazards from maars recorded in crater morphologies

Alison Graettinger, Alexander Bearden

University of Missouri-Kansas City, Kansas City, Missouri, USA.graettingera@umkc.edu

Keywords: crater shape; lateral migration; explosion location.

The shape of maars following an eruption is the result of excavation, depositional processes and collapse. A global catalog of intact Quaternary maars from the MaarVLS database (Graettinger 2018) shows the dominance >85% of non-circular shapes. Elliptical, peanut, chain and other non-circular shapes require more than one location for subsurface phreatomagmatic explosions that migrated laterally during the eruption. Observations of Ukinrek in 1977 documented the formation of two craters separated along a fissure that were at times active simultaneously, with the eastern crater hosting two vent locations (Kienle et al. 1980). Further evidence for lateral migration of explosion locations in maars, not limited to the direction of the feeder dike, has been recognized from tephra ring stratigraphy, bomb sag orientations, and the distribution of debris jets in diatremes (van Otterloo et al. 2013; Firestein and Hildreth 2017; Ort and Carrasco-Núñez 2009; Ross et al. 2006).

Methods: The shape of intact maar craters provides an opportunity to constrain the distance and minimum number of explosion locations (vents) in past maar forming eruptions. This is first accomplished by using craters with shapes composed of identifiable overlapping circles (e.g. peanut shape on the right in Fig 1). The diameter of component circles are measured, and the distance between the centers of the component circles is measured. The component circles are assumed to represent explosion footprints (with associated growth through collapse) and the number of circles represents the minimum number of vent locations.

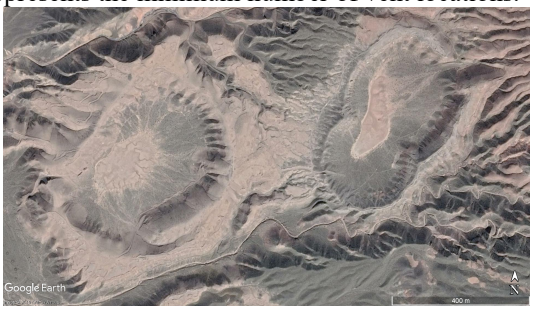

Fig. 1 – The majority of Quaternary maars on Earth have non-circular shapes such as those featured above from the Qal'eh Hasan Ali volcanic field in Iran.

Experimental work by Valentine et al. (2015) show that subsurface explosions spaced <1 radius apart produce a circular shape, explosions spaced near 1 radius produce ellipses, explosions spaced> 1 radius make peanut/chains, and explosions spaced>2 crater radii make separate craters.

Results: Based on 70 craters, most component circles were <600 m in diameter (Fig. 2) with some footprint sizes as large as 1.5 km. These footprints centers were mostly<700 m apart. Of these craters most shapes contained 2-3 component circles, with 4 recognizable overlapping circles occurring <5% of the time. The number of preserved explosion footprints represents a minimum number of vent locations to form the observed shape.

This number is likely low for more complex shapes as vent positions reconstructed from stratigraphy at some maars have been reported as >6 Tecuitlapa, Mexico (Ort and Carrasco-Núñez 2009), and 13 Mt. Gambier, Australia (van Otterloo et al. 2013), and >13 at Ubehebe, USA (Fierstein and Hildreth 2017).

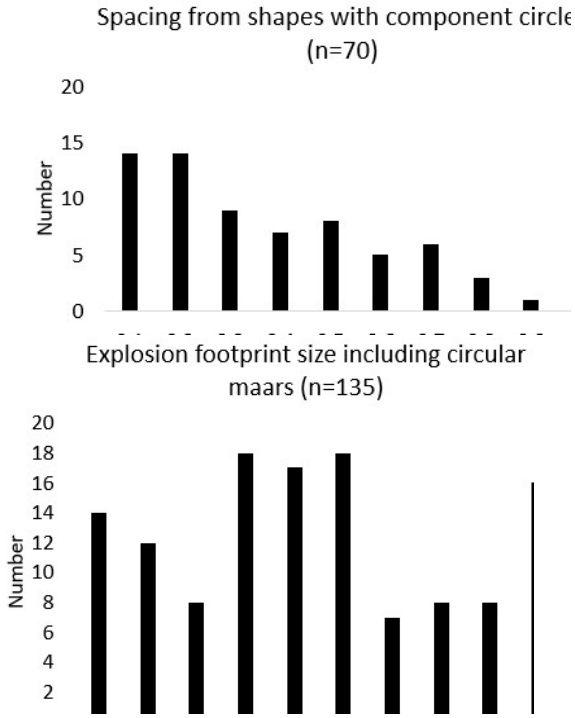

Fig. 2 – Frequency of values for the spacing between and diameter of component circles (explosion footprint) from non-circular maars.

Circular maars represent ~12% of the MaarVLS database and range in size from 100-3900 m in diameter. As estimates of explosion energies for phreatomagmatic explosions have been estimated to be 10^9 -10^{14} J (Valentine et al. 2014) and experiments with non-migrating explosions reveal an asymptotic growth of craters (Sonder et al. 2015) it is possible to estimate a size of crater size related to multiple explosions of the same energy in a single

location with added collapse by up to 60% of the initial explosion crater. This estimate indicates that the largest maar craters that can be produced without lateral migration should be between 650-1000 m in diameter. This suggests that lateral migration of explosion locations is required to produce large circular craters like Laguna Potrok, Argentina (~3900 m in diameter). To produce a crater of that diameter, phreatomagmatic explosions of 10^{14} J would have to move at least 8 times, and possibly as many as 20, to produce a circular crater of the size of Laguna Portok.

This analysis focused on craters whose shape have easily resolvable circular components, but >30% of the maars in the MaarVLS database are elliptical in shape. If ellipses are produced by explosion locations separated by roughly one crater radius (Valentine et al. 2015), the major diameter of the ellipse can be used to estimate two component circle diameters, that are spaced diameter/2 apart (Fig. 3). As these estimates assume a minimum number of explosion locations (two), the footprint estimates are maximums, however, they are consistent with the estimates from the more distinctly shaped crater analysis. There, are however, tens of footprints that are larger than the proposed maximum of 1 km, which suggests either more explosion locations, or that the maximum energy for phreatomagmatic explosions may be currently underestimated.

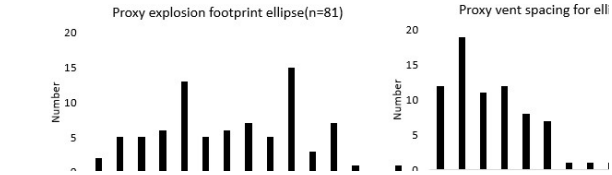

Fig. 3 – Frequency of proxy component circle diameters and spacing for elliptical maars in the MaarVLS database.

Conclusions: The number and distance of explosion locations during maar formation eruptions can be estimated from intact Quaternary maar shape. Analyses indicate that most component circles are <600 m in diameter, but examples up to 1 km are observed. The spacing between these explosion locations are similarly more abundant below 600 m, with rare examples at distances 1 km and above. The spacing of preserved component circles (explosion footprints) increases with increasing footprint size. In cases where this relationship is not maintained is likely represented by craters that do not preserve distinct component circles.

The causes of this lateral migration of explosions are many, including local hydrology, rock strength, and dynamic stresses from previous explosions. Detailed study of volcanic fields to identify the local dominant external factors are important to constraining future eruption scenarios, but are resource and time intensive. The estimates provided here, by global morphometric studies, represent a critical first step to better preparing for future phreatomagmatic eruptions in distributed volcanic fields by providing the order of magnitude for the distance explosions may migrate in a maar forming eruption. Constraining the common distances of vent migrations in maars is valuable to producing accurate hazard models and eruption event trees.

Acknowledgements

We would like to thank the UMKC undergraduate SEARCH and SUROP grants for supporting A. Bearden's participation in this research.

References

Fierstein J, Hildreth W (2017) Eruptive history of the Ubehebe Crater cluster, Death Valley, California. Journal of Volcanology and Geothermal Research 335:128-146.

Graettinger AH (2018) Trends in maar crater size and shape using the global Maar Volcano Location and Shape (MaarVLS) database. Journal of Volcanology and Geothermal Research 357:1-13

Kienle J, Kyle PR, Self S, Motyka RJ, Lorenz V (1980) Ukinrek Maars, Alaska, I. April 1977 eruption sequence, petrology and tectonic setting. Journal of Volcanology and Geothermal Research 7:11-37

Ort MH, Carrasco-Núñez G (2009) Lateral vent migration during phreatomagmatic and magmatic eruptions at Tecuitlapa Maar, east-central Mexico. Journal of Volcanology and Geothermal Research 181:67-77

Sonder I, Graettinger AH, Valentine GA (2015) Scaling multiblast craters: general approach and application to volcanic craters. Journal of Geophysical Research 120:6141-6158

Valentine GA, Graettinger AH, Macorps E, Ross P-S, White JDL, Dohring E, Sonder I (2015) Experiments with vertically and laterally migrating subsurface explosions with applications to the geology of phreatomagmatic and hydrothermal explosion craters and diatremes. Bulletin of Volcanology 77:15

Valentine GA, Graettinger AH, Sonder I (2014) Explosion depths for phreatomagmatic eruptions. Geophysical Research Letters 41

van Otterloo J, Cas RAF, Sheard MJ (2013) Eruption processes and deposit characteristics at the monogenetic Mt. Gambier Volcanic Complex, SE Australia: implications for alternating magmatic and phreatomagmatic activity. Bulletin of Volcanology 75:737

Apparently "dry" rootless littoral cones, ʻAuʻau Point and PuʻuKī, Hawaiʻi

Sam Holt, Jocelyn McPhie, and Rebecca Carey

School of Natural Sciences, University of Tasmania, Hobart, Tasmania, Australia. j.mcphie@utas.edu.au

Keywords: rootless littoral cone, steam-driven explosion, confined mixing.

Rootless cones form when lava interacts with external water, resulting in explosive lava–water interactions and the formation of a pyroclastic cone above, or adjacent to, the feeder lava flow (Fisher and Schmincke, 1984). Rootless cones that are formed within the littoral zone where lava crosses the coast are referred to here as rootless littoral cones. Rootless littoral cones may be regarded as special case of monogenetic volcano – they are small and typically have a single vent that is used once in a single eruption episode; all known examples are basaltic. Rootless littoral cones are reasonably common features of the coasts of basalt-dominated volcanic islands such as Hawaiʻi, the Canary Islands and Reunion Island, and several examples have been observed, including during the 2018 eruption of Kilauea.

In simplest terms, the steam-driven explosions that build rootless littoral cones occur in response to mixing of lava and water. Heat transfer from the lava to the water leads to rapid production and expansion of steam that fragments the lava. Mattox and Mangan (1997) defined two lava–water mixing regimes for rootless littoral cones. Open mixing occurs when lava flows into a body of water and lava–water interaction occurs freely. Rootless littoral cones that have formed during periods of observed explosive activity driven by open mixing share similar cone geometries and deposits. The cones have a characteristic half-cone geometry, as only the half-cone onshore is preserved, and the half-cone may be bisected by the lava into two onshore quarter-cones. The cones range greatly in height from 10 m (Waikupanaha) to 35 m (Sand Hills) and are dominated by thinly planar-bedded to cross-bedded deposits composed mainly of ash (70-90%) and minor lapilli and bombs. The deposits are poorly sorted and have high proportions of coarse ash. Such features are widely considered to be typical of the deposits from explosive hydrovolcanic activity (e.g., Walker and Croasdale, 1971; Zimanowski et al., 2015).

Confined mixing occurs when tube-fed lava interacts with water that enters via fractures in the tube wall, and has been observed to produce small (8 m high) circular mounds of welded bombs and lapilli with minor amounts of ash (Mattox and Mangan, 1997).

Rootless littoral cones at ʻAuʻau Point and PuʻuKī on the southwestern flank of Mauna Loa, Hawaiʻi show none of the characteristics of explosive hydrovolcanic activity driven by open mixing of lava and water common to other historic rootless littoral cones on Hawaiʻi. Both cones are much larger than the mounds observed to result from confined mixing and the cone-forming units are, in fact, more akin to those produced by "dry" explosive activity found elsewhere on Hawaiʻi and on many other basalt-dominated subaerial volcanoes.

PuʻuKī consists of two littoral cones, North Cone and South Cone, which both formed on the Pohūe Bay tube-fed lava (750-1500 years old) that was erupted from the Southwest Rift Zone of Mauna Loa (Jurado-Chichay et al., 1996).The South Cone is almost a complete circle in plan view and consists of two main units (Fig. 1): (A) thermally oxidized, slightly welded lapilli and coarse bombs arranged in planar beds defined by grain size and variations in the degree of welding; (B) alternating grey clastogenic lavas and thermally oxidized, slightly to moderately welded lapilli and bombs. The clastogenic lavas are laterally continuous over distances up to 50 m and range in thickness from tens of cm to 1 m. The pyroclastic beds between the clastogenic lavas contain ≪5% ash, are up to 4 m thick and include abundant round cored bombs.

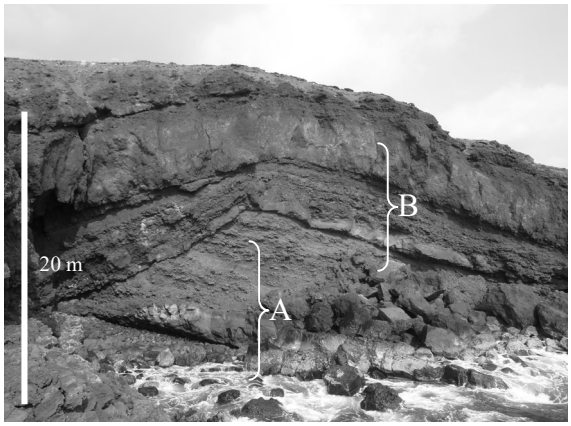

Fig. 1 – Cross-section through PuʻuKī showing the two main units, both of which are red due to thermal oxidation.

ʻAuʻau Point is a rootless littoral cone that was fed by a pahoehoe branch of the Kolo lava flow erupted from the Southwest Rift Zone of Mauna Loa between 200 and 750 years ago (Jurado-Chichay et al., 1996). The cone is 30 m high and appears to have originally been circular, but the seaward side is cut by an escarpment. The main cone-forming unit is 15 m thick and comprises alternating clastogenic lavas and thermally oxidized, slightly-welded lapilli and bombs, similar to Unit B at PuʻuKī South Cone. The welded lapilli and bomb layers are 1 to 7 m

thick and the clastogenic lavas have thicknesses up to 3 m. This unit is mantled by a non-welded, ash-rich, internally bedded layer approximately 15 m thick. The uppermost unit consists solely of very large bombs (Fig. 2) on the inner wall and proximal outer walls of the cone. This unit was deposited simultaneously with lava effusion from a vent in the southwestern quadrant of the crater. The lava covered the floor of the crater and flowed over the escarpment down to sea level, forming the current surface of the lava bench.

Fig. 2 – ʻAuʻau Point rootless littoral cone. Large bombs within the uppermost unit draping the proximal parts of the cone.

The cone-forming units at ʻAuʻau Point and PuʻuKī South Cone show many features traditionally attributed to "dry" explosive magmatic activity: mainly fluidal lapilli and bombs, very low ash abundance, extensive thermal oxidation, a high degree of welding, presence of clastogenic lavas. These characteristics are surprising given that rootless littoral explosions must involve external water as the source of gas (steam). Magmatic volatiles play no significant role because the lava flows have undergone extensive outgassing and the explosions take place far away from the primary subterranean magmatic plumbing system of the volcano. In fact, it is not possible for these cones to be the result of "dry" explosive magmatic activity, despite their apparently "dry" facies characteristics. The circular geometry of the cone-forming units at ʻAuʻau Point and PuʻuKī South Cone also sets them apart from most other rootless littoral cones on Hawaiʻi.

Given that these cones must be hydrovolcanic in origin, they most likely formed from confined mixing as described by Mattox and Mangan (1997) but sustained for much longer periods and on a larger scale than in observed events. The alternating clastogenic lavas and variably welded lapilli and bomb beds could reflect cycles of higher and lower eruption intensity and accumulation rate over time. During periods of littoral lava fountaining (high energy, high frequency explosions; Mattox and Mangan, 1997), high proximal accumulation rates resulted in the formation of clastogenic lavas. During periods of lower-intensity lava bubble bursts (low energy, intermittent explosions; Mattox and Mangan, 1997), lower proximal accumulation rates formed the thick, variably-welded lapilli and bomb lithofacies.

The deposits of ʻAuʻau Point and PuʻuKī South Cone suggest that prolonged confined mixing of lava and water can result in the formation of rootless littoral cones that show very few of the diagnostic field characteristics of hydrovolcanic activity. Without geographical context, cones of this nature could easily be interpreted as products of "dry" explosive magmatic activity at primary vents. Furthermore, rootless littoral cones formed from confined mixing are much more likely to be preserved in the ancient rock record than rootless littoral cones formed from open mixing, as their deposits are more consolidated and less prone to erosion.

References

Fisher, R.V., Schmincke, H.-U., 1984. Pyroclastic rocks. Springer-Verlag Berlin.

Jurado-Chichay, Z., Rowland, S.K., Walker, G.P., 1996. The formation of circular littoral cones from tube-fed pāhoehoe: Mauna Loa, Hawai'i. Bulletin of Volcanology 57: 471-482.

Mattox, T.N., Mangan, M.T., 1997. Littoral hydrovolcanic explosions: a case study of lava-seawater interaction at Kilauea volcano. Journal of Volcanology and Geothermal Research 75: 1-17.

Walker, G., Croasdale, R., 1971. Characteristics of some basaltic pyroclastics. Bulletin Volcanologique35: 303-317.

Zimanowski, B., Büttner, R., Dellino, P., White, J.D., Wohletz, K.H., 2015. Magma–Water Interaction and Phreatomagmatic Fragmentation. The Encyclopedia of Volcanoes (Second Edition), Elsevier, p. 473-484.

Post-caldera monogenetic volcanism at Deception Island, Antarctica: landform recognition and volcanic hazards implication

Dario Pedrazzi[1], Gabor Kereszturi[2], Agustin Lobo[1], Adelina Geyer[2] and Janina Calle[3]

[1] *ICTJA, CSIC, Group of Volcanology, SIMGEO UB-CSIC, Institute of Earth Sciences Jaume Almera, Lluis Sole i Sabaris s/n, 08028 Barcelona, Spain.* dpedrazzi@ictja.csic.es
[2]*Volcanic Risk Solutions, School of Agriculture and Environment, Massey University, Palmerston North, New Zealand.*
[3]*Gli Studies & Projects GLISP S.A., Principal Florida Norte s/n, Guayas, Guayaquil, Ecuador*

Keywords: tuff cone, tuff and tephra ring, hydrovolcanism

Interest in monogenetic volcanism, with special reference to volcanic hazards and risk studies, has risen in the last decade. This is especially true in areas where monogenetic volcanic fields are close to population centres, critical infrastructure, and shipping routes, as for example the Michoacán-Guanajuato and Chichinautzin Volcanic Fields in Mexico, Auckland Volcanic Field in New Zealand, Deception Island in the Antarctica, Garrotxa Volcanic Field and Canary Islands in Spain. Volcanic hazard assessment requires information to be obtained from the geomorphology of volcanic edifices and deposit characteristics, such as volumes, crater shapes, grain size distributions, and edifice geometries. Such attributes of a volcanic edifice often provide quantitative information for long-term eruptive volumes, magma eruption rates, and relative chronologies (Conway et al. 1998; Guilbaud et al. 2012).

Eruptive and associated sediment transport processes of a monogenetic volcano critically control the resultant morphology of volcanic edifices (Bemis and Ferencz 2017; Wood 1980b), which in turn capture vital information about the volcanic processes. These are often overprinted by post-eruptive degradation modification (Hooper and Sheridan 1998; Kereszturi et al. 2013a; Wood 1980a).

Deception Island (DI), an active Quaternary volcano with a large central collapse caldera, is characterized by monogenetic post-caldera landforms (mainly tuff cones and rings; Fig. 1) dominated by explosive eruptions driven by magma-water interaction (Pedrazzi et al. 2018). More than 20 eruptions have been registered at Deception Island over the past two centuries (Roobol 1982; Smellie et al. 2002), demonstrating that the occurrence of a new eruption is fully plausible, being a concern for tourists, scientists, and the logistics personnel working on or near the island.

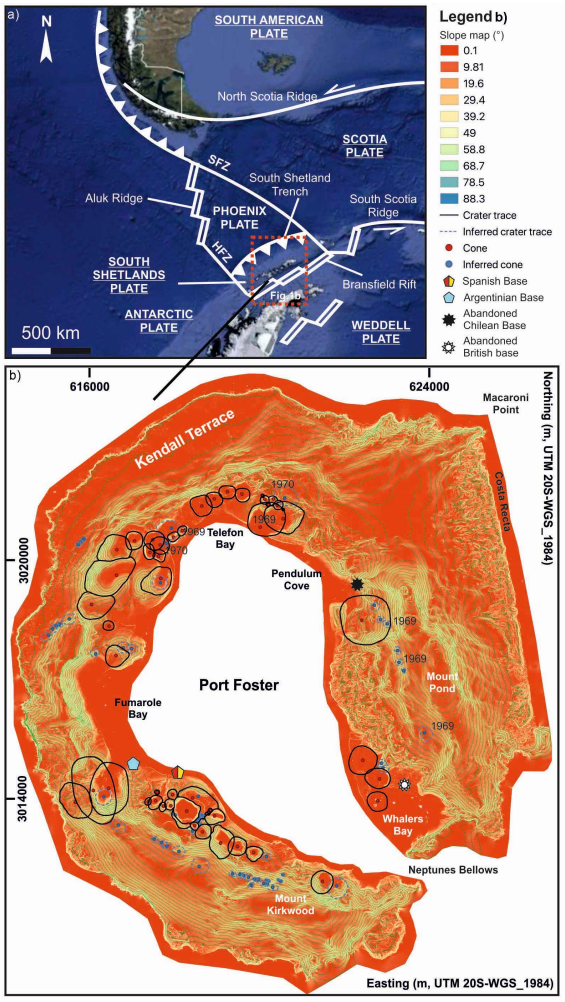

Fig. 1 – a) Location of the South Shetland Archipelago (Google Earth 2019—Image US Geological Survey) and geodynamic setting of the area (modified from Ibáñez et al., 2003);b) Slope map of DI with the location of the post-caldera explosive vents and recent volcanic activity (1967, 1969, and 1970 eruptions).

The described geometry and morphologies might be interpreted to be shaped by a combination of erosional and eruptive processes: the histograms of slope angles of the volcanic structures at DI are complex since they present a multimodal and skewed distribution (Fig. 2), making the reliability of the mean values less comparable than for scoria cones that are more often unimodal (Kereszturi et al. 2013a). This variability of the slope angles of the volcanic structures (craters and cones) is unforeseen being relatively young structures, which must be most likely, eruptive in origin—without discarding the influence of external environmental controls.

The geomorphology of the studied edifices (major/minor crater diameter, crater elongation and breaching direction, and crater or slope angle of the

crater wall) and physical properties of the exposed outcrops (poorly vesiculated bombs and lapilli scoria deposits, high lithic content, and palagonitisation of glass in the matrix; Fig. 2) are also largely consistent with a hydrovolcanic origin, forming tuff rings and tuff cones, due to the explosive interactions of magma with porous - or fracture-controlled groundwater aquifers or surface water (White 1996; Wohletz 1986).

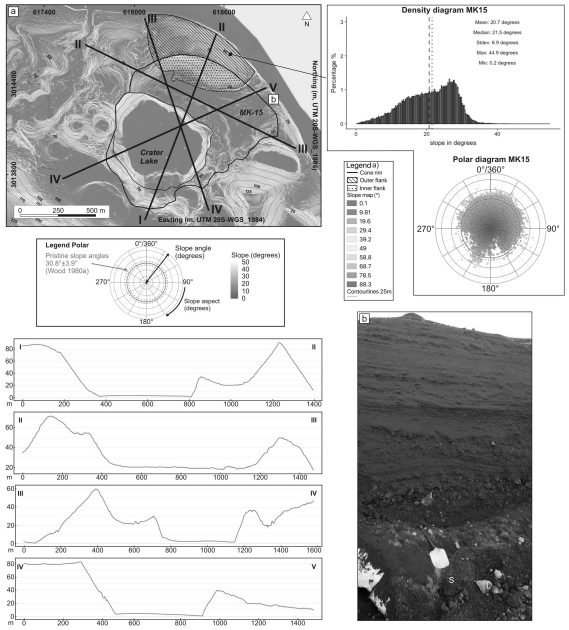

Fig. 2 – Example of one of the studied edifice: a) slope map with the density slope diagram of the northern flank and topographic profiles; b) alternation of clast-supported lithic-rich layers of lapilli and bombs (shovel is about 1 m long).

The geometry of the resultant volcanic edifice is in sharp contrast with subaerial scoria cone morphologies that are common subjects of morphometric analyses. This study shows that the basic shape parameters are important; in combination with slope angle analysis, which can provide valuable observations to discriminate among different types of monogenetic volcanoes

Hazard implication of the eruption styles at DI has shifted from the early Surtsey-type to phreatomagmatic due to spatial changes in the availability of the external water within an actively evolving collapse caldera. The water depth must have been changing over time due to sea-level change and change in the local topography during the Holocene. This aspect of the evolution of Deception Island needs to be investigated in the future.

Acknowledgements

This research was supported by the MICINN grant CTM2011-13578-E and was partially funded by the POSVOLDEC project (CTM2016-79617-P) (AEI/FEDER-UE). A.G. is grateful for her Ramón y Cajal contract (RYC-2012-11024). D.P. is grateful for his Beatriu de Pinós (2016 BP 00086) and Juan de la Cierva (IJCI-2016-30482) contracts. This research is part of POLARCSIC and AntVolc activities.

References

Bemis, K.G. and Ferencz, M., 2017. Morphometric analysis of scoria cones: the potential for inferring process from shape. Geological Society, London, Special Publications 446.

Conway, F.M., Connor, C.B., Hill, B.E., Condit, C.D., Mullaney, K. and Hall, C.M., 1998. Recurrence rates of basaltic volcanism in SP cluster, San Francisco volcanic field, Arizona. Geology 26(7): 655-658.

Guilbaud, M.-N., Siebe, C., Layer, P. and Salinas, S., 2012. Reconstruction of the volcanic history of the Tacámbaro-Puruarán area (Michoacán, México) reveals high frequency of Holocene monogenetic eruptions. Bull. Volcanol. 74(5): 1187-1211.

Hooper, D.M. and Sheridan, M.F., 1998. Computer-simulation models of scoria cone degradation. J. Volcanol. Geotherm. Res., 83(3-4): 241-267.

Ibáñez, J.M., Almendros, J., Carmona, E., Martínez-Arévalo, C. and Abril, M., 2003. The recent seismo-volcanic activity at Deception Island volcano. Deep Sea Res. Part II, 50(10-11): 1611-1629.

Kereszturi, G., Geyer, A., Martí, J., Németh, K. and Dóniz-Páez, F.J., 2013a. Evaluation of morphometry-based dating of monogenetic volcanoes—a case study from Bandas del Sur, Tenerife (Canary Islands). Bull. Volcanol., 75(7): 1-19.

Kereszturi, G., Bebbington, M. and Németh, K., 2017. Forecasting transitions in monogenetic eruptions using the geologic record. Geology, 45(3): 283-286.

Pedrazzi, D., Németh, K., Geyer, A., Álvarez-Valero, A.M., Aguirre-Díaz, G. and Bartolini, S., 2018. Historic hydrovolcanism at Deception Island (Antarctica): implications for eruption hazards. Bull. Volcanol., 80(1): 11.

Roobol, M., 1982. The volcanic hazard at Deception Island, South Shetland Islands. British Antarctic Survey Bulletin, 51: 237-245.

Smellie, J., López-Martínez, J., Headland, R., Hernández-Cifuentes, F., Maestro, A., Millar, I., Rey, J., Serrano, E., Somoza, L. and Thomson, J., 2002. Geology and geomorphology of Deception Island. British Antarctic Survey.

White, J.D.L., 1996. Impure coolants and interaction dynamics of phreatomagmatic eruptions. J. Volcanol. Geotherm. Res., 74(3-4): 155-170.

Wohletz, K.H., 1986. Explosive magma-water interactions: Thermodynamics, explosion mechanism and field studies. Bull. Volcanol., 48(5): 245-264.

Wood, C.A., 1980a. Morphometric analysis of cinder cone degradation. J. Volcanol. Geotherm. Res. 8(2-4): 137-160.

Wood, C.A., 1980b. Morphometric evolution of cinder cones. J. Volcanol. Geotherm. Res. 7(3-4): 387-41

Destruction of emergent tuff cones in Faial Island, Azores: influence of tectonics and marine erosion

Dario Pedrazzi [1], Vittorio Zanon[2,3], Adriano Pimentel[4], Fernando Tempera [5]

[1] *ICTJA, CSIC, Group of Volcanology, SIMGEO UB-CSIC, Institute of Earth Sciences Jaume Almera, Lluis Sole i Sabaris s/n, 08028 Barcelona, Spain. dpedrazzi@ictja.csic.es*
[2]*Instituto de Investigação em Vulcanologia e Avaliação de Riscos (IVAR), Universidade dos Açores, Rua Mãe de Deus, Ponta Delgada 9500-123, Portugal*
[3]*Institut de Physique du Globe de Paris, Université de Paris, CNRS UMR-7154, Paris 75005,France*
[4] *Centro de Informação e Vigilância Sismovulcânica dos Açores (CIVISA), Rua Mãe de Deus, 9500-123 Ponta Delgada, Portugal*
[5]*Departamento de Oceanografia e Pescas, Universidade dos Açores, 9901-862 Horta, Portugal*

Keywords: tuff cone, hydrovolcanism, marine geology, basaltic magmatism

The island of Faial is the westernmost of the central islands of the Azores archipelago (North Atlantic Ocean), and is located east of the Mid-Atlantic Ridge. The Azores are in a unique geodynamic setting at the triple junction of the North-American, Eurasian and Nubia lithospheric plates (Searle, 1980; Madeira and Ribeiro, 1990; Vogt and Jung, 2004) (Fig. 1a)

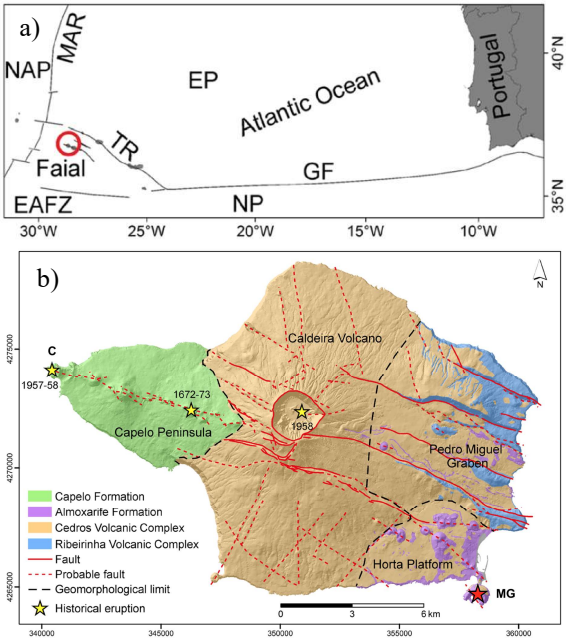

Fig. 1 –a) Geological setting of the Azores Islands. NAP: North American Plate, EP: Eurasian Plate, NP Nubian Plate, MAR: Mid-Atlantic Ridge, TR: Terceira Rift, EAFZ: East Azores Fracture Zone, GF: Gloria Fault; b) simplified geological map of Faial Island, C-Capelinhos, MG-Monte da Guia (modified from Pimentel et al., 2015).

The central part of Faial is dominated by the Caldeira central volcano, which corresponds to the main massif of the island, truncated by a summit collapse crater of 2 km across and 400 m deep (Fig. 1b). Horta fissure zone, located on the south-east of Faial, is a lava platform with several scoria cones and one tuff cone (Monte da Guia; Fig. 1b).

On the western end of the island, the Capelo fissure zone is a ridge formed by cinder cones and the remnant of the tuff cone formed during the1957-58historic eruption of Capelinhos (Fig. 1b).

The Azores are located in the northern hemisphere subtropical anticyclones zone dominated by the Azores anticyclone that influences the circum North Atlantic climate.

Between autumn and winter, these islands are frequently affected by low-pressure systems, associated to the southern migration of the polar front, causing recurrent storms and periods of high winds. During spring and summer, the climate is regulated by the establishment of the Azores High closer to the archipelago reducing the precipitation.

The ocean circulation pattern in the Azores area is governed by two main branches the Gulf Stream: the North Atlantic Current and the Azores Current. The coasts of the islands are, therefore, considered as wave dominated coasts following the Davis and Hayes (1984) classification scheme.

In this work, we focused on Capelinhos and Monte da Guia tuff cones (Fig. 1b) as case study to show the influence of tectonic and marine erosion on destruction of monogenetic landforms at oceanic islands.

Capelinhos tuff cone is located at the western tip of Capelo peninsula (Fig. 1b). The tuff cone is the product of three distinct eruptive pulses that begun up to 1.2 km off-shore the Costado da Nau cliff in 1957-1958 (e.g. Castelo Branco et al., 1959; Zbyszewski and Veiga Ferreira, 1959). Today, about 3/5 of the original tuff cone have been removed by partial collapses, and the joined action of wind and waves (Fig. 2).

Fig. 2 –Capelinhos cliff showing the remaining tuff and scoria cones with a complex network of dykes

The careful study of the structure of the palagonitized tuff sequences around the remnant of the cone, revealed the existence of an incompletely

developed network of both radially-and tangentially-arranged fractures similarly to other tuff-cones in the area (Zanon et al., 2009). The intensive erosion allowed the exposure of the inner structure of the cone, where there are three main dyke complexes which survived to the erosion.

.Monte da Guia is a tuff cone located in the south-east of Horta platform (Fig. 1b). It is connected to the main land by a narrow isthmus composed of sand and pebbles that contact with a deeply eroded and collapsed older scoria cone (Fig. 3). Differently from Capelinhos, there are neither scoria cones nor lava flows associated. The steep slopes are constituted by highly palagonitized hydromagmatic tuff, with scattered basaltic bombs which plastered upon the surface on landing. The tuff cone is higher in the northern part, while progressively grades to the sea towards the S. A considerable mass movement has affected the SE flank of Monte da Guia. The run-out of this mass movement succession attains a depth of 750 m and extends across a flow-wise distance exceeding 6 km.

Fig. 3 – Monte da Guia tuff cone. Google Earth (2020).

At Capelinhos, regional tectonic influenced the morphology of the submerged basement along this direction, favored magma intrusion along parallel feeder dykes and determined the breaching of the cone towards the west. Partial gravitational collapse and rock-falls also keep on occurring along this direction, acting a strict morphological control on the erosion of the cone.

It is speculated that the emplacement of the Monte da Guia cone very close to the shelf edge overloaded this section of the island margin and eventually led to the collapse which produced the incision extending across the shelf margin and slope. Likely, seismic activity and the fact that the heavy volcanic load was possibly emplaced over shelf sediment deposits may have facilitated the failure.

Acknowledgements

D.P. is grateful for his Juan de la Cierva (IJCI-2016-30482) contract.

References

Castelo Branco, A., Zbyszewski, G., Moitinho de Almeida, F., Veiga Ferreira, O., 1959. Rapport de la Premiere mission Geologique. Serv. Geol. Port. Mem., 4, 9–27.

Davis, J.R.A., Hayes, M.O., 1984. What is a wave-dominated coast? Marine Geology, 60, 313.

Madeira, J., Ribeiro, A., 1990. Geodynamic models of the Azores triple junction: a contribution from tectonics. Tectonophysics 184, 405–415.

Pimentel, A., Pacheco, J., & Self, S. (2015). The~1000-years BP explosive eruption of Caldeira Volcano (Faial, Azores): the first stage of incremental caldera formation. Bulletin of Volcanology, 77(5), 42.

Searle, R., 1980. Tectonic pattern of the Azores spreading centre and triple junction. Earth Planet. Sci. Lett. 51, 415–434.

Vogt, P.R., Jung, W.Y., 2004. The Terceira Rift as hyper-slow, hotspot-dominated oblique spreading axis: a comparison with other slow-spreading plate boundaries. Earth Planet. Sci. Lett. 218, 77–90.

Zanon, V., Pacheco, J.M., Pimentel, A., 2009. Growth and evolution of an emergent tuff cone: Considerations from structural geology, geomorphology and facies analysis of São Roque volcano, São Miguel (Azores). J. Volcanol. Geotherm. Res., 180(2–4), 277–291.

Zbyszewski, G., Veiga Ferreira, O., 1959. Rapport de la Deuxieme mission Geologique. Serv. Geol. Port. Mem., 4, 29–55.

Statistical analysis of spatial patterns and characteristics of monogenetic volcanoes (maars vs scoria cones) in the Los Tuxtlas Volcanic Field (Veracruz, Mexico)

Katrin Sieron[1], Sergio Juárez Cerillo[2], and Karime González Zuccolotto[3]

[1] *Centro de Ciencias de la Tierra of Universidad Veracruzana, Xalapa, Veracruz, 91000 Mexico.ksieron@gmail.com*
[2]*Facultad de Estadística e Informática of Universidad Veracruzana, Xalapa, Veracruz, 91000 Mexico.*
[3]*Centro de Investigaciones en Geografía y Geomática (CentroGeo), Distrito Federal, 14240 Mexico.*

Keywords: monogenetic field, spatial analysis, statistics.

The Los Tuxtlas Volcanic Field (LTVF) is located in southern Veracruz State at the Coast of the Gulf of Mexico, almost 200 km to the South of the easternmost limit of the Trans-Mexican Volcanic Belt (Fig 1). Although extension-related volcanism has been identified (Negendank et al., 1985), calc-alkaline chemical fingerprints clearly indicate subduction-related volcanism (Nelson et al., 1995).

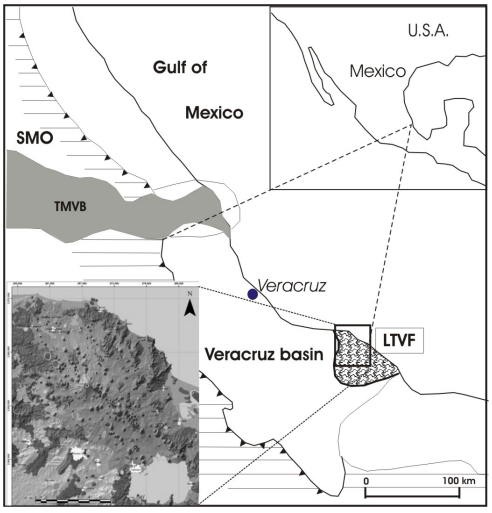

Fig. 1 – Location of the Los Tuxtlas volcanic Field and study area.

Although the LTVF includes several polygenetic volcanoes (as there are San Martín Tuxtla, Santa Martha, Yohualtajapan and San Martín Pajápan) it is composed by more than 350 monogenetic vents, mainly scoria cones and explosion craters (predominantly maars) of late Quaternary and Holocene ages (Fig 1). Although geologic studies date back to 1923 (Friedlaender and Sonder), detailed information about eruptive history of the polygenetic volcano and the surrounding monogenetic field is scarce. Only about 3% of the volcanic edifices have been dated so far, which complicates comprehension of spatial-temporal patterns of eruptions and hazard assessment. Nevertheless, existing dates point towards very recent eruptions affecting prehispanic settlements (e.g. Jaime-Riverón y Pool, 2009). Related hazards to monogenetic volcanism in the LTVF are manifold. Strombolian eruptions related to scoria cone construction can produce extensive ash and lapilli fallout; maar volcano eruptions are generally associated to pyroclastic surge emissions threatening the population living in the area. About 15% of the scoria cones have associated lava flows, some of which showing considerable volumes and travel distances of up to >10 km from the source.

The volcanic field shows the second highest cone-density (up to 6/km^2) compared to the other Mexican Volcanic Fields, after Michoacan-Guanajuato Volcanic Field. It also represents the field with highest maar-volcano abundance in Mexico (at least 41 young maar craters).

Comparing morphological traits of the edifices, 4 age groups have been identified, showing a distribution of the youngest volcanoes throughout the volcanic field.

It is clearly visible (Fig 2) that individual volcanic field members are not evenly distributed throughout the LTVF compared to other Mexican volcanic fields; further, there is a different spatial arrangement for the explosion craters and the scoria cones, which has its origin in the subsurface (local and regional faults and water table).

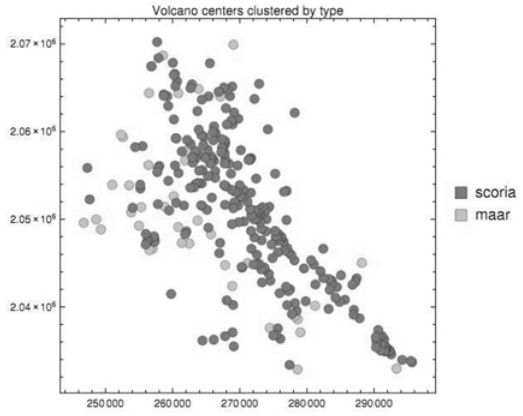

Fig. 2 – Distribution of monogenetic volcanoes of scoria cone and maar type throughout the Los Tuxtlas Volcanic Field.

In order to further characterize the monogenetic volcanism, morphological parameters have been determined for scoria cones and maars. For this purpose high resolution Lidar images have been used. Specific parameters have been determined by using the GIS-measure tool, and the zonal statistics tool applied to individually delimited edifices

(polygons). Subsequent statistical analyses were carried out by using R-software.

The results of the latter reveal specific distributions of the most voluminous edifices, breached craters and lava flows associated to volcanoes, as well as characteristics like cone and crater-width are clearly trending across and along the LTVF (e.g. Fig 3). Additionally, correlations (bi-plots, etc) between morphometric parameters reveal clearly related and not related parameter-pairs. Spatially dependent parameters have been further analyzed using kriging, which reveals for example that the most voluminous volcanoes are expected to get constructed within a narrow stripe at the center line of the NW-SE trending field. .

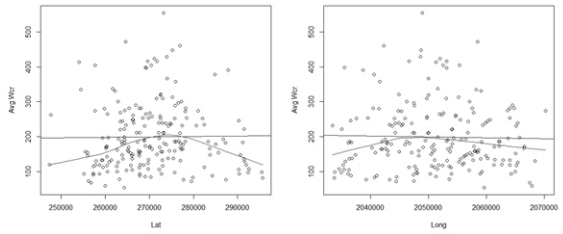

Fig. 3 – Example of spatial variation (linear and smooth trends) of edifice width along and across the Los Tuxtlas Volcanic Field.

References

Friedlaender, I, Sonder, R.A. 1923. Über das Vulkangebiet von San Martín Tuxtla in Mexiko. Zeit. Vulkan. 7, 162-187.

Jaime-Riverón, O., Pool, C. 2009. The impact of volcanic hazards on the ancient Olmec and Epi-Olmec economies in the Los Tuxtlas region, Veracruz, Mexico. En: Jones, E.C., Murphy, A.D. (Eds.) In the Political Economy of Hazards and Disasters. Altamirano Press, Lanham, p. 133-154.

Magill, C.R., McAneney, K.J., Smith, I.E.M., 2001. Probabilistic assessment of vent locations for the next Auckland volcanic field event. Mathematical Geology 37: 227-242.

Negendank, J.F.W., Emmermann, R., Krawczyk, R., Mooser, F., Tobschall, H., Werle D. (1985), Geological and geochemical investigations on the eastern Trans Mexican Volcanic Belt. Geofis. Int., 24, 477-575.

Nelson, S.A., González-Caver, E., Kyser, T.K. 1995. Constraints on the origin of alkaline and calc-alkaline magmas from the Tuxtla Volcanic Field, Veracruz, Mexico. Contrib. Mineral. Petrol., v.122, p. 191-211.

The January 02, 1996 eruption in Akademii Nauk Caldera: the formation of maars and its limnological consequences

Ilya Svirid[1], Viktor Dvigalo[1] and Alina Shevchenko[1,2]

[1]*Institute of volcanology and seismology FEB RAS, Petropavlovsk-Kamchatsky 683006, Russia.*
i.yu.svirid@gmail.com
[2]*Deutsches Geo Forschungs Zentrum GFZ, Helmholtz-Zentrum Potsdam*

Keywords: Karymsky Volcanic Center, Maar, Limnic Explosion

Akademii Nauk Caldera is a unique volcanic object. Considered extinct over the past 4800 years, it unexpectedly activated together with Karymsky volcano in early 1996.

On January 1, 1996, a swarm of shallow earthquakes with magnitudes of up to 6.9 was detected within the Karymsky Volcanic Center. That is the highest crust magnitude that has ever been detected in the history of seismological survey in Kamchatka. Following this, on January 2, 1996, the simultaneous eruption of the Karymsky volcano began, as well as in the northern part of the Akademii Nauk Caldera - in the shallow zone (Belousov et al., 1997) at the bottom of Karymsky Lake. The consequences of this eruption were recorded by aerial photography in 1996, and also there was pre-eruption aerial data available (from September 11, 1984). Further, aerial photography was carried out in 2000, 2003, 2004, and 2010. Using all these data, we can evaluate not only the effects of the eruption, but also the post-eruptive changes.

The eruption caused a tsunami in Karymsky Lake. The splash heights in the northern part of the lake reached 50 m, and in the southern part, up to 10 m. Vegetation was destroyed along the coastline, the soil was eroded, and the terrain changed on the part of the coast directly adjacent to the eruptive center due to slipping of the slope. The amplitude of the changes was up to 6 meters horizontally and up to 1.5 m vertically.

The eruption was phreatomagmatic (Fedotov, 1997). According to (Andreev and Latkin, 2004), a series of explosions occurred with the ejection of both clastic rocks and fresh material. As a result of the eruption, a peninsula was formed with a crater named Tokarev Crater, 600 m in diameter. Its round shape, gently sloping outside shafts and a flat subaerial part lead us to raise the question of its belonging to one or another type of hydro-volcanic objects. In previous works (Fedotov, 1997, Andreev and Latkin, 2004) it was suggested that it could be an example of Surtseyan volcanism.

This assumption is based on one argument - the underwater conditions of the eruption. But besides this circumstance, there are other signs. (Brand and Heiken, 2009) distinguish such signs as morphological, petrological and related to the presence of abundant liquid water in the eruption column. The underwater morphology of the crater was studied in (Belousov et al., 1997). Its shape is symmetrical, on the south side it also has a pronounced rim that goes under water no more than 10 m; its central part has a depth of about 50 m. The subaerial part of the Tokarev crater, adjacent to the shore of the lake, was named Novogodniy Peninsula. Its surface is absolutely flat with a slight down inclination to the south, which fundamentally distinguishes it from typical tuff cones of the Surtseyan type, with steep slopes. Tokarev Crater has very similar shape and size to Valentina's Maar, located 6 km to the NE from the Karymsky volcano.

The petrological features of the maars and tuff cones are limited to the percentage of fresh magmatic material in the eruption products. For maars it is 0–100 (typically <30%), for tuff cones - 90-100% (Brand and Heiken, 2009). Unfortunately, the surface of the Novogodniy Peninsula, exposed to landslides from the lake and tsunamis, and therefore it is not representative of this indicator. Andreev and Latkin, 2004 conducted a study of outcrops of deposits of explosive eruption products in areas of the northern shore of Lake Karymsky that were not subjected to landslide formation. In a three-meter-deep outcrop, he identified five layers of large (tens of centimetres) and small (centimetres) of volcanic bombs, lapilli, resurgent fragments, and debris alternating with each other, which demonstrates a pulsating character typical of hydro-volcanic eruptions (Brand and Heiken, 2009). Although the percentages of fresh material are not given in Andreev and Latkin, 2004, it is indicated that clastic rocks are more predominant for deposits of the initial eruption phases, and bombs and lapilli are more prevalent for later ones. Thus, we can conclude that the proportion of fresh and matured rocks was about the same order. Only new field studies can give more detailed data, but in any case, this order of values does not fit into the 90-100% of new material that is typical of the Surtseyan type.

The third indicator of the genetic difference between maars and tuff cones is the water saturation of rocks, through which igneous material makes its way to the surface. Brand and Heiken, 2009 classify such phenomena as dry-phreatomagmatic and wet-phreatomagmatic eruptions. Although the formation of maars usually occurs in dry conditions, and in humid conditions - apparently corresponding to the situation on the bottom of the Karymsky lake - tuff cones usually

form, it is stipulated that under conditions of low magma mass flux and high groundwater recharge, wet maars can form, like, for example, on the Tihany Peninsula in Hungary (Nemeth et al., 2001). In the work Lorenz, 1986, the conditions for the formation of this type of volcanic objects are examined in detail using the example of the formation of the maars of the West Eifel volcanic fields. We can assume that the conditions for the formation of the Troitsky crater, obviously a Maar rather than a tuff cone, were somewhat similar to the dyke fissure zone of West Eifel.

On the surface of the New Year's Peninsula, in addition to the main crater, there are: one large funnel with a diameter of 30 m and two groups of small funnels with diameters of no more than 10 m. The distance between the farthest of them is 180 m. These funnels are obviously second-order Maars formed in the next stage after the main eruption. An interesting feature of these Maars is the close to linear arrangement with the north-south-western strike. Large funnel and southern group are located on the same line with the center of the Tokarev crater, but northern group departs from this line 50 m to the east, closer to Piip's hot springs, which also appeared after this eruption.

To the north of Novogodny Peninsula along the Karymskaya River extends a zone of tectonic discontinuities. Most of them were formed as a result of earthquakes on January 1, 1996, however, among them there are old cracks - existing long before the events of 1996, and having a similar extension to the new ones. These discontinuities reached almost the Lagerny cone in the north. This is a monogenetic dome-shaped volcanic object surrounded by a field of lava flows poured from under it. Its estimated age is approximately 5,000 years (Belousov et al., 1997).

Such a neighbourhood of old and new volcanic and tectonic objects may indicate the interaction of the processes that generate them. We suggest that this area is a zone of fissure volcanism with periodically occurring monogenic eruptive centers. In this case, the type of eruption can be determined by the conditions for the lava outflow. The formation of the maars during the events of January 2-3, 1996, occurred due waters of Lake Karymsky, which predetermined the phreatic component in the type of eruption.

The previous eruption in this place - the northern part of the Akademii Nauk caldera took place 4,800 years ago, the nature of its deposits suggests that it was also phreatomagmatic (Belousov et al., 1997). The eruptive subaerial landforms associated with it are absent. It is obvious that until 1996 they were hidden by the waters of Karymsky Lake. As detailed bathymetry of its bottom was not performed we cannot estimate where exactly it is located. The 1996 eruption had such significant effect on the relief of the northern part of the lake bottom that now it is impossible to find out for sure.

The main post-eruptive event was the damming of the Karymskaya River, which flows out of the lake, with eruption materials. It was followed by a breakthrough of the dam and the mud flows going downstream. The largest part of their deposits was formed in the Volkanostantsii valley, in the area to the north from the lava fields of the Lagerny cone. Also, over time, as we can see from aerial photographs of different years, there was a restructuring of certain sections of the riverbed and overgrowing of the Karymsky Lake coastline with new vegetation.

On the ASTER image of Karymskoye Lake taken on 19 December 2006 a thaw in ice up to 50 m wide was observed extending from the NNE coast (the area of the Grimuchie springs) to the SW coast (near the Medvezhie springs). This indicates a high hydrothermal activity in the lake, and possibly the existence of a fissure zone at its bottom, traced by melting ice above it.

References

Andreev, E.I. & Latkin A.S. 2004. Influence of the vortex-related events upon the dynamics of the subaqueous 02.01.1996 Akademii Nauk Caldera Eruption. (in Russian). The Vortex-related events of the geological processes Workshop proceedings, Kamchatka regional association "Educational-scientific center". p. 229–240.

Belousov, A.B., Belousova, M.G., Muravev, Y.D. 1997. Holocene Eruptions it the Akademii Nauk Caldera and Age fo the Karymsky Stratovolcano (Kamchatka). (in Russian). Doklady Akademii Nauk, 1997, Jun, V354, N5. PP. 648–653.

Brand, B.D & Heiken, G. 2009. Tuff cones, tuff rings, and maars of the Fort Rock–Christmas Valley basin, Oregon: Exploring the vast array of pyroclastic features that record violent hydrovolcanism at Fort Rock and the Table Rock Complex. *GSAComplex Field Guides,* **15,** 521–538, doi: 10.1130/2009.fld015(25)

Fedotov, S.A. 1997. Study and Mechanism of the Simultaneous 1996. Karymsky Volcano and Akademii Nauk Caldera Eruptions in Kamchatka. Volcanology and Seismology, Volume 19, Number 5, p 525–566.

Lorenz, V., 1986. On the growth of maars and diatremes and its relevance to the formation of tuff rings: Bulletin of Volcanology, v. 48, p. 265–274, doi: 10.1007/BF01081755

Nemeth, K., Matrin, U., and Harangi, Sz., 2001. Miocene Phreatomagmatic volcanism at Tihany (Pannonian Basin, Hungary): Journal of Volcanology and Geothermal Research, v. 111, p. 111–135, doi: 10.1016/S0377-0273(01)00223-2

Silicic lava dome growth and associated tephra deposits, Tokaj Mts Hungary

János Szepesi[1,2], Ildikó Soós[1], Bianka Németh[1], Máté Szemerédi[13], Csaba Bogos[3], Péter Sipos[3], Andrea Di Capua[4], Gianluca Groppelli[4], Gianluca Norini[4], Roberto Sulpizio[4,5], Szabolcs Harangi[1,6], Réka Lukács[1]

[1] *MTA-ELTE Volcanology Research Group, Budapest, Hungary* szepeja@gmail.com
[2]*Isotope Climatology and Environmental Research Centre (ICER), Institute for Nuclear Research, Debrecen, Hungary*
[3] *Department of Mineralogy, Geochemistry and Petrology,University of Szeged, Szeged, Hungary*
[4]*Istituto di GeologiaAmbientale e Geoingegneria, Consiglio Nazionale delleRicerche, Milano, Italy*
[5] *Dipartimento di Scienzedella Terra e Geoambientali, UniversitàdegliStudi di Bari, Bari, Italy*
[6] *Department of Petrology and Geochemistry, Eötvös University, Budapest, Hungary*

Keywords: rhyolite, dome complex, tephra.

Introduction

Rhyolitic domes are commonly regarded as monogenetic volcanoes (Carrasco-Núñez and Riggs 2008) and characterized by short-lived successions of pyroclastic and effusive activity. The small volume eruptions include tephra rings, bedded fallout deposits or pyroclastic density currents (Németh, 2010). The studies of young volcanic terrains are mainly focused on short term morphological changes, tephra transport and depositional processes. The older Miocene volcanic landforms provide an advantage to see the deeper architecture of edifices, characterizing depositional-erosional events and transformation of the syn-eruptive landscape.

Geological settings

Regionally repeated andesitic to rhyolitic volcanic eruptions took place from ca. 15 Ma until 10 Ma in the Tokaj Mountains (TM) within the Carpathian-Pannonian region, Eastern-Central Europe. The volcanic edifices were partially developed at shallow marine environment (Szepesi et al. 2019) followed by subaerial volcanism. ThePáska Hill rhyolitic lava dome and the associated volcaniclastics are located in the northern part of TM. Based on the dating of the surrounding lava domes, the eruption occurred around 12 Ma and is contemporaneous with the Late Miocene silicic volcanic activity of the TM (Szepesi et al. 2019).

The edifice is a west to east tending erosional ridge (~2km^2) with 200m relative elevation. Several outcrops are located in surrounding valleys and a detailed research drilling performed between 1980-1992 (Cseh-Németh et al. 1991). Active quarrying is currently exploiting the deposit and provide exposures for the lithofacies correlations. The overall evolution of the complex is poorly described and interpreted as a submarine lithofacies association. The stratigraphy of 50 boreholes have been revised and correlated to fieldwork results to characterize the major lithofacies zones.

Lithofacies architecture

The simplified local stratigraphy is given in Fig. 1. The complex facies architecture is subdivided into proximal (lava dome), medial (dome slope) and distal (fallout and ignimbrite) sections.

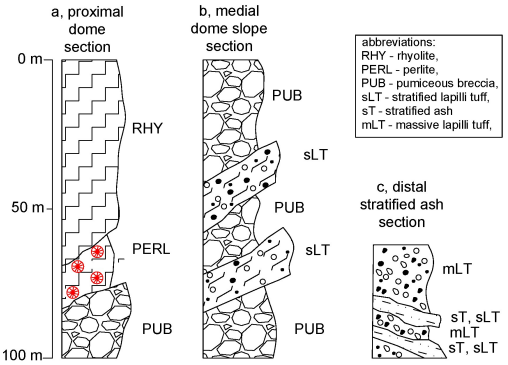

Fig. 1 –Stratigraphy and facies architecture of the Páska Hill.

Proximal dome section

The proximal (western) section of edifice encloses two distinct overlapping dome units (Fig.1.). The lower is a poorly to unsorted monomictic, pumiceous breccia (PUB). The appearance is highly variable from matrix (reddish, oxidized) to clast supported domains (Fig. 2)

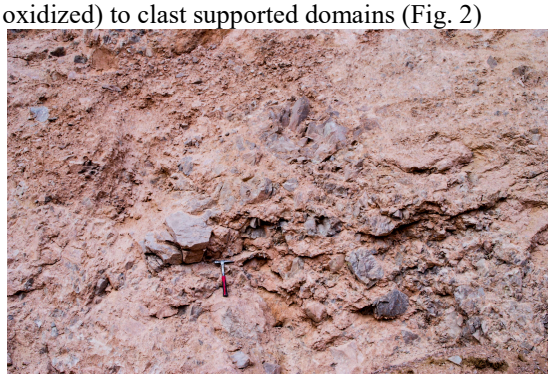

Fig. 2 – Clast (grey) and matrix (red) supported domains in the pumiceous, monomictic breccia (PUB).

The clasts size varies from cm to meter large angular boulders, coherent and devitrified parts are subordinate. The thickness is varied between 50-180 m. The upper dome is exposed at top of the edifice with a maximum thickness over 50 m. The basal zone of it (5m) is perlitic glass while the devitrified banded coherent rhyolite core (30m<) is developed through a transitional (15m) zone. The glass usually contains relict obsidian grains (2-7 mm). The expected upper glassy zones have been eroded.

Medial (dome slope) section

The outcrops of the medial section are restricted to the lower part of the operational quarry at the southeastern part of the edifice. At outcrop scale, two horizons of dense stratified lapilli tuff can be recognized as intercalation between the pumiceous breccia (PUB, Fig. 1b, 2.) lithofacies. The maximum vertical extent of lapilli tuff stratigraphy ranges from 5-15 m in the boreholes with a general 30° NE dipping. The thickness of the individual horizons range between cm to dm and are usually fine poor. Planar stratification with normal or reverse grading is observed. The clast size varies from coarse ash to lapilli (5-8cm), occasionally with larger clasts (20-40cm). The clast composition is uniform in the whole sequence with sub-rounded to angular banded perlite (dense or pumiceous) and reddish rhyolite. Three lenses (2-5 m long, 10-50 cm thick) of fine ash contains accretionary pellets (Øcm).

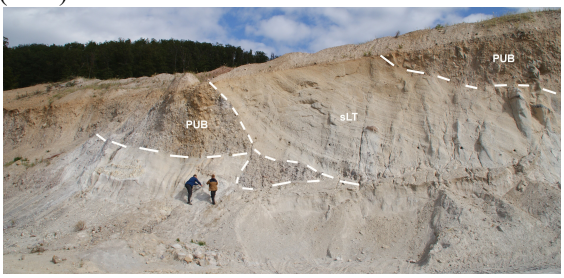

Fig. 3 – Stratified lapilli tuff layers (white, sLT) intercalated between the dome related breccias (dark, PUB).

Distal (sLT-mLT) section

Distal outcrops are mapped at the eastern margin of the edifice. The dome material is totally absent. The stratified lapilli tuff layers (30-80 cm) are alternating with massive lapilli tuff horizons.

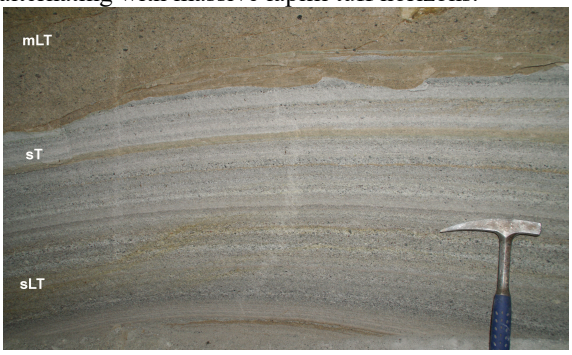

Fig. 4 – Erosional unconformity on the top of sT/sLT unit.

At the top of sLT layers erosional unconformities are observed (Fig. 4.). The thickness of the laterally continuous beds is 0.5-5 cm with usually good sorting. The grain size varies from coarse ash to fine lapilli. The clast types are identical with the medial section. The upper, mLT dominated part of the succession is more voluminous (10 m<). The massive, poorly sorted, non-welded lithics bearing lapilli tuff crops out over a wider area in the surroundings.

Discussion

Dome forming eruptions are commonly associated with hydrovolcanic explosive activity resulting from the interaction of rising magma with external aquifer (Tait et. al 2009, Kósik et al. 2019). At the Páska Hill, the multiphase dome growth is combined with contemporaneous tephra deposition. The sLT units deposited on the dome breccias as well sorted fallout layers and give important stratigraphic markers for the correlation. The presence of accretionary lapilli suggests sub-Plinian, phreatomagmatic activity but the existence of a larger tuff ring structure is not confirmed. The appearance of unsorted (mLT) deposits in distal settings indicate small granular pulses of pyroclastic density currents (ignimbrite) and changing in eruptive style. The topmost dome is a mostly eroded silicic flow which played an important role preserving the succession during 10 Ma erosion.

Acknowledgements

This research has been funded by the Hungarian–Italian MTA-CNR bilateral research project 2018–2021 (led by S. Harangi and G. Groppelli) and part of the FK131869project of National Research, Development and Innovation Office (Hungary). The work was also supported by the European Union and the State of Hungary, co-financed by the European Regional Development Fund in the project of GINOP-2.3.2-15-2016-00009 'ICER'.

References

Carrasco-Núñez G., Riggs N.R., 2008. Polygenetic nature of a rhyolitic dome and implications for hazard assessment: Cerro Pizarro volcano, Mexico J. Volcanol. Geoth. Res. 171, 307–315.

Cseh-Németh, J., Mátyás E., Sántha P., 1991. Nagybózsva, Páska Hill, comprehensive report and stock estimation, Manuscript, 1-125 (in Hungarian)

Kósik, S., Németh,, K., Lexa, Procter J.N., 2019 Understanding the evolution of a small-volume silicic fissure eruption: Puketerata Volcanic Complex, Taupo Volcanic Zone, New Zealand Journal of Volcanology and Geothermal Research 383. 28–46.

Németh, K., 2010. Monogenetic volcanic fields: Origin, sedimentary record, and relationship with polygenetic volcanism, in Cañón-Tapia, E., and Szakács, A., eds., What Is a Volcano? Geological Society of America Special Paper 470: 43–66.

Szepesi, J., Lukács, R., Soós, I., Benkó, Zs., Pécskay, Z., Ésik, Zs., Kozák, M., Capua D., A., Groppelli, G., Norini, G., Sulpizio, R., Harangi, Sz.Telkibánya lava domes: Lithofacies architecture of a Miocene rhyolite field Tokaj Mountains, Carpathian-Pannonian region, Hungary Journal of Volcanology and Geothermal Research, 385, 179-197.

Tait M.A., Cas R.A.F., Viramonte J.G., 2009 The origin of an unusual tuff ring of perlitic rhyolite pyroclasts: The last explosive phase of the Ramadas Volcanic Centre, Andean Puna, Salta, NW Argentina. Journal of Volcanology and Geothermal Research 183:1–16.

Session 2. Eruption mechanism of maars and associated volcanoes

Originally maars were considered as craters of pure gas eruptions which ejected no juvenile magmatic material. Later quenched juvenile pyroclasts were recognized in most of the maar deposits and it became widely accepted that maars are products of phreatomagmatic eruptions from a highly explosive interaction between ascending magma and groundwater. Recently however appeared evidences that at least some maars were formed by violent release of CO_2 probably of mantle origin. This session invited multidisciplinary submissions that can provide insight into eruptive mechanisms of maars based on investigation of lithology of maar deposits, properties of the erupted juvenile material. Presentations that investigate the link between maar forming eruption mechanism and more magmatic explosive eruption-driven eruption styles (such as Strombolian for instance) were particularly welcome.

Maars of Kamchatka

Alexander Belousov, Marina Belousova

Institute of volcanology and seismology FEB RAS, Petropavlovsk-Kamchatsky 683006, Russia. belousov@mail.ru

Keywords: Kamchatka, maar, phreatomagmatic eruptions.

Maars have distinctive edifice morphology (low profile with broad crater that commonly contains a lake). Such morphology allows maars to be easily identified at aerial and space images. We have examined space images as well as topographic maps and aerial images of Kamchatka Peninsula and identified, in total, 24 maars with crater diameters ranging from 0.2 to 2 km (Table 1). It turned out that maars constitute approximately 2% of the total number (about 1000) of monogenic volcanic edifices of the peninsula (represented mostly by scoria cones).

Analysis of the geographic distribution of the maars throughout the area of Kamchatka (Fig. 1), shows that their number in each particular area is not proportional to the number of other types of monogenic volcanoes in the area. For example, Klyuchevskaya group of volcanoes in Holocene produced numerous monogenic scoria cones and only two maars.

Such as maar-forming eruptions are phreato-magmatic and require the presence of ground water that explosively interacts with magma, we estimated relative abundance of water in the areas where the maars were formed (Fig.1). The largest number of the maars was formed in the southern part of Kamchatka Peninsula. Comparison of the map of the maar distribution with the map of annual atmospheric precipitation revealed that maars tended to form in volcanic areas of Kamchatka having the highest precipitation rates. Some maars of Kamchatka, such as Nachikinsky, Krokur, and Chasha, were formed close to large natural water reservoirs (the Bering Sea, Lake Kronotskoye and Lake Tolmachevo, correspondingly). Obviously, water of these reservoirs migrated through aquifers, and contributed to phreatomagmatic mechanism of the maar-forming eruptions. Most of the maars of Kamchatka were formed in lowlands, where groundwater was most abundant. For example, Maar Dal'neye Lake was formed inside the swamped area of Uzon Caldera.

Most of the maars resulted from eruptions of mafic magmas, although there are several maars formed by evolved magmas (up to rhyolitic).

Table 1. Characteristics of maars of Kamchatka (from north to south).

Name	Geographic coordinates	Age, Ka	Crater, km	Composition
Nachikinsky	57°50'46.46"N, 162°30'54.47"E	>10	1.6	Basalt
Kinenin 1 (Blyudechko)	57°20'29.35"N, 160°57'57.8"E	1.1	1.2	Basalt?
Kinenin 2	57°23'18.37"N, 161°10'33.6"E	?	0.2	
Kinenin 3	57°22'37.6 "N, 161°10'39.56"E		0.3	
Kroton 1	57° 2'24.21"N, 162° 0'8.22"E	>9	0.7	Basalt?
Kroton 2	57° 2'4.12"N, 162°3'54.65"E		0.5	
Baidarny (Shiveluch)	56°34'0.95"N, 161°7'33.72"E	7.6	>0.5	Basalt
Tolbachinsky1	55°42'52.86"N, 160° 2'36.06"E	?	1	Basalt
Tolbachinsky2	55°41'43.03"N, 160° 1'57.19"E		0.7	
Krokur	54°41'56.41"N, 160°22'9.39"E	4.9	1.3	Basalt
Dal'neye lake	54°30'27.22"N, 160° 2'22.95"E	3.3	1.2	Basaltic andesite
Valentina	54° 5'56.35"N, 159°29'0.61"E	>10	0.8	Basalt
Sukhoye Lake	54° 4'46.45"N, 159°34'52.25"E	>10	2	Basalt
Koldobische	53°48'40.04"N, 158° 2'43.69"E	1.2	0.2	Basalt
Chasha (2 craters)	52°37'43.25"N, 157°33'21.2"E	4.6	1.2	Rhyolite
Barany amphitheater	52°31'21.47"N, 157°24'54.1"E	1.5	1.4	Rhyolite
Temny (3 craters)	52°23'25.05"N, 57°15'11.9"E	8	0.7, 0.2, 0.3	Basalt
Chernoye lake (2 craters)	52° 5'44.61"N, 157°39'47.59"E	?	0.8, 0.3	?
Khodutkinsky (2 craters)	52° 5'15.32"N, 157°38'26.45"E	2.8	1.5, 0.4	Rhyolithic dacite
Khetik	52° 5'20.39"N, 157° 5'31.31"E	?	0.3	Basalt (?)
Krugloye lake	51°48'8.86"N, 157°17'34.27"E	9	0.8	Basalt (?)
Krestovka	51°49'4.82", 156°49'43.46"E	?	0.8	Basalt (?)
Iliinsky 2	51°31'10.44"N, 157° 8'10.88"E	<7.6	0.3	?
Iliinsky 1	51°30'12.11"N, 57°13'34.45"E	1901 AD	1	Andesite

Note: Ages of Barany amphitheater and Khodutkinsky maars after Braitseva et al. (1992), Krokur after Ponomareva (1987), Koldobishe after Dirsen, Melekestsev (1999), Chasha after Dirksen (2002), Baidarny after Churikova et al. (2010), Nachikinsky, Kinenin, and Kroton maars after Pevzner (2015). Other ages are estimations by the authors.

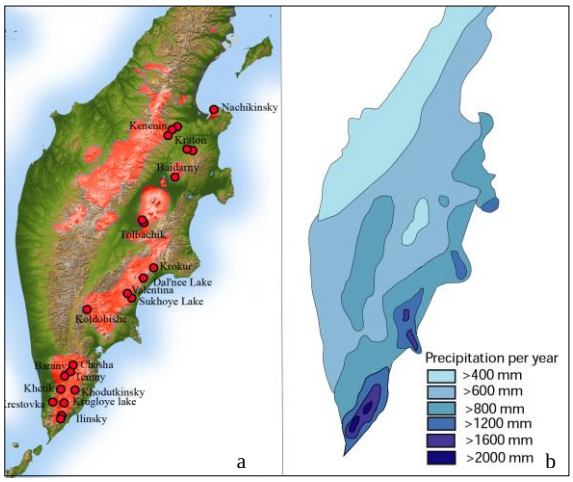

Fig.1 – (a) Geographic distribution of maars in the Kamchatka Peninsula. Red-coloured areas indicate the distribution of Pleistocene-Holocene volcanic rocks. (b) Amount of atmospheric precipitation in the Kamchatka Peninsula. Most of the maar-forming eruptions took place in areas where volcanism occurs against the background of a wet climate.

References

Belousov, A. 2006. Maars of Kamchatka: distribution and mechanism of their formation. Transactions of the Russian Academy of Sciences. Earth Science Sections 406: 492–495.

Braitseva, O. A., Melekestsev, I. V., Ponomareva, V. V., Kirianov, V. Y., Litasova, S. N., & Sulerzhitsky, L. D., 1992. Tephra of the largest prehistoric Holocene volcanic eruptions in Kamchatka. Quaternary International, 13: 177–180.

Braitseva, O.A., Melekestsev, I.V. and Ponomareva, V.V., 1994. Age of Active Volcanoes in the Kuril–Kamchatka Region. Journal of Volcanology and Seismology: 5–32.

Churikova,T.G., Gordeichik B.N., Belousov A.B., Babansky A.L., 2010. Funding of eruptive center on the slopes of Shiveluch volcano. Conference devoted to 25 anniversary of volcano observatory at Kamchatka.

Dirksen O., Melekestsev I.V., 1999. Chronology, Evolution and Morphology of Plateau Basalt Eruptive Centers in Avacha River Area, Kamchatka, Russia. Journal of Volcanology and Seismology, 21: 1–27.

Dirksen, O. V., Ponomareva V. V., and Sulerzhitsky L. D. 2002. Eruption from Chasha Crater – a unique large silicic eruption at a monogenetic basaltic lava field. Volcanology and Seismology 5: 3–10.

Ponomareva, V.V., 1987. Krasheninnikov volcano: history of formation and activity. Journal of Volcanology and Seismology 5: 28–44 (In Russian).

Pevzner, M. M., 2015. Holocene volcanism of Sredinny Ridge, Kamchatka. Transactions of Geological Institute 608, 248 p.

The characteristics of phreatomagmatic ash particles from maar complex of Lamongan Volcanic Field, East Java, Indonesia

Andriansyah Gurusinga and Tsukasa Ohba

Department ofEarth Resource Science, Akita University, Akita 010-8502, Japan. magurusinga11@gmail.com

Keywords: maar, phreatomagmatic eruption, volcanic ash

The Lamongan Volcanic Field (LVF) is located *c*. 140km to the SE of Surabaya, capital city of East Java, Indonesia. LVF is a unique in term of its characteristic which is surrounded by dry maars and water-filled maars.

Petrology and geochemistry of lavas from the western of LFV have been reported by Carn and Pyle, 2001, but the characteristics of maars and formation process are still not clear. Lamongan volcano is a basaltic stratovolcano comprising three main vents. The LVF contains up to 61 cinder or spatter cones and at least 29 maars, distributed on the flank of Lamongan volcano (Fig. 1). An assessment of the LVF longevity was suggested an age of the order of 13-14 ka based on a range of eruptive rates and erupted volume (Carn, 2000). These ages are comparable to other volcanoes along Sunda Arc.

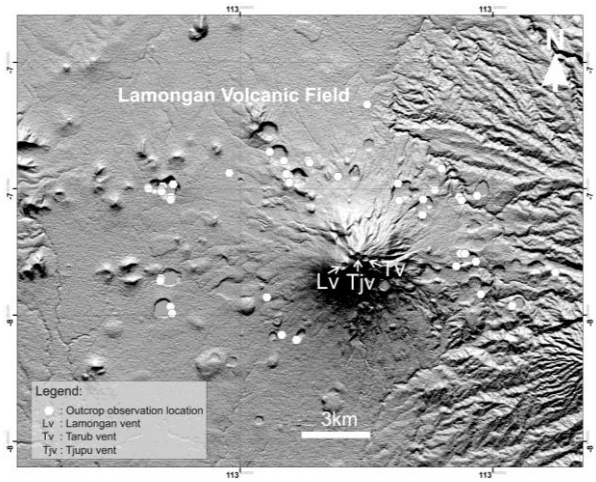

Figure 1 – The distribution of outcrop observation location around the maar complex in LVF. The three vents of Lamongan volcano are Lamongan vent (Lv), Tarub vent (Tv), and Tjupu vent (Tjv).

The interaction of water and magma is known as molten-fuel-coolant-interaction (MFCI). The initial phase of contact between water and surface of magma generates a thin vapor film. The instability of the vapor film on magma surface causes rapid expansion by heat energy transfer. The cause of explosive eruption can also be reinforced by the expansion of dissolved gas as a result of decompression during magma ascent.

The analysis of shape of volcanic particles is important to infer some eruptive parameters (e.g. magma viscosity, volatile content, and degree of magma-water interaction) which could describe the fragmentation and transportation associated with volcanic eruptions (Maria and Carey, 2002).

The distribution of maars was identified through field observation and morphological analysis using satellite imagery. These maars are present to the east, north, and west of LVF at 170-600 m elevation. The deposit of maar complex is mainly composed of pyroclastic density current deposit which is characterized by the presence of accretionary lapilli and cross-laminated layers. These features can be formed as a result of explosive phreatomagmatic eruption when magma contacts with shallow groundwater.

A total of 27 thin sections were prepared from field investigation of LVF. Under the light microscopy, the volcanic ash particles are categorized into five types (Fig. 2): black non-vesicular (bnv), black vesicular (bv), clear non-vesicular (cnv), weathered (w), and free crystal (fc).

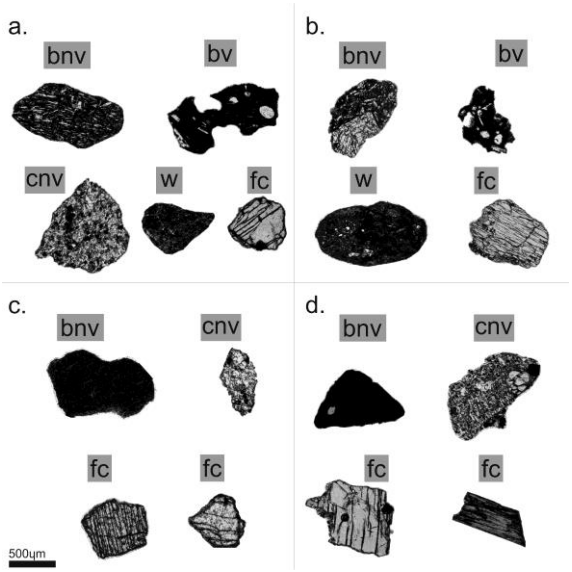

Figure 2 – Type of ash particles in LVF with comparable scale of 500μm (a. Ranu Pakis maar; b. Ranu Bedali maar; c. Ranu Yoso maar; d. Ranu Segaran maar).

Analysis of shape, morphology, and chemistry of volcanic ash particles (500 μm – 250 μm) from representative maar samples are still being conducted in order to obtain new insights about the

influence of magma degassing to phreatomagmatic eruption.

Acknowledgments

This research is financially support by the Ministry of Education, Culture, Sports, Science and Technology of Japan (MEXT) and Akita University, Japan.

References

Carn, S., A., 2000. The Lamongan volcanic field, East Java, Indonesia: physical volcanology, historic activity and hazards. Journal of Volcanology and Geothermal Research 95:81–108.

Kervyn, M., Ernst, G., G., J., Carracedo, J., -C., Jacobs, P., 2012. Geomorphometric variability of "monogenetic" volcanic cones: Evidence from Mauna Kea, Lanzarote and experimental cones. Geomorphology 136: 59–75.

Maria, A., Carey, S., 2002. Using fractal analysis to quantitatively characterize the shape of volcanic particles. Journal of Geophysical Research 107: ECV 7-1-ECV 7–17.

Maria, A., Carey, S., 2007. Quantitative discrimination of magma fragmentation and pyroclastic transport processes using the fractal spectrum technique. Journal of Volcanology and Geothermal Research 161(3):234–246.

Németh, K., 2010. Volcanic glass textures, shape characteristics and compositions of phreatomagmatic rock units from the Western Hungarian monogenetic volcanic fields and their implications for magma fragmentation. Central European Journal of Geosciences 2: 399–419.

Paulsen, T., S., Wilson, T., J., 2010. New criteria for systematic mapping and reliability assessment of monogenetic volcanic vent alignments and elongate volcanic vents for crustal stress analyses. Tectonophysics 482: 16–28.

Rausch, J., Grobéty, B., Vonlanthen, P., 2015. Eifel maars: Quantitative shape characterization of juvenile ash particles (Eifel Volcanic Field, Germany). Journal of Volcanology and Geothermal Research 291: 86–100.

Rodriguez-Gonzalez, A., Fernandez-Turiel, J., L., Perez-Torrado, F., J., Paris, R., Gimeno, D., Carracedo, J., C., Aulinas, M., 2012. Factors controlling the morphology of monogenetic basaltic volcanoes: The Holocene volcanism of Gran Canaria (Canary Islands, Spain). Geomorphology 136: 31–44.

Saucedo, R., Macías, J., L., Ocampo-Díaz, Y., Z., E., Gómez-Villa, W., Rivera-Olguín, E., Castro-Govea, R., Sánchez-Núñez, J., M., Layer, P., W., Torres Hernández, J., R., Carrasco-Núñez, G., 2017. Mixed magmatic–phreatomagmatic explosions during the formation of the Joya Honda maar, San Luis Potosí, Mexico. Geological Society, London, Special Publications 446: 255–279.

Smith, I., E., M., Németh, K., 2017. Source to surface model of monogenetic volcanism: a critical review. Geological Society, London, Special Publications 446: 1–28.

Soledad, M., V., Corina, R., 2019. El Pozo Volcanic Complex: Evolution of a group of maars, central Mendoza province, Argentina. Journal of Volcanology and Geothermal Research 371: 177–191.

Tongxin Volcano, from the onset of lava fountaining to phreatomagmatic directed blasts along a propagating fissure in an intramountain basin in Arxan-Chaihe Volcanic Field (ACVF), NE China

Boxin Li[1], Károly Németh[1], Julie Palmer[1], Alan Palmer[1], Jonathan Procter[1], Jing Wu[2]

[1]School of Agriculture and Environment, Massey University, Palmerston North, New Zealand; doomlee1216@hotmail.com
[2]Institute of Geology and Geophysics, Chinese Academy of Science

Keywords: monogenetic, intracontinental, phreatomagmatic.

Monogenetic volcanism in northeastern China has created phenomenal landscapes and preserves a range of spectacular features many with huge geological value, e.g. research, geoheritage, as well as tourism. However, the origins of the syn-eruptive and post-eruptive processes of these volcanic fields are still poorly known. Based on previous studies, the Arxan-Chaihe Volcanic Field (ACVF) formed in intracontinental settings within intramountain basins (Németh et al., 2017) with at least 45 vents covering an area of c.3000 km^2. The location is on the southwest flank of the Great Xing'an Range, bounded by a series of normal faults, believed to form a rifting shoulder of the Songliao Graben (Liu, 1989; Liu, 1993; Liu et al., 2001).

Tongxin Volcano is located in the northeastern corner of the ACVF. This location is suspected to be the eastern terminus of the field. The area of the ponded Tongxin lake is nearly 2 km^2 (Fig. 1). The ring-shaped mountain range surrounding Tongxin Lake is composed of Paleozoic and Mesozoic granitoid rocks with smaller amounts of greenish coloured metasediments. On the southern part of the range, mafic pyroclastic density current (PDC) deposits are seen covering basement rocks. Field relationships suggest a range of energetic phreatomagmatic blasts were involved in their formation. The Chaihe River, which flows from the west then veers south across the area, exposes lava flows in both banks of the river channel (Fig. 2). The lava flows cover the whole broad fluvial valley of Chaihe River and along its length from the northwest to the south is typified by columnar jointing and flow-shaped pahoehoe surface textures.

Fig. 1 – The Tongxin Volcano. The picture was taken from the eastern rim. The western rim capped by phreatomagmatic pyroclastic deposits.

Field work undertaken in September of 2018 and 2019 established the eruption history of the area and preliminary geological mapping of Tongxin Volcano. An area c.60 km^2 was mapped locating and recording key sites.

Fig. 2 – Lava flows are well exposed on the bank of the Chaihe River.

Well preserved PDC deposits related to typical phreatomagmatic eruptions are present on the western rim of the lake (Fig. 3).The deposits are predominantly interbedded coarse and fine units. The coarse layers are lapilli-rich units containing very angular shaped juvenile pyroclasts indicating phreatomagmatic fragmentation produced them. The PDC deposits are commonly horizontal and parallel bedded. The typical bedform characteristics are dune structures and cross-bedding. These two distinct features indicate transportation processes changed during deposition possibly caused by changes in local topography, vent migration or flow conditions (e.g. velocity, energy, particle concentration, moisture and temperature).

Fig. 3 – Dune and cross-bedding structures seen in PDC deposits on the western rim. The face of the section is more or less perpendicular to the flow direction. Tongxin crater is behind the image.

Lava spatter deposits are mapped on the NW side of the pyroclastic rim; they quickly thin laterally. Within the middle section of the spatter unit, highly vesicular, welded lava spatters formc.70-90 cm thick spatter lenses. Ac. 20-25 cm thick PDC deposit overlies the spatter unit. These two contrasting eruptive successions imply the eruption styles changed from magmatic fragmentation dominated by mostly lava fountaining events (dry phase) to phreatomagmatic explosive events (wet phase).

Pyroclastic deposits resting directly on pre-volcanic country rock were observed at two sites. The deposits clearly represent a nearly or even the first eruptive phase. Based on field observation, one site with unequivocal "*first*" eruption material is located on the southeastern side of the lake where a succession of interbedded coarse and fine layers overlie a relatively thin black, glassy bed about 25 cm thick. Below this glassy deposit, the country-rock crops out. Another site discovered with the first eruption deposits is nearly 13 km away from Tongxin Volcano, where interbedded PDC deposits, containing up to a 1.5 cm thick scoriaceous layer, is suspected to be a correlative of the spatter deposits from the proximal area. Perhaps the evidence of a dry eruption phase in the early stages.

Juvenile clasts predominate each PDC deposit. Country-rock debris and small quantities of crystals, e.g. olivine, pyroxene and hornblende, are the most common non-juvenile fragments. The features of deposits from proximal areas contain a range of very angular country-rock clasts with multiple grain sizes, consistent with the excavation processes occurring during an explosive eruption.

Proximal deposits are located on the top of the basement ridges to the west and east. Mapping on the northwest and southeast sides of the lake, from the inner side of the depression (lake basin and fluvial fan), suggest that PDC likely mantled the inner slopes of the crater wall.

The stratigraphic position of the lava flows covering the fluvial valley of the Chaihe River is ambiguous. They are not covered by any pyroclastic deposits from Tongxin despite their low-lying position in the landscape. Their proximity to the tephra ring suggests they might be younger than Tongxin crater. Alternatively, the lava flows are older than Tongxin and they have been partially covered by Tongxin eruptive product that has been subsequently eroded by the broad braided river system of the Chaihe River.

Geochronology of the region from previous research is loosely constrained (Liu, 1993; Liu et al., 2001). It is believed the ACVF formed during the late Pliocene to early Pleistocene. However, field observations suggest the erosional processes were very high intensity. Field relationships with post eruptive fan deposits, soil mantles and the fresh nature of the deposits suggest a young age for both the Tongxin eruptives and the lava flows. They may well be post Last Glacial Maximum (<20,000 years) in age. On-going work will attempt to constrain the age of both deposits.

Acknowledgements

The authors would like to thank gratefully the support provided by Massey University, Chinese Academy of Sciences, the China Science and Technology Exchange Center (CSTEC), and the China-New Zealand Scientist Exchange Program 2019, as well as their family.

References

Liu, J., 1989. On the origin and evolution of continental rift system in Northeast China. Chinese Journal of Geology, 3, 209–319.

Liu, J., 1993. The northeast China rift system and opening of the Japan sea: a volcano-chronological review. Sci. Geol. Sinica, 2(2), 157–162.

Liu, J., Han, J., & Fyfe, W. S., 2001. Cenozoic episodic volcanism and continental rifting in northeast China and possible link to Japan Sea development as revealed from K–Ar geochronology. Tectonophysics, 339(3-4), 385–401.

Németh, K., Wu, J., Sun, C., & Liu, J., 2017. Update on the Volcanic Geoheritage Values of the Pliocene to Quaternary Arxan–Chaihe Volcanic Field, Inner Mongolia, China. Geoheritage, 9(3), 279–297. doi:10.1007/s12371-017-0224-5.

Products of the Surtsey eruption in 2017 SUSTAIN drill core

Jocelyn McPhie[1], James DL White[2], Carolyn Gorny[3], Marie D Jackson[4], Magnús Gudmundsson[3], Samantha Couper[4]

[1]*School of Natural Sciences, University of Tasmania, Hobart, Tasmania, Australia. j.mcphie@utas.edu.au*
[2]*Geology Department, University of Otago, Dunedin 9016, New Zealand.*
[3]*Nordvulk, Institute of Earth Sciences, University of Iceland, Sturlugata 7, 101 Reykjavik, Iceland.*
[4]*Department of Geology and Geophysics, University of Utah, Salt Lake City, Utah, US.*

Keywords: Surtsey eruption, 2017 drill core, lapilli tuff.

Surtsey was created by submarine and then subaerial basaltic eruptions from 1963 to 1967 (Thórarinsson et al., 1964; Jakobsson and Moore, 1982). The eruptions began in sea water ~130 m deep, eventually building an island that grew to a height of 150 m above sea level. Two vents were active on Surtsey during the main subaerial activity (Fig. 1). Explosive eruptions began at Surtur in late 1963 and lasted for about 2.5 months. Explosive eruptions then began at a second vent, Surtungur, ~500 m to the northwest of Surtur. The explosive activity was driven by steam generated by the interaction between basaltic magma and seawater or a water-saturated slurry, and dominated by tephra jets and continuous uprush. Explosions at Surtungur stopped on 4 April 1964, when fountains and effusion of lavas began, eventually ending in May 1965. However, effusive activity resumed at Surtur in August 1966, and continued until the end of the eruption in June 1967.

In 1979, a vertical hole 181 m deep was drilled through the rim of Surtur (SE-01; Jakobsson and Moore, 1982, 1986), providing information on lithofacies, structure, alteration and temperature. In 2017, the Surtsey Underwater volcanic System for Thermophiles, Alteration processes and INnovative Concretes (SUSTAIN) project, sponsored partly by the International Continental Scientific Drilling Program, drilled three cored holes on Surtsey (Jackson et al., 2019). Two of the 2017 drill holes, SE-02a and SE-02b, are vertical and the third, SE-03, is inclined, plunging 55º to the west. The four drill hole collars, SE-01 (1979) and SE-02a, SE-02b, and SE-03 (2017), lie within a 10-m-wide area on the southeastern rim of Surtur (Figs 1, 2).

Variably altered lapilli tuff composed of vesicular basaltic lapilli and ash is the most abundant lithofacies (>95%) in the 2017 drill holes. Armoured lapilli are common in the sections above ~70 m depth but are difficult to identify at deeper levels where the lapilli tuff is more strongly altered. All of the lapilli tuff except the top ~20 m was erupted from Surtur during its 1963 to 1964 activity; the top ~20 m was erupted from Surtungur in 1964.

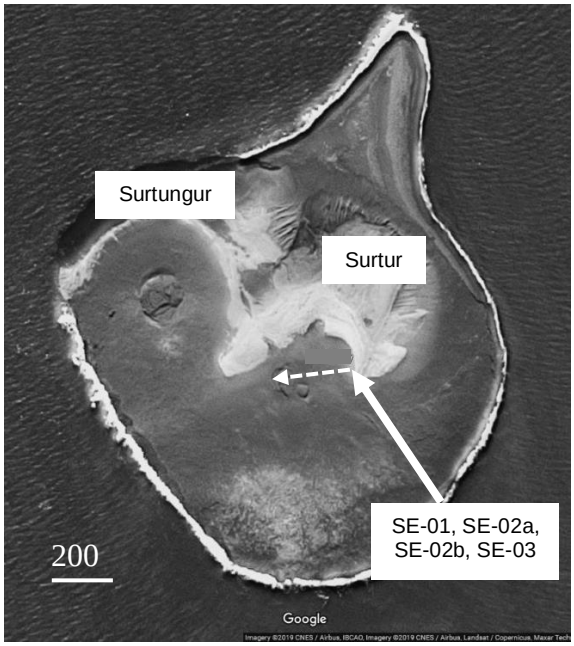

Fig. 1 - Surtsey showing Surtunger, Surtur and the location of the 1979 (SE-01) and 2017 (SE-02a, SE-02b, SE-03) drill hole collars. The white dashed line is the approximate trace of angled drill hole SE-03. Base from Google Maps.

The lapilli tuff consists of ash (<2 mm), vesicular lapilli, armoured lapilli, composite clasts, feldspar and olivine crystal fragments, and a variety of non-juvenile clasts. The composite clasts (lapilli and rare bombs) consist of vesicular tachylitic basalt and comprise multiple smaller vesicular clasts loosely held within a larger, less vesicular fragment. Composite clasts typically have highly irregular shapes and appear to be less altered than the enclosing lapilli tuff, typically retaining original porosity. Beds defined by grain size and color differences occur throughout the lapilli tuff sections but are more distinct in the less altered upper part above ~70 m, vertical depth.

Coherent basalt amounts to <4% of the drill sections and occurs in two narrow intervals in SE-02b, and in two narrow (<1.5 m) and one thick (~10 m) intervals in the angled drill hole, SE-03. The basalt is dark gray, vesicular, aphanitic, almost aphyric and magnetic; coarse tabular translucent feldspar crystals (3-10 mm) and olivine phenocrysts (1 mm) are present; subtle changes in vesicle abundance define subparallel bands. The contacts of the basalt intervals intersected by the drill holes are sharp and planar, implying that the basalt intervals are dykes that intruded the pyroclastic facies.

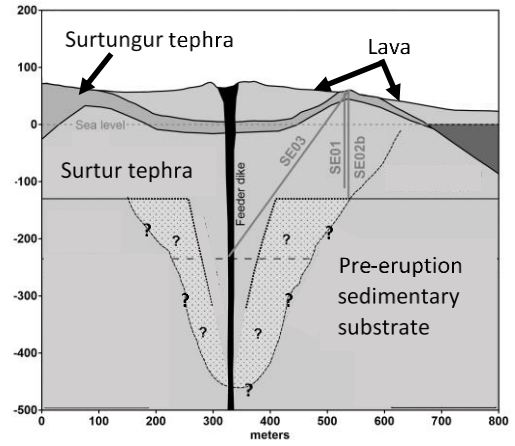

Fig. 2 – West-east cross-section through Surtur showing the positions of the four drill holes in relation to the major facies produced 1963-1967. Modified from Jackson et al. (2019).

When first deposited, the subaerial tephra on Surtsey was unconsolidated, unaltered and yellowish brown or gray. The color of the 2017 drill core varies among black, dark gray, dark greenish gray, brown, yellowish brown and pinkish brown, and all of it is altered and lithified. The contrast between the fresh, unconsolidated Surtsey tephra and the rock in the 2017 drill cores reflects the effects of alteration during the ~50 years since deposition.

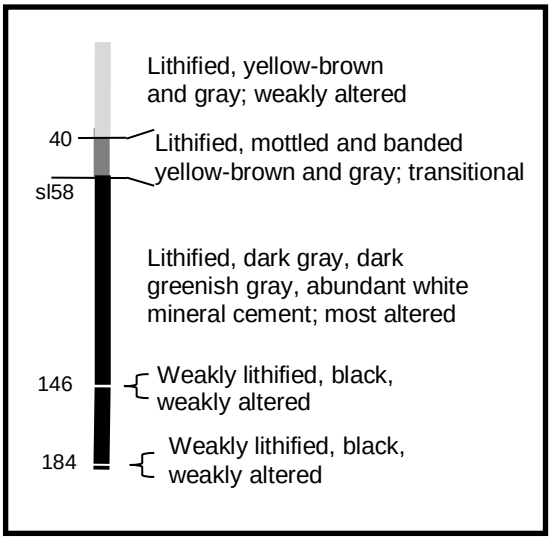

Fig. 3 - Macroscopic vertical variations in alteration intensity in the SE-02a – SE-02b vertical drill cores. sl, sea level.

In the vertical drill holes (SE-02a, SE-02b; Fig. 3), a weakly altered, lithified, brown or yellowish brown interval extends from the top to ~54 m depth. Minor white mineral cement is present and there are many examples of armoured lapilli. There is a gradation into progressively more-altered lapilli tuff with depth. From ~54 m to ~70 m, the vesicular basaltic lapilli are dull grayish black; white mineral cement infills or lines intraparticle pores. The interval from ~70 to ~182 m is the most altered; the lapilli tuff is dark gray or dark green, and white mineral cement is abundant. However, at 146 to 148 m and in the lowermost core (~182 to 185 m), there is an abrupt change to weakly altered, weakly lithified lapilli tuff. The entire section of lapilli tuff and armoured lapilli tuff in angled drill hole SE-03 is lithified and altered.

SE-03 was drilled to explore the crater- and conduit-fill of Surtur and perhaps help constrain the depth excavated into the pre-eruption sea floor by the 1963 to 1964 explosions. The section in SE-03 comprises texturally uniform, variably altered, lithified lapilli tuff for some 342 m of the total drilled length of ~354 m (97%). This continuous section of lithified lapilli tuff presumably originated as unconsolidated pyroclastic deposits that formed Surtur crater walls and that filled the crater and conduit. In such a proximal setting, it is likely that the section almost entirely comprises facies resedimented from unstable depositional sites and/or recycled through the vent perhaps multiple times.

Thick coherent basalt occurs just above the base of SE-03 (~342 to 352 m). At least two feeder dykes are evident in this interval. These dykes intruded the deepest part of the lapilli tuff section, consistent with the expectation that the end of this drill hole crossed Surtur's conduit.

The pre-Surtsey sea floor was ~130 m below sea level (Jakobsson and Moore, 1982) and underlain by volcanogenic sedimentary rocks (Alexandersson, 1968) (Fig. 2). The end of SE-03 reached ~100 m below the pre-eruption sea floor. However, no in situ sedimentary rocks were intersected implying that Surtur's explosions excavated the pre-eruption sea floor at the vent to minimum depth of ~100 m.

References

Alexandersson, T., 1968. The sedimentary xenoliths from Surtsey: Marine sediments lithified on the sea-floor. A Preliminary Report. Surtsey Research Progress Report 5: 83–89.

Jackson, M.D., Gudmundsson, M.T., Weisenberger, T.B., Rhodes, J.M., 38 others, 2019. SUSTAIN drilling at Surtsey volcano, Iceland, tracks hydrothermal and microbiological interactions in basalt 50 years after eruption. Scientific Drilling, 25: 35–46.

Jakobsson, S.P., Moore, J.G., 1982. The Surtsey research drilling project of 1979. Surtsey Research Progress Report 9: 76–93.

Jakobsson, S. P., Moore, J. G., 1986. Hydrothermal minerals and alteration rates at Surtsey volcano, Iceland. Geological Society of America Bulletin 97: 648–659.

Thórarinsson, S., Einarsson, Th., Sigvaldason, G.,Elísson, G., 1964. The submarine eruption off the Vestmann Islands 1963–64. Bulletin of Volcanology 29: 435–455.

Emplacement model of maar volcanoes in Altiplano-Puna (Northern, Chile)

Gabriel Ureta[1,2,3], Felipe Aguilera[1,3,4], Károly Németh[5]

[1]*Núcleo de Investigación en Riesgo Volcánico - Ckelar Volcanes, Universidad Católica del Norte, Av. Angamos 0610, Antofagasta, Chile.gabriel.ureta@ucn.cl*
[2]*Programa de Doctorado en Ciencias Mención Geología, Universidad Católica del Norte, Av. Angamos 0610, Antofagasta, Chile.*
[3]*Centro Nacional de Investigación para la Gestión Integrada del Riesgo de Desastres (CIGIDEN), Av. Vicuña Mackenna 4860, Santiago, Chile.*
[4] *Departamento de Ciencias Geológicas, Universidad Católica del Norte, Av. Angamos 0610, Antofagasta, Chile.*
[5]*VolcanicRiskSolutions, School of Agriculture and Environment, Massey University, Palmerston North, New Zealand.*

Keywords: phreatomagmatism, Central Andes Volcanic Zone, monogenetic volcanism.

Maar volcanoes are the result of externally driven fragmentation when the melt interacts with external water (e.g. seawater, water-saturated sediments, lakes, groundwater table, littoral cone or rootless cone). The direct interaction between magma and water is known as phreatomagmatic or taalian eruption, and forms one of the most common subaerial volcanic crater types of explosive volcanism such as the maar-diatremes.

The evidences of phreatomagmatism and the role of the water in the formation of maars have been proofed by many studies (e.g. White and Valentine, 2016 and references therein). These diagnostic criteria are the typical features described for the maar studies around the world and for the current models on the phreatomagmatic emplacement of maar-diatreme volcanoes in subaerial continental environments (Lorenz, 1985, 2003; Valentine and White, 2012). However, what happens when there are a lack of information or if on the deposits it may not be possible to find the typical features of models on the phreatomagmatic emplacement of maar-diatreme? Here we present an emplacement model of maar volcanoes from field observations such as lithology of maar deposits and features of erupted material, which will provide insights into eruptive mechanisms of maars based on link between magmatic explosive eruption-driven styles and maar forming eruption mechanism on maars from northern Chile.

Among of the maars in the northern Chile, Cerro Overo (Fig. 1) is the least silicic yet analyzed from this area with 52-54% SiO_2 wt., where rocks from Cerro Overo are characterized by the presence of olivine and clinopyroxene crystals. Its crater is468x583 m; depth reaches 72 m and an estimated eruptive volume of 0.0093 km^3, which is represented by two units. The first one is lying over the Tuyacto and Cajón Ignimbrites, which corresponds to a lava unit with fluid textures and breccia's fragments, whereas the second one is a pyroclastic deposit that is covering the lava unit. This unit is characterized by presence of scoriaceous fragments (ash and lapilli) that present a wide range of vesicularity, cooling crack, cauliflower textures, chilling border, and breccia fragments with juvenile material and lithic clasts.

Fig. 1 – Cerro Overo maar looking toward the NW.

Tilocálar volcanoes present a maar crater (Fig. 2) of 380x294 m, depth reaches 34 m and an erupted bulk volume of 0.0025 km^3. The syn-eruptive landscape level of this crater corresponds to the Tucúcaro Ignimbrite, which is covered by a pyroclastic deposit from Tilocálar Sur volcano (TCS), which is 55-62 % SiO_2 wt. Around the crater rim, lie individual rock fragments that correspond to scoriaceous material (ash and lapilli) with cauliflower texture, cooling crack and chilling border, and fragments from TCS pyroclastic deposit, Tucúcaro Ignimbrite, volcanic, sedimentary and granitic rocks (basement).

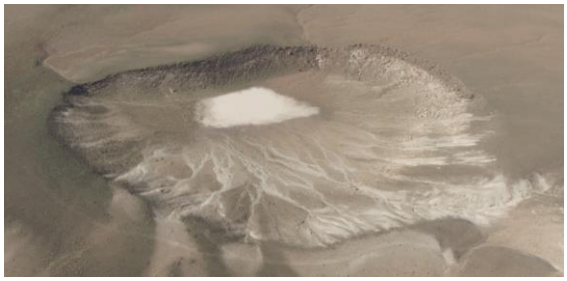

Fig. 2 – Tilocálar Sur maar with the pyroclastic deposit from Tilocálar Sur volcano (black and red color); looking toward the N.

A similar kind of deposit is observed and linked to the preserved deposit of Cerro Tujle (Fig. 3), which has an andesitic composition (56-58% SiO_2wt). The deposit is compound by the lower andesitic lava flow, which is emplaced over the Tucucaro Ignimbrite, and the upper pyroclastic deposit characterized mainly by lapilli and block/bomb fragments with dacitic to rhyolitic xenoliths. Breccia's fragments with lithic and juvenile clasts are also recognized. Cerro Tujle has

is an elliptical crater of 333x279 m and depth reaches 73 m. The crater's cavity presents a volume of the right circular cone of 0.002 km^3 with an estimated erupted bulk volume of 0.024 km^3.

Fig. 3 – Cerro Tujle maar looking toward the NW, where is possible to see the andesitic lava unit under the tephra ring.

On the other hand, Corral de Coquena(Fig. 4) is a felsic maar composed by rhyolite lava (72-74% SiO_2 wt.) emplaced over Pampa Chamaca Ignimbrite in La Pacana caldera. Covering this rhyolite lava is present a clastogenic and agglutinated andesitic lava. The crater cavity is 209 m deep (cut into the Pampa Chamaca Ignimbrite), 2.5x2.7 km diameter sediment filled crater, and with an erupted bulk volume of $4.0468x10^{-10}$ km^3.

Fig. 4 – Corral de Coquena maar looking toward the N. The clastogenic and agglutinate lava (dark color) is covering the rhyolite lava (white-brown color).

The examples from northern Chile show: a preserved crater that cut into the pre-eruptive landscape (maar), a surrounding pyroclastic deposit (tephra ring), a continuous deposit sequences of lavas and scorias (short timescale), lapilli fragments and breccias, a single volcanic structure, a simple conduit system (plumbing), a small volume of erupted magma (< 1 km^3), different magma compositions (from basaltic andesite to rhyolite) and, a host rock mainly composed mainly by ignimbrites with the permeability required to confining water layers.

Recently some studies (e.g. Berghuijs and Mattson, 2013; Jordan et al., 2013) argues that the maar volcanoes can be produced by the effects of magmatic gases that excavate a vent, followed by continued upward streaming of gas (violent release of CO_2 probably of mantle origin) through vent-filling debris and may not necessarily by a magma-water interaction (dry-maar). According our data there are some features from these maars cannot support the idea of a magma that initially carried a large amount of volatiles, which must have largely been released or exsolved upon ascent due to decompression and adiabatic cooling generating an explosive condition with the enough energy to produce a crater at least 600 m of diameter. These features are the thickness of the crust (67 km), degree of magma composition which is related to the volatile contents (basaltic andesite to rhyolite), number and amount of mineral that can contain wt.% water to support crystal growth in a volatile-rich environment (lack of phlogopite and range of Mg#), and volume of magma batch (< 1 km^3).

Despite of the absence of evidences of a typical magma-water interaction such as surge levels, cross-bedded tuffs and lapilli tuffs, abundant clasts emplaced from ballistic trajectories and the other features described in Lorenz (1985), and White and Valentine (2016), we suggest that each maar must have erupted in at least two stages. The first stage is an ephemeral magmatic condition where the magma may ascend and feed intrusions, which does not interact with water in the conduit and explode reaching the surface to erupt lava. The second stage is an explosive condition by magma-water interaction at various depths along feeder dike, forming a crater, tephra ring (such as ash and lapilli fragments that present a great range of vesicularity, cooling crack, cauliflower textures, chilling border, and breccia fragments with juvenile material and lithic clasts) and domains of brecciated country rock in the subsurface.

Acknowledgements

We thank to Comisión Nacional de Investigación Científica y Tecnología (CONICYT) for the GU Doctoral Grant "Becas de Doctorado Nacional CONICYT - PCHA / Doctorado Nacional / 2016-21161286", which allows funding this research.

References

Berghuijs, J. F., Mattsson, H. B., 2013. Magma ascent, fragmentation and depositional characteristics of "dry" maar volcanoes: similarities with vent-facies kimberlite deposits. Journal of Volcanology and Geothermal Research, 252, 53–72.

Jordan, S. C., Cas, R. A. F., Hayman, P. C., 2013. The origin of a large (> 3 km) maar volcano by coalescence of multiple shallow craters: Lake Purrumbete maar, southeastern Australia. Journal of Volcanology and Geothermal Research, 254, 5–22.

Lorenz, V., 1985. Maars and diatrems of phreatomagmatic origin: a review. Trans. Geol. Soc. S. Afr., 88, 459–470.

Lorenz, V., 2003. Maar-diatreme volcanoes, their formation, and their setting in hard-rock or soft-rock environments. Geolines, 15, 72–83.

Valentine, G. A., White, J. D., 2012. Revised conceptual model for maar-diatremes: Subsurface processes, energetics, and eruptive products. Geology. 40. 1111–1114.

White, J. D., Valentine, G. A., 2016. Magmatic versus phreatomagmatic fragmentation: absence of evidence is not evidence of absence. Geosphere, 12(5), 1478–14.

Session 3. Monogenetic volcanoes: eruption dynamics, magma plumbing systems, structure, physical and petrological modeling

This session invited scientific contributions about eruption dynamics of monogenetic volcanoes, their internal structure, and the physical and petrological modelling of its magma plumbing system.

Small-scale basaltic volcanic systems are the most widespread forms of magmatism on the planet and are expressed at the Earth's surface as fields of small volcanoes which are the landforms resulting from explosive and effusive processes triggered by the rise of small batches of magma. This session concerned with the growth, geomorphology, eruption dynamics, geodynamic distribution and degradation of this type of volcanism. Monogenetic volcanoes distribution inside a volcanic field depends in each case on their regional and local tectonic controls. The great variety of eruptive styles, edifice morphologies, and deposits shown by monogenetic volcanoes are the result of a complex combination of internal (magma composition, gas content, magma rheology, magma volume, etc.) and external (regional and local stress fields, stratigraphic and rheological contrasts of substrate rock, hydrogeology, etc.) parameters, during the magma transport from the source region to the surface. This meant to be a multi-disciplinary session and we invited contributions that include different type of methods, such as; field studies, geophysical methods, numerical and analogue modeling of volcanic processes, GIS analysis, and petrological studies focused on its magma plumbing system and eruption dynamics.

Origin of monogenetic volcanoes in Malko-Petropavlovsk zone of the transverse dislocation (Kamchatka): geological setting, geophysical parameters and geochemical data

Olga Bergal-Kuvikas[1,2,3], Anna Skorkina[4], Ilya Bindeman[3,5], Olga Khubaeva[1]

[1] *Institute of Volcanology and Seismology FEB RAS, Petropavlovsk-Kamchatsky 683006, Russia*
olgakuvikas@gmail.com
[2]*Institute of Geology of Ore Deposits, Petrography, Mineralogy and Geochemistry RAS, Moscow, 119017, Russia*
[3]*Fersman Mineralogical Museum, Moscow, 115162, Russia*
[4]*Institute of Earthquake Prediction Theory and Mathematical Geophysics RAS, Moscow, 117997, Russia*
[5]*Dept. of Earth Sciences, 1272 University of Oregon, Eugene, OR 97403, USA*

Keywords: monogenetic volcanoes, Malko-Petropavlovsk zone of the transverse dislocation, Kamchatka

Geodynamic setting of Kamchatka has a complicated structure and was formed by the accretion of various aged terrains on north from the Malko-Petropavlovsk zone of transverse dislocations (MPZD) and a long-lived volcanic arc in southern Kamchatka (Lander and Shapiro, 2007). MPZD is located on trajectory of deep transform fault (Seliverstov, 2009) and can be considered as a boundary between various aged slabs and generated volcanic belts on Eastern volcanic belt, Sredinny Range and southern Kamchatka (Fig. 1).

On the Earth's surface MPDZ detected by numerous regional faults, which are orthogonal to the present location of subduction zone (Geological map, 2000) (Fig. 1b). Geophysical researches using the earthquake converted-wave method and magnetotelluric sounding suggest for fragmentations of the crust and intrusions of magmatic bodies in various depths inside the MPDZ (Nurmukhamedov, Sidorov, 2019).

Complex geological structure of Kamchatka region can be seen also from seismic recordings. Firstly, operating seismic stations can be divided into three groups considering the frequency content of its waveforms (Gusev, Skorkina, 2020) on “southern”, “northern” stations and Bering (BKI), with a boundary within Russkaya-Nalychevo (RUS-NLC) stations. Another feature which can be seen from seismic data is a shift of the third corner frequency. Source spectra for earthquakes of Kamchatka region are known to have a complex shape which in the broad frequency range fits best the three-corners source spectra model (Skorkina, Gusev, 2017). It was found that for subduction earthquakes of 2011–2014 with $K_S = 10–12$ registered between 52–54°N the shift of third corner frequency can be observed from 7 Hz around 54°N to 4.5 Hz around 52°N. The origin of this shift should be studied further because there are two controversial hypotheses: it can be either a source effect or propagation effect. However, in both cases it indicates the complex geological media.

Geological and geochemical studies of magmatic complexes in MPDZ give a unique chance to investigate genesis of their formations and evolution throw the time. The oldest rocks (>38 Ma) in MPDZ are pillow lavas with basaltic-andesitic compositions in north-west edging of Avacha bay (Fig. 1). The next stage of magmatic evolution are magmatic rocks, e.g. lava flows, extrusive domes, which were formed 14.4–11.5 Ma. Large caldera-forming eruption were active since 5.1–1.6 Ma, e.g. the Karymshina caldera (Leonov and Rogozin, 2007) and Verhneavachinskaya caldera (Bergal-Kuvikas et al, 2019). In Pleistocene-Holocene time magmatic activities presented by stratovolcanoes and monogenic cinder cones. Locations of stratovolcanoes controlled by slab and situated on 213–230 km from the trench. Whereas locations of monogenic volcanoes are independent from the slab and localized on 197– 233 km from the trench (Fig. 1). Monogenetic volcanoes represented by numerous basaltic andesitic cinder cones in the valley of Paratunka river, coastline of Pacific ocean and extrusive andesitic domes in north edging of Avacha bay (Fig. 1).

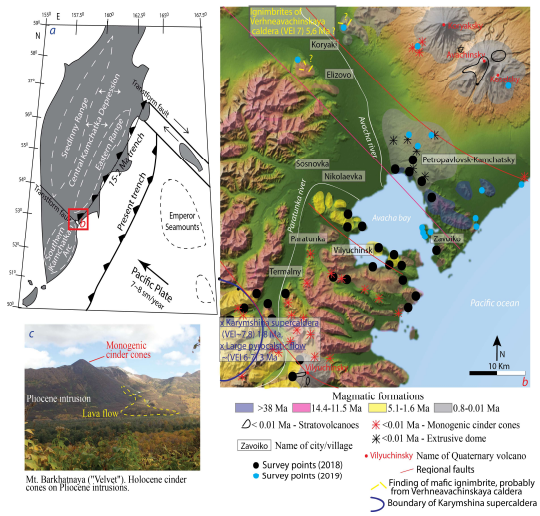

Mt. Barkhatnaya ("Velvet"). Holocene cinder cones on Pliocene intrusions.

Fig. 1. (a) General tectonic setting of Kamchatka, (b) Geological formations of MPZD according to Geological map (2000) in survey points, (c) Monogenic cinder cone in MPZD.

Compositions of magmatic rocks in MPDZ vary from basalts to rhyolites (47–76 wt.% SiO_2). Large caldera-forming eruptions of the Karymshina caldera have more acid compositions (>60 wt.% SiO_2), at

the same time with acid intrusions in the valley of Paratunka river. Most mafic, low alkali magma (50–53 wt. % SiO_2, 6.5–7.7 wt.% MgO, 0.8–0.9 wt.% K_2O) belong to monogenic cinder cones in the valley of Paratunka river, near the Vilyuchinsky volcano. Monogenic cinder cones were formed during two stages of activities: 7000–10000 BP and 2000–4000 BP (Dirksen, 2009). Localizations of monogenic cinder cones were controlled by deep regional faults (Florensky and Bazanova, 1989; Sheimovich and Patoka, 2000). Extrusive domes (e.g. Mishennaya Mount) in north edging of Avacha bay characterized by hornblende bearing andesites. They are localized on thick sedimentary deposits in basement and consequently more fractionated in comparing with monogenic cinder cones in valley of Paratunka river.

Preliminary results of seismic data analyses and morphological structures on the Earth surface enable identify deep dislocation zone (e.g. deep regional faults) in MPDZ. They have control localizations of monogenic volcanism. Magma compositions of monogenic volcanoes are more mafic and low alkali in comparing with other various aged magmatic formations in MPZD. The effect of crystal process (e.g. assimilation, fractional crystallization) is suggested to be a minimum in comparing with other magmatic formations in MPDZ.

Acknowledgements

We are gratefully thanking grant N14.W03.31.0033 from the Russian Ministry of Education and Science of the Russian Federation for support field works and grant 19-17-00241 of Russian Science Foundation for analytical measurements.

References

Bergal-Kuvikas, O.V., Leonov, V.L., Rogozin, A.N., Bindeman, I.N., Kliapitskiy, E.S., Churikova, T.G., 2019. Stratigraphy, structure and geology of late Miocene Verkhneavachinskaya caldera with basaltic-andesitic ignimbrites at Eastern Kamchatka. Journal of geosciences, 4 (accepted).

Dirksen, O.V., 2009. Late Quaternary areal volcanism of Kamchatka (structural positions, geological and geomorhological effects and spatial variations). Dissertation of PhD thesis. Sankt-Petersburg University. P.172 (in Russian).

Florensky, I.V., Bazanova, L.I., 1989. Volcanism during cenozoic time in South-East of Kamchatka (Beregovoy ridge). Volcanology and seismology, 6, 30–41 (in Russian).

Geological map of Russian Federation, 2000. Scale 1:200 000. Issue Sothern Kamchatka. Lists N-57-XXVII, N-57-XXXIII. Moscow, 302 (in Russian).

Gusev, A.A., Skorkina, A.A., 2020. Site responses in Kamchatka from records at strong-motion seismic stations. Russian Geology and Geophysics, 61(2), 224–233.

Lander, A. V., Shapiro, M. N., 2007. The origin of the modern Kamchatka subduction zone. Washington DC American Geophysical Union Geophysical Monograph Series, 172, 57–64.

Leonov, V. L., Rogozin, A. N., 2007. Karymshina, a giant supervolcano caldera in Kamchatka: Boundaries, structure, volume of pyroclastics. Journal of Volcanology and Seismology, 1(5), 296–309.

Nurmukhamedov, A. G., Sidorov, M. D., 2019. Deep structure and geothermal potential along the regional profile set from Opala Mountain to Vakhil'River (Southern Kamchatka). In IOP Conference Series: Earth and Environmental Science, 249, 1, 012041

Seliverstov, N. I., 2009. Geodynamics of the Junction Zone of the Kuril–Kamchatka and Aleutian Island Arc. Petropavlovsk-Kamchatsky: KamGU, 191 (in Russian).

Sheimovich, V.S., Patoka, M.G., 2000. Geological setting of zones with active Cenozoic volcanism. Moscow: Geos, 208 (in Russian).

Skorkina, A.A., Gusev, A.A., 2017. Determination of corner frequencies of source spectra for subduction earthquakes in Avacha Gulf (Kamchatka). Russian Geology and Geophysics, 58(7), 844–854.

Imagery of fluid circulation and inner structure of Parícutin volcano (Mexico) by self-potential data, temperature measurements, and 3D resistivity model

Xavier Bolós[1], Alexander Delgado-Torres[1, 2], José Luis Macias[1], Gerardo Cifuentes[1], Mario Boijseauneau[1, 2], David Salguero[2]

[1] Institute of Geophysics, UNAM, Campus Morelia, 58190 Morelia, Michoacán, Mexico. xavier.bolos@gmail.com
[2] Escuela Nacional de EstudiosSuperiores, UNAM, Campus Morelia, 58190 Morelia Michoacán, Mexico.

Keywords: Parícutin, geophysical surveys, monogenetic structure.

Parícutin eruption is one of the most well-known examples of monogenetic volcanism worldwide. This volcano is the youngest edifice of the Michoacan-Guanajuato volcanic field (MGVF), which is located in the west-central sector of the Trans-Mexican Volcanic Belt (Fig. 1).

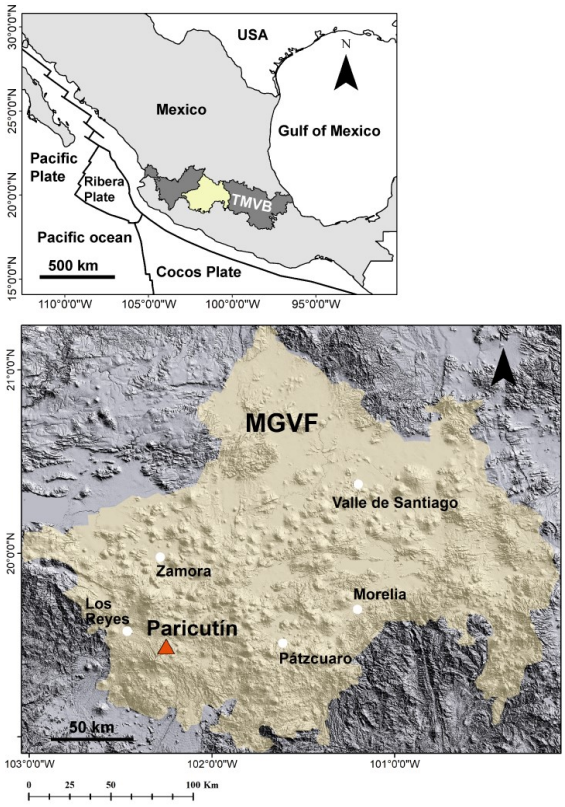

Fig. 1 – Digital elevation model of the Michoacán-Guanajuato Volcanic Field (MGVF, yellow area) showing the location of Parícutin volcano (red triangle), and the main towns (white dots). Inset map at the upper shows the location of the MGVF within the Trans-Mexican Volcanic Belt (TMVB).

MGVF has an area of about ~40,000 km^2 that contains the largest concentration of monogenetic vents on Earth associated with a subduction-related continental arc, holding more than 1,500 edifices consisting of abundant scoria cones, semi-shield volcanoes with large effusive magma volumes, tens of lava domes, several maars, tuff rings and spatters (Hasenaka and Carmichael, 1985). Interesting enough the Parícutin and Tacámbaro area (80 km southeast of Parícutin) holds the highest density of Quaternary scoria cones in the whole MGVF (11 to 14 cones/100 km^2, respectively) (Hasenaka and Carmichael, 1985).

Parícutin eruption began on February 20, 1943, and ended on March 4, 1952, producing a volume of ~ 2 km^3 that included effusive, Strombolian and violent Strombolian phases (Pioli et al., 2008). This volcano started to develop in the middle of a cornfield become an iconic monogenetic volcano in the world. Its eruption dynamics and magma composition have been described in numerous papers using the detailed accounts of the local people, visitors, and scientists who witnessed the eruption from the early beginning to its end. In this way, we know that the volcano began with a fissural eruption, with the emission of pyroclasts, ashes, and gases. The main cone grew rapidly with a very intense explosive activity, reaching ~ 150 m high at the end of the first month, from a total of ~ 280 m high (Fries, 1953). The eruption produced most of the pyroclastic material involved in the construction of the cone during its first three years (~75% of total eruption volume) (Fries, 1953). The formation of lava flows occurred in parallel to the explosive activity during the nine years of eruption, taking place at different emitting points along the eruptive fissure (Luhr and Simkin, 1993). The fall of ash and especially the lava flows were the main causes of the destruction of two populations: Parícutin-Combutzio and San Juan Parangaricutiro.

This work focuses on the study of the internal structure and the sub-surface fluid circulation of the Parícutin main cone, from geophysical prospecting methods. The most important variation in the physical properties of rocks, besides the flow temperature in the hydrothermal system, is the change in their electrical conductivity. An increase of the temperature produces an increment of the ionic mobility and therefore an increase in the electrical conductivity (Lachenbruch, 1971). In order to study the electrical conductivity in the Parícutin main edifice, self-potential surveys combined with surface temperature measurements were successfully applied (Fig. 2). This allowed us to identify the main infiltration and ascent zones of hydrothermal fluids under the volcano, as well as the specific surface temperature crossing the fumarolic areas. In addition, electrical resistivity tomography (ERT)

measurements were performed using a non-conventional array in order to get profiles with any geometry. We applied this methodology for the first time in volcanology in order to assess the internal structure of the Parícutin cone, and the role of the basement in the region attempting to understand the geometry of the feeder dike, which until now lacked any detailed geophysical data. ERT is presented in a 3D resistivity model showing high resistivity values inferred as proximal Spatter facies and welded pyroclasts aligned in the same direction of the described eruptive fissure (Fig. 2).

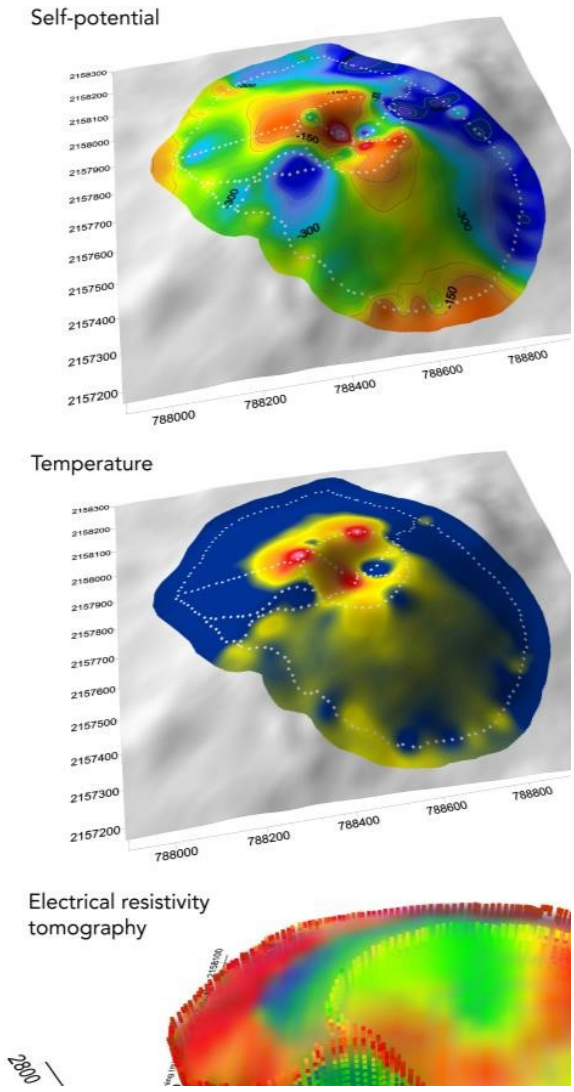

Fig. 2 – Self-potential map, temperature map, and 3D resistivity model of the Parícutin cone with its topography. White dots represent the measure points. Note the correspondence of the temperature, and self-potential anomalies with the low values of resistivitiy reaching the surface, as well as, the interpolation of the high resistivity values on the crater showing the orientation of the feeder dike.

At depth, we infer this zone of low conductivity as the feeder dike, were high-temperature fumaroles appear at the surface around them but not in the middle. Therefore, hydrothermal fluids rise to the surface through the non-consolidated pyroclastic deposits of the cone that are the most permeable zone. Parícutin presents normal faults produced by the overburden of pyroclastic materials deposited during the eruption. The SP data suggest that these faults in the non-consolidated pyroclasts constitute the main pathways whereby hydrothermal fluids rise to the surface, generating visible hydrothermal alteration zones.

In conclusion, the combination of SP, temperature, and 3D ERT data provides enough accuracy to detect meter-sized convective zones in which up and downflow circulation occurs in the hydrothermal system, moreover, it allows us to infer the feeder dike and its geometry beneath the volcano. The results obtained in this study will help to understand the inner structure of other monogenetic volcanoes of similar characteristics lacking direct observations of its eruption, but with possibilities to apply geophysical surveys.

Acknowledgements

Funding for this research was provided by Fronteras de la Ciencia project: 2016-01-2406 of CONACyT to J.L. Macías. X. Bolós was funded by a UNAM-DGAPA postdoctoral fellowship (2016–2018). We are also grateful to Víctor Del Angel and the students of ENES-UNAM for their collaboration during the field campaign.

References

Fries Jr., C., 1953. Volumes and weights of pyroclastic material, lava, and water erupted by Parícutin volcano, Michoacán. EOS Trans. Am. Geophys. Union 34, 603–616.

Hasenaka, T., Carmichael, I.S.E., 1985. A compilation of location, size, and geomorphological parameters of volcanoes of the Michoacan–Guanajuato volcanic field, central Mexico. Geofis. Int. 24, 577–607.

Lachenbruch. A. H., 1971. Vertical gradients of heat production in the continental crust, 1. Theoretical detectability from near-surface measurements. J. Geophys. Res., 76:3842-3851.

Luhr, J.F., & Simkin, T., 1993. Paricutín: The Volcano Born in a Mexican Cornfield. Geoscience Press, Inc., Phoenix, Arizona. 427.

Pioli, L., et al., 2008. Explosive dynamics of violent Strombolian eruptions: the eruption of Parícutin Volcano 1943–1952 (Mexico). Earth Planet. Sci. Lett. 271, 359–368.

The structure and geomorphology of Salton Sea-type Miocene mud calderas, northern Gulf (Kuwait)

Michael J Duane[1]

[1] *Department of Earth & Environmental Sciences, Kuwait University, PO Box 5969, Safat 13060, Kuwait.*
phytokarst@gmail.com

Keywords:mud, volcanoes, caldera.

The results of a survey of sulphate-siliciclastic mud pots in the Middle Miocene rocks of the Subiya mud volcano complex (Kuwait; Fig. 1), are recorded. Pot loci, and related geothermal structures are described, and were found to cluster along a northwest-trending line that is indicative of a Zagros-induced strike-slip fault. The small-scale (<50 m) structure and geomorphology of these calderas (Fig. 2) consists of passive venting and expulsion of water, mud and gas from pools, and small cones, by seismically-induced collapse (Fig. 3). The mud pools are considered products of subaerial expulsion into a shallow terrestrial vent linked by subsurface evaporitic/siliciclastic chambers. Geomorphological surveys recognized several different classes of landforms that include ground deformations, alluvium, and conjugate fractures. The larger mud pools appear to have subsided due to chamber withdrawal and subsidence of the calderas, and accounts for the lack levee deposits on the rim of the craters. They are remarkably similar to the Salton Sea mud pots.

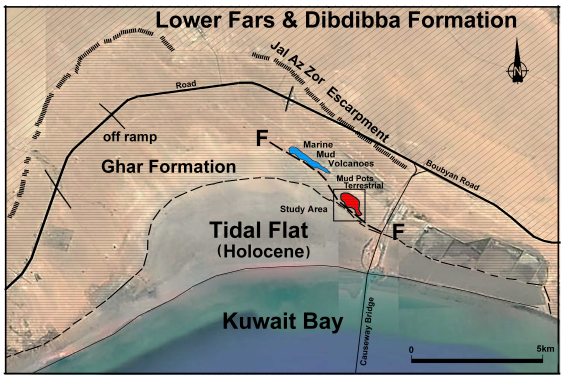

Fig. 1 – Location of Miocene mud volcanoes and mud pots (Kuwait).

The evaporitic-sandy nature of the eruptions are clearly visible as planed off vents with subdued topography (Fig. 2-3). The method of model assemblage was to map the structures by drone and geographically insert the geological structures on a Google plan map.

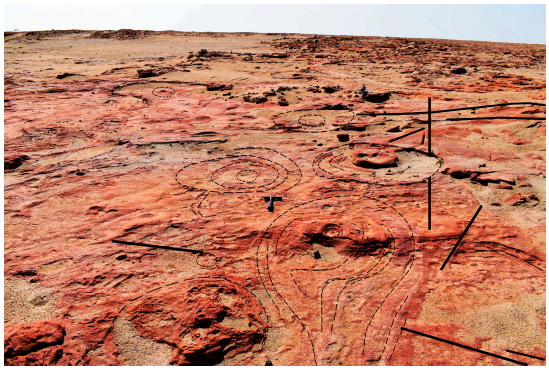

Fig.2 – Interpretation of surface features. Crater diameters are indicated by geological hammer for scale.

The original annular ring structures at the surface of undisturbed vents have been modified by internal collapse (Fig. 3) of the feeder bodies, which are analagous to nuclear explosion-induced stress of layered media (Fig. 4).

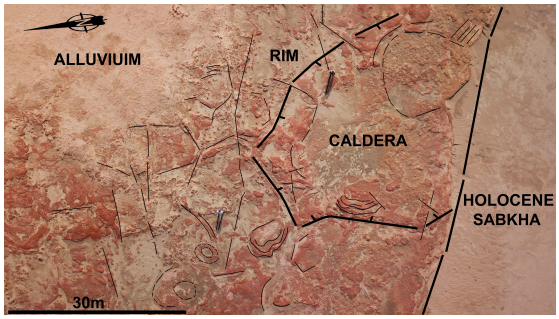

Fig.3 – Aerial structural interpretation of a single caldera.

The analogue model by Howard (1969) best fits the surface features manifested by subaerial collapse.

It is concluded that the Subiya Mud volcano complex in Kuwait hosts a variety of site-specific mud pools that are common to terrestrial sites worldwide. The unique Mid-Miocene eruptions are suggestive of a mixed low- to high-viscosity evaporite-bearing sandy mud emitting micro-breccias that are closely connected to the landward side of a proactive fault (The Subiya Fault). The concentric structural zoning in collapse structures varying from symmetric in box models to Kuwait trapdoor floor morphology suggests analogous subsurface fault geometries, and chamber withdrawal mechanisms.

The mud pools are a result of overpressured fluids below the edifice which are suddenly withdrawn by reservoir evacuation and produced a pressure differential between the fluids in the fractures and the fluids in the sedimentary column. This will exceed the minimum principal stress field,

causing dilation and passive fluid flow through the fractures (Jolly & Lonergan, 2002; Howard, 2010). The fact that the MP structures lie within a prolonged seismic zone (Zagros Belt), makes them ideal candidates for further studies on the interaction between seep activity and seismic fracturing. They are Miocene analogues to the present-day Salton Sea mud pools.

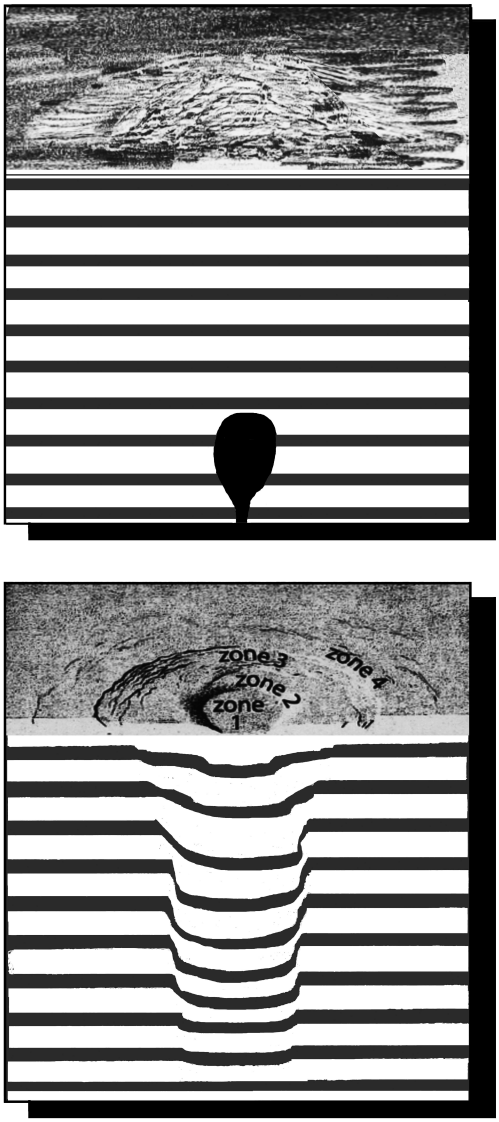

Fig. 4 – Analogue model of Howard (2010) applied to caldera collapse in Miocene rocks of Kuwait.

References

Duane, M.J., Reinink-Smith, L., Eastoe, C., Al-Mishwat, A.T., 2015. Mud volcanoes and evaporite seismites in a tidal flat of northern Kuwait – implications for fluid flow in sabkhas of the Persian (Arabian) Gulf.GeoMarine Letters 35: 237–246.

Howard. K.A., 2010. Caldera collapse: Perspectives from comparing Galapagos volcanoes, nuclear-test sinks, sandbox models, and volcanoes on Mars. GSA Today 20; 4–10.

Jolly, R.J.H., Lonergan, L., 2002. Mechanisms and controls on the formation of sand intrusions. Journal of Geological Society, London 159: 605–617.

Volcanological evolution of the maar of Lechminen'Aït el Haj (Middle Atlas, Morroco)

Sara Mountaj[1], Toufik Remmal[1], Samira Makhoukhi[1], Benjamin Van Wyk De Vries[2]

[1] *Faculty of Sciences AïnChok. Université Hassan II Casablanca Morocco.* sara.mountaj@gmail.com
[2]*Laboratoire Magmas etVolcans, UMR6524 CNRS, Observatory of Globe Physics of Clermont, Université Blaise Pascal - Clermont-Ferrand II. France.*

Keywords: Maar, Karst, Lechmine n'Aït el Haj.

Monogenetic volcanoes are the most common type of subaerial volcanoes (Tchamabé et al., 2016). They result from a single volcanic eruption or several volcanic eruptions that have occurred in a short period of time, not exceeding a few days. The eruptions are usually provoked by the intrusion of small amounts of magma (Németh, 2010; Walker et al., 2000). Among monogenetic volcanoes, those of phreatomagmatic type, resulting from the interaction between the ascending magma and superficial water, lead to the formation of a «maar». The Lechmine n'Aït el Haj maar (LNH) located in the Middle Atlas, Morocco (33°22'50"N,5°04'15"O), is an excellent example of this type of monogenetic volcano.

This work aims to investigate the volcanic mechanism of the Lechmine n'Aït el Haj maar based on tephrostratigraphy, in order to improve the knowledge about the evolution of tephra ring around LNH. The geochemical, mineralogical, and petrographic features constrain the origin and type of magma.

The LNH environment is characterized by outcrops of the Liasic limestone substrate mostly in the NW. The latter records intense fracturing. Locally, in the northwestern flank, 1.5 m of lacustrine deposits are at the base of the pyroclastic deposits (Mountaj et al., 2014). Based on stratification criteria and deposition, transport and fragmentation mechanisms, five main units were distinguished. The first two units, U1 and U2, consist of beds of lapilli tuff, composed of juvenile clasts and accidental lithics and a small proportion of xenoliths. These elements are cemented by fine volcanic ash. The distinction between the three units is based on the observation of the distribution, the size, the shape and the proportion of accidental lithics and juvenile clasts.

This variation depends on the intensity of the explosion, the water/magma ratio and the location of the eruptive vent. The passage towards the third unit (U3) is branded with a figure of mud cracks. U3 consist on massive breccia tuffs. It contains scoria, lava blocks and volcanic bombs, forming a kind of lava breccia rich in of peridotites and pyroxenites xenoliths. This unit is devoid of accidental lithics. The upper and last unit (U4) is represented by thin level of lapilli tuff, located mostly in the SE flank, with few outcrops in the NW. The southern side of the crater is covered by massive lava flow.

The LNH mafic lavas show a fluidal microlitic texture. The phenocrysts are mostly composed of clinopyroxene and olivine (fig. 1). Mineralogical analysis allows classifying the clinopyroxenes using the ternary diagram enstatite/wollastonite/ferrosilite (Morimoto, 1989); they plot generally in the augite-diopside field. Olivines show a resorbed texture due to their destabilization or rapid cristallisation. Olivine (Fo_{74-87}) also show a forsterite composition. Major elements data were obtained on 14 samples**.** The LNH rocks are very similar in composition, and have comparable ranges of major and trace element concentrations. The chemical analyzes show that the mafic samples display low silica content 38.5-40.8 wt %, and very high concentrations of Ni and Cr (220 - 318 ppm and 330 - 451 ppm, respectively). The TiO_2 vary from 2.87 to 3.12 %, MgO from 11.45 to 11.16 % and Mg# from 40.62 to 45.42. Those values reflect the primitive character of the magma.

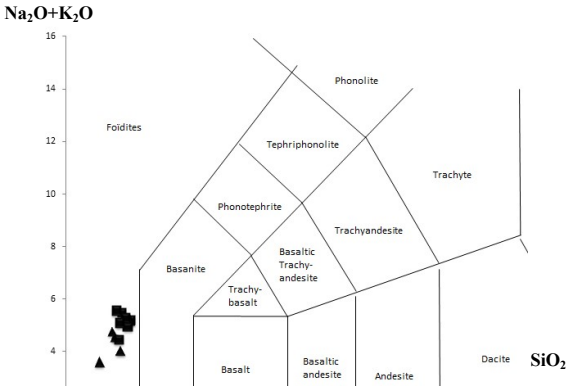

Fig. 4: TAS plot for the LNH lavas (Bas et al., 1986)

The pyroclastic deposits are influenced by the conditions of the eruption, namely the water/magma ratio (Fisher and Schmincke, 1984). In LNH, the first burst was caused by the arrival of ascending magma into water from a pre-existing lake highlighted by the lacustrine deposits; this generated a strong phreatomagmatic first explosion, and consequently the birth of the LNH maar (Lorenz, 2003; White and Ross, 2011; Wohletz and Sheridan, 1983) (fig. 2). The tephrostratigraphic study allowed to reconstructing the evolution of the maar. The units U1 and U, are composed of lapilli tuff; and are inherent of phreatomagmatic activity (presence of

lake water). The intensity of every explosion depends on the water/magma ratio. Toward the summit of the second unit (U2), the proportion of accidental lithics decreases inversely to the juvenile clasts, which become very abundant, mean that the volume of water also decreased until it dried. This is attested by the structures of mud cracks at the top of U2. At this stage the dynamic of eruption changed from a phreatomagmatic to a Strombolian one, and the formation of the third unit of breccia tuff. Meanwhile, a lava flow came from the plateau of the Middle Atlas and poured into the LNH crater from the south. A second transition of the eruptive occurs at the forth unit (U4), which consists of lapilli tuff; the ascending magma met water again and provoked the final phreatomagmatic explosion.

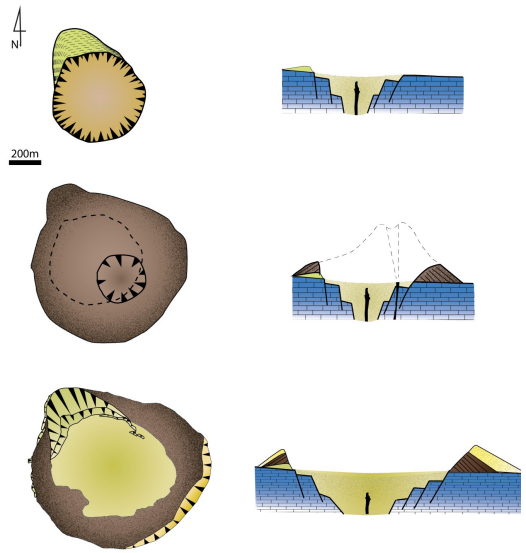

Fig. 1 –Volcanogenic reconstruction of the maar of Lachemine n'Aït el Haj.

The mafic lavas of LNH are basanites. They derived from a primary magma that is near primary. The phenocrysts of LNH lavas consist of olivine and diopside. The enrichment of incompatible element (Ni, Cr) suggests a low degree of partial melting (2%) of a mantle source located at 65 km deep (2 GPa) (Bosch et al., 2014). This depth corresponds to the lithosphere-asthenosphere boundary under the Middle Atlas (60-80 km) (Bosch et al., 2014).

This study presents the first detailed volcanological stratigraphy of tephra composing the maar of Lechmine n'Aït el Haj. From an old lake to an exceptional and didactic maar. The LNH is characterized by a double transition of eruptive style; starting by a phreatomagmatic to a strombolian dynamic, then from a strombolian to a final phreatomagmatic explosion. The petrological, mineralogical and geochemical analyses show that the LNH nephelinites were not been fractioned, with formation via a low degree of partial melting degree (2%). The origin of this magma is the lithosphere-asthenosphere boundary.

Acknowledgements

Many thanks to "Laboratoire Magmas et Volcans, Observatoire du Physique du Globe de Clermont, Université Blaise Pascal-Clermont, for their support for the Geochemical Analyzes. We are grateful to Pr. Pierre Boivin Pr. M'hamed Benbakkar for their technical assistance.

References

Bas, M.J.L., Maitre, R.W.L., Streckeisen, A., Zanettin, B., 1986. A Chemical Classification of Volcanic Rocks Based on the Total Alkali-Silica Diagram. J. Petrol. 27, 745–750. Bosch, D., Maury, R.C., Bollinger, C., Bellon, H., Verdoux, P., 2014. Lithospheric origin for Neogene–Quaternary Middle Atlas lavas (Morocco): Clues from trace elements and Sr–Nd–Pb–Hf isotopes. Lithos 205, 247–265.

Fisher, R.V., Schmincke, H.-U., 1984. Pyroclastic Rocks. Springer Berlin Heidelberg, Berlin, Heidelberg.

Lorenz, V., 2003. Maar-diatreme volcanoes, their formation, and their setting in hard-rock or soft-rock environments. Geolines 15, 72–83.

Morimoto, N., 1989. Nomenclature of pyroxenes. Mineral. J. 14, 198–221.

Mountaj, S., Remmal, T., El Amrani El Hassani, I.-E., Van wyk de vries, B., 2014. Reconstruction of the morphological evolution and the eruptive dynamics of the lachminen'Ait el Haj Maar in the Middle Atlas. Karstic province of Morocco. Proceeding 5th Int. Maar Conf. Quéretaro Mex. 4–5.

Németh, K., 2010. Monogenetic volcanic fields: Origin, sedimentary record, and relationship with polygenetic volcanism, in: Geological Society of America Special Papers. Geological Society of America, pp. 43–66.

Tchamabé, B.C., Kereszturi, G., Németh, K., Carrasco-Núñez, G., 2016. How Polygenetic are Monogenetic Volcanoes: Case Studies of Some Complex Maar-Diatreme Volcanoes, in: Nemeth, K. (Ed.), Updates in Volcanology - From Volcano Modelling to Volcano Geology. InTech.

Walker, G.P.L., Sigurdsson,, H., Houghton, B., Rymer, H., Stix, J., McNutt, S., 2000. Basaltic volcanoes and volcanic systems, in: Encyclopedia of Volcanoes. Academic Press, pp. 283–9.

White, J.D.L., Ross, P.-S., 2011. Maar-diatreme volcanoes: A review. J. Volcanol. Geotherm. Res., From maars to scoria cones: the enigma of monogenetic volcanic fields 201, 1–29.

Wohletz, K.H., Sheridan, M.F., 1983. Hydrovolcanic explosions; II, Evolution of basaltic tuff rings and tuff cones. Am. J. Sci. 283, 385–413.

The isolated dacitic Tapias dome and its relation to the magmatic reservoir of Cerro Machín volcano, Colombia

Hugo Murcia[1,2], Jonathan Ortiz[3], Johan García[3], Dayana Schonwalder[4], Carlos Errazuriz[5], Susana Osorio[6]

[1] *Department of Geological Sciences, Universidad de Caldas, Colombia. hugo.murcia@ucaldas.edu.co*
[2]*Instituto de Investigaciones en Estratigrafía, Universidad de Caldas, Colombia.*
[3]*GeologyProgram, Universidad de Caldas, Colombia.*
[4] *Earth Observatory of Singapore, Nanyang Technological University, Singapore.*
[5]*Master in Earth Sciences, Universidad Nacional de Colombia, Colombia.*
[6]*EarthSciencesPostgraduate, Universidad Nacional Autónoma de México, México.*

Keywords: Andes volcanism, magma reservoirs, monogenetic volcanoes.

The Tapias dome (4°27'55.3''N; 75°21'47.43''W; 2525 m.s.n.m.) is a monogenetic volcanic expression, emplaced in a Jurassic metamorphic basement (Fig. 1). The dome is located 5 km SE of the Cerro Machín volcano (CMV), one of the most recognised, highly explosive, active volcanoes of the Colombian Andes. The CMV is located 13 km from Ibagué city, a medium size city with ~500,000 inhabitants.

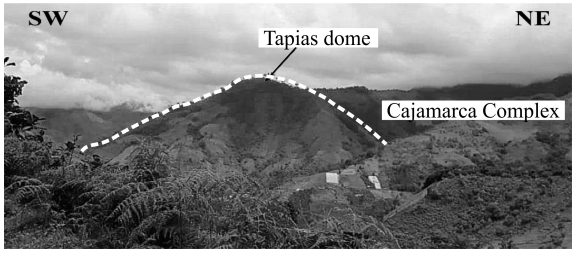

Fig. 1 –The Tapias dome in the Jurassic Metamorphic basement (Cajamarca Complex).

Using whole-rock, mineral and isotopic chemistry, we characterize the Tapias dome, calculate the crystallization conditions and investigate its relation to Cerro Machín volcano.

The dome displays n homogeneous dacitic composition (66.5 wt. % SiO_2, 6.2 wt. % Na_2O + K_2O on anhydrous base) within the calc-alkaline series. It exhibits a mineral assemblage of plagioclase (An_{28-48}), amphibole (magnesiohastingsite), biotite (Fe_{47-48}), quartz, and Fe and Ti oxides. Isotopic ratios such as Sr, Pb, Nd and Hf, indicates common values for subducted-related magmas in the region (e.g. $^{87}Sr/^{86}Sr$ = 0.70491).

Two types of amphiboles, with similar core compositions, were identified in the dome. Type I, has homogeneous composition along the entire crystal, whereas type II has Mg-enriched rims. Geothermobarometric analysis indicates that the cores crystallized at 11.73 ± 5.72 km depth, 310 ± 151 MPa and 905 ± 48 °C. The Mg-enriched rims crystallized at 9.39 ± 2.61 km depth, 256 ± 54 MPa and 931 ± 58 °C. These results suggest that a mafic magma reached a more evolved magma in a level where amphibole had already started to form. This magma mixing then formed the Mg-rich rims for the type II amphiboles.

Our results are similar to the characteristics described for the intracrateric dome of Cerro Machín volcano (e.g. Laeger et al., 2013; Errazuriz et al., 2019), which formed in the most recent eruption (i.e. 900 years BP). Its composition is also dacitic (~66 wt. % SiO_2, ~6.6 wt. % Na_2O + K_2O), with a calc-alkaline signature. Isotopic ratios values such as $^{87}Sr/^{86}Sr$ = 0.70497, are also similar, as well that the mineral assemblage characterized by plagioclase (An_{24-54}), amphibole (tschermakite and pargasite/magnesio-hastingsite) and biotite (Fe_{42-43}). There are also, two types of amphiboles with crystallization conditions of 13 ± 2 km depth, 360 ± 70 MPa and 910 ± 30 °C, and 14 ± 2 km depth, at 410± 100 MPa and 970 ± 25 °C. These characteristics were interpreted by Laeger et al. (2013) as a mafic magma intrusion into a rhyolitic resident magma.

Taking into account our results for the Tapias dome, its location with respect to CMV and the similarities with the CMV's intracrateric dome, we conclude that, both domes are fed by the same magmatic reservoir. Consequently, the Tapias dome rather than a monogenetic volcano is a monogenetic expression related to a shallow feeding system.

References

Errázuriz-Henao, C., Gómez-Tuena, A., Duque-Trujillo, J., Weber, M., 2019. The role of subducted sediments in the formation of intermediate mantle-derived magmas from the Northern Colombian Andes. Lithos 336: 151–168.

Laeger, K., Halama, R., Hansteen, T., Savov, I. P., Murcia, H. F., Cortés, G. P.,Garbe-Schönberg, D., 2013. Crystallization conditions and petrogenesis of the lava dome from the~900 years BP eruption of Cerro Machín Volcano, Colombia. Journal of South American Earth Sciences 48: 193–208.

The youngest multiple long-lived volcanic systems and the role of fissure eruptions in Arxan-Chaihe, NE China

Károly Németh[1], Boxin Li[1], Julie Palmer[1], Alan Palmer[1], Jonathan Procter[1], Jing Wu[2]

[1]School of Agriculture and Environment, Massey University, Palmerston North, New Zealand;K.Nemeth@massey.ac.nz
[2]Institute of Geology and Geophysics, Chinese Academy of Science

Keywords: scoria cone, lava flow, fissure.

The monogenetic Arxan-Chiahe Volcanic Field (ACVF) is field located in Eastern Inner Mongolia, NE China. It is located at the southwestern end of Great Xing'an Range, an active fault zone believed to be in a rift setting (Liu, 1989; Liu, 1999; Liu et al., 2001). ACVF includes approximately 45 vents in an area of c.3000 km^2 (Németh et al., 2017). Several types of small-volume, mostly mafic, volcanoes are recognised as tuff rings and scoria cones, but other vent types such as fissure-triggered lava flows that interacted with the region's fluvial systems also occur.

Arxan contains scoria cones as well as fissure-aligned vents which emitted large volume lava flows that covered the paleo-valleys and eventually joined the ancestral fluvial network of the present day Halaha River. This region includes the iconic Arxan Heaven Lake, Wusulangzi Lake, Dichi Lake, Moon Lake and Tuofengling Lake. All of these are small-volume volcanoes with shallow lakes in their crater and have a young morphological appearance. Their distribution shows a distinct pattern which indicates the general tectonic trend from the southwest to northeast. This is the inferred orientation of the erupting fissure. Field observations suggest the volcanism at ACVF might have been controlled by regional tectonic events.

Fissure vents have been identified on the east flank of Heaven Lake and the west side of Dichi Lake. The lava from these fissures ponded in the palaeo-valley topography, possible channels of Halaha River. The surface textures of the lava flows are typical of aa and slabby pahoehoe types. In some areas, it looks like younger lava has flowed over older ones. The relative position of the lava flow to its source is not always certain as major ponding areas behind develop around topographic obstacles. It appears that high volumes of lava have poured out rapidly from fissure-aligned vents. This raises the question of volcanic risk assessment and evaluation of the risk ACVF poses. The youngest eruptions that formed ponded lava fields along the Halaha River provide the opportunity to assess this risk. We believe that studying the style of volcanism, eruption styles, syn and post-eruptive processes, as well as reconstructing the post-eruptive environments, will provide the best assessment of the regional hazards and the opportunity to mitigate the effects of an eruption of any type or scale.

Alongside small vents such as Heaven Lake which is located on the southeastern part of the ACVF, several morphologically young, large and well-preserved scoria cones are located with extensive well preserved lava flows.

Fig. 1 –Yanshan, "*the triple vents*", it is suspected to formed through sustained and long-lived continuous lava fountaining eruption, and it might be the youngest vent of the ACVF.

The Yanshan volcano, informally called as "*the triple vents*", is typical of these multiple vent volcanic centres from which fissure-oriented lava fountaining eruptions, such as that recorded in thick clastogenic lava successions surrounds its elongated crater, occurred. The triple vents of Yanshan volcano were observed during field work. On the south flank, the lava flow is aa type and flows onto the older lava flow. Eventually, the lava flows joined and formed ponds in the Halaha River valley. Topographic and flow relationships indicate these most likely formed at a very young age, perhaps younger than 2000 years (Fig. 1). The southern side of the cone, approximately 47 degrees, is steeper than the north side as a result of an armour of spatter. This could have been caused by collapse on the northwestern flank due to cone-rafting during vigorous lava outpouring events. The three vents appear to have formed in succession, one built upon another. The aa lava flow on the southern side of Yanshan contains a range of lava tumuli in a linear trend. Also, on the top of the lava flow there are scoria deposits, suspected to be the deposits of subsequent Strombolian type explosive events that followed the major lava outpouring.

The Dichi Lake, located on the southwestern side of Yanshan, is about 12.6 km away from the others. This volcano is the smallest volcanic lake in ACVF.

The lake was built on aa type lava flow ponding in the fluvial channel of Halaha River. It is suspected that if formed by a single eruption. The lava flow is covered by a thin soil and exposed in the crater lake wall where the pre-eruptive rock units can be observed. This volcanic landform is the best evidence Dichi Lake is a maar (Fig. 2). The surrounding areas preserve a few large basaltic boulders, which might be projectiles from a single explosive eruption. These basaltic boulders are suggested as remnants from the overlying lava flow that formed the lake wall and its bottom. On the eastern side of Dichi Lake, fissure structures preserve a typical W-E orientated linear trend. Within the fissure there are several small, well-preserved scoria vents composed of reddish basaltic scoria. The fissure clearly shows Dichi Lake lies on a fissure. It seems that the vents located in the NE gradually migrated SW forming an c. 2 km long fissure. In the SW, the propagating dykes must have hit some confined aquifer and generated a single blast-like explosion to create Dichi Lake.

Fig. 2 – Dichi Lake, it is the smallest lake, and suspected to be a maar formed in the SW-edge of a fissure.

Tuofengling Lake (Fig. 3), another scoria cone complex with an elongated shape, is located on the eastern side of ACVF, about 11 km away from Yanshan to the NW. On top of the lake rim, there is scoria containing abundant peridotite lherzolites. The lava flow from Tuofengling is extending down its eastern flank c. 400 m. On the outer side of the southern flank of the lake, a series of phreatomagmatic pyroclastic units are exposed beneath the youngest scoria units. These phreatomagmatic deposits are generally parallel bedded, composed of unsorted, coarse lapilli. One of the deposits contains angular basaltic blocks with cracks, which might suggest that it was formed by an eruption-triggered landslide or collapse event. Tuofengling also appears to be located on a fissure with a W-E orientation.

Fig. 3 –Tuofengling Lake, the shape of this lake is like double humps of a camel. Scorias are overlying on the rim of the lake. Double vents, this assumption is under investigation.

Acknowledgements

The authors would like to thank gratefully the support provided by Massey University, Chinese Academy of Sciences, the China Science and Technology Exchange Center (CSTEC), and the China-New Zealand Scientist Exchange Program2019, as well as their family.

References

Liu, J., 1989. On the origin and evolution of continental rift system in Northeast China. Chinese Journal of Geology, 3, 209–319.

Liu, J., 1999. Volcanoes in China. In: Beijing: Science Press.

Liu, J., Han, J., Fyfe, W. S., 2001. Cenozoic episodic volcanism and continental rifting in northeast China and possible link to Japan Sea development as revealed from K–Ar geochronology. Tectonophysics, 339(3-4), 385–401.

Németh, K., Wu, J., Sun, C., Liu, J., 2017. Update on the Volcanic Geoheritage Values of the Pliocene to Quaternary Arxan–Chaihe Volcanic Field, Inner Mongolia, China. Geoheritage, 9(3), 279–297. doi:10.1007/s12371-017-0224-5

Lomo Negro (El Hierro) – geology, archaeomagnetic dating and emplacement dynamics of a "monogenetic" eruption

Claudia Principe[1], Stavros Meletlidis[2], Daniele Giordano[1, 3], Stephan Kolzenburg[4], Sonia La Felice[1], Avto Gogichaishvili[5], Marina Devidze[1,6], Ruben Cejudo[7], Gianluigi Groppelli[8], Donald Bruce Dingwell[9], Joan Martì Molist[10]

[1]Archaeomagnetic Laboratory of the Istituto di Geoscienze e Georisorse, CNR, via G. Moruzzi 1, Pisa 56124, Italy
c.principe@igg.cnr.it
[2]Instituto Geografico Nacional, Calle La Marina 20, Santa Cruz de Tenerife, Espana
[3]Dipartimento di Scienze della Terra, Università degli studi, Torino, Via Valperga Caluso, 35, 10125 Torino, Italy
[4]Department of Geology, 126 Cooke Hall, University of Buffalo, North Campus, Buffalo, NY 14260-4130
[5]Servicio Arqueomagnetico Nacional, Instituto de Geofisica - Campus Morelia, Universidad Nacional Autonoma de Mexico (UNAM), Ciudad Universitaria, Morelia, Mexico
[6]M. Nodia Institute of Geophysics, Ivane Javakhishvili Tbilisi State University, Tbilisi, Georgia
[7]Laboratorio Universitario de Geofisica Ambiental, Instituto de Geofisica - Campus Morelia, Universidad Nacional Autonoma de Mexico (UNAM), Ciudad Universitaria, Morelia, Mexico
[8]Istituto di Geologia Ambientale e Geoingegneria, CNR, Via M. Bianco 9, 20131 Milano, Italy
[9]Department für Geo- und Umweltwisshenchaften, Ludwig-Maximiliams Universtät München. Theresienstrasse 41, 80333 Munich, Germany
[10]Institut de Ciencias de la Terra Jaume Almera, Barcelona, Spain

Keywords: El Hierro, archaeomagnetic dating, geological mapping, lava viscosity

The island of El Hierro, at the southwestern end of the Canary archipelago, is the youngest of the Canary Islands. Together with La Palma, to its north, and in contrast to the rest of the islands, El Hierro is thought to be in its main subaerial constructive phase, although several giant lateral landslides have already modified its previous structure (Carracedo et al. 2001, 2002).

The products of the small Lomo Negro eruption, located at the westernmost end of El Hierro, was firstly described by Hernàndez-Pacheco (1982) as constituted by pyroxene-olivine-rich alkaline basalts (ankaramite) lava flows. Following Hernàndez-Pacheco (1982) Lomo Negro eruption, dubitatively attributed to the 1793 AD, could have been related to the seismic crisis occurred at El Hierro in the same year.

In more recent times Villasante-Marcos and Pavòn-Carrasco (2014) used the average palaeomagnetic direction of Lomo Negro lavas to perform a palaeomagnetic dating using the master PSVCs for El Hierro, computed from the SHA.DIF.14k global geomagnetic field model (Pavòn-Carrasco et al. 2014). The palaeomagnetic direction of Lomo Negro obtained by their work, also with the imprecision deriving from quite high

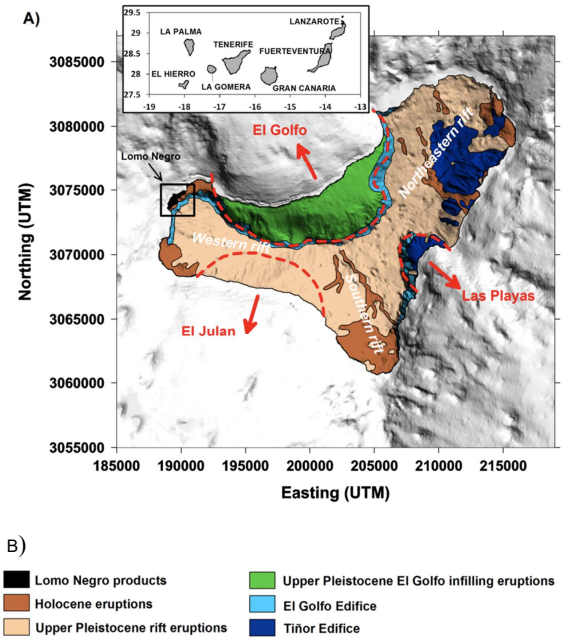

Fig. 1 – A) Simplified geological map of El Hierro (modified from Balcells & Gòmez 1997) over topographic and bathymetric Digital Elevation Model (25 m, Instituto Geografico Nacional data). B) Legend from Villasante-Marcos and Pavòn-Carrasco (2014)

α95 values, precludes the 1793 AD as the year of the eruption, and identifies the following three possible age intervals for Lomo Negro lavas: 115BC-7AD, 410-626 AD and 1499-1602 AD.

To solve this ambiguity, we performed an accurate geological and archaeomagnetic survey of the volcanic deposits lying on the Lomo Negro marine terrace. Our geological survey has allowed to obtain an accurate geological map of the Lomo Negro area where at least twelve stratigraphic units has been identified and mapped on the Digital Terrain Model of El Hierro Island, as provided by the Instituto Geografico National (IGN). The new map has allowed to establish, unlike previous authors, a geological scenario, where at least two ankaramitic lava flows have been recognized. In particular, we could distinguish (i) a younger lava flow originated from a scoria cone positioned on the coastal platform and (ii) an older lava flow originated from a cone on the top of the cliff. The path of this second lava flow can still, in part, be recognized on the steep wall of the cliff himself.

On the other hand, the archaeomagnetic survey performed on these two ankaramitic flows discerned during field mapping has permitted to date these two units. A total of 26 samples distributed on 3 sites has

been collected by employing the big sample plaster method (BSPM) (Tanguy et al, 2003). Sample preparation necessary to the successive analysis has been performed in the Archaeomagnetic Laboratory of IGG-CNR at Villa Borbone (Viareggio, Lu) in Italy. Directional measurements have been performed by means of the large cell induction magnetometer of the Saint Maur des Fossés Laboratory (Institute de Physique du Globe de Paris) in Paris. Lastly, the magnetic intensity measurements and magnetic mineralogy experiments were conducted at the facilities of the Servicio Arqueomagnetico Nacional, of UNAM in Morelia (Mexico). Archaeomagnetic dating allowed us to obtain two different ages for the two ankaramitic lava flows. The resulting directional measurements show $\alpha 95$ values from 1.90 to 1.03 and a viscous magnetic remanence of about 1-2%.

Finally, in order to improve the description of the dynamics of emplacement of the investigated lava flows, we have performed high temperature viscosity measurements at the Earth and Environmental Sciences Department of the University of Munich (Germany). The measured samples have shown that the liquid viscosity of the Lomo Negro ankaramitic products has the lowest value amongst those measured for natural samples (Fig. 2). The measured viscosities also indicate that for cooling rate of ca 3K/min and 5 K/min, the crystallization temperatures are of the order of 1240 and 1220°C, respectively. Finally, these preliminary measurements indicate that at the above reported cooling rates a rheological death may have occurred at cut off temperatures (Giordano et al., 2007; Kolzenburg et al., 2016, 2017, 2018) of the order of 1220 and 1200 °C, respectively and corresponding viscosity values about two orders of magnitude lower than those typical of basaltic melts such as Etnean trachybasalts (Giordano and Dingwell, 2003, Kolzenburg et al., 2018).

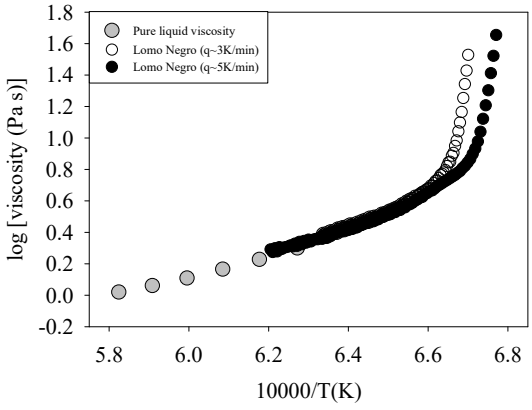

Fig. 2 – Preliminary super-liquidus and sub-liquidus viscosity data as measured at cooling rates of 3 and 5 K/min.

Acknowledgements

Maxim Le Goff from Saint Maur des Fossés Archaeomagnetic Laboratory of the IPGP, is acknowledged for making available the facilities of the Saint Maur archaeomagnetic Laboratory. This work was supported by funds of a CNR short-term mobility assigned to CP. Maria Josè Blanco of Instituto Geografico National is thanked for making all logistical facilities available.

References

Balcells, R., Gomez, J.A., 1997. Memorias y mapas geolo´gicos del Plan MAGNA a escala 1:25000 de las hojas correspondientes a la isla de El Hierro. Hojas de: Valverde, Sabinosa, Tigaday, Taibique y La Restinga. IGME, Madrid, Spain.

Carracedo, J.C., Badiola, E.R., Guillou, H., de la Nuez, J., Pe´rez-Torrado, F.J., 2001. Geology and volcanology of La Palma and El Hierro, Western Canaries, Estudios Geolo´gicos, 57, 175–273.

Carracedo, J.C. et al., 2002. Cenozoic volcanism II: the Canary Islands, in The Geology of Spain, pp. 439–472, eds. Gibbons, W. & Moreno, T., Geological Society.

Giordano, D., Polacci, M., Longo, A., Papale, P., Dingwell, D. B., Boschi, E., Kasereka, M., 2007. Thermo-rheological magma control on the impact of highly fluid lava flows at Mt. Nyiragongo. Geophysical Research Letters, 34, L06301.

Giordano, J. K. R., Dingwell, D. B., 2008. Viscosity of magmatic liquids: A model. Earth and Planetary Science Letters, 271(1–4), 123–134. https://doi.org/10.1016/j.epsl.2008.03.038

Herna´ndez-Pacheco, A., 1982. Sobre una posible erupcio´n en 1793 en la isla de El Hierro (Canarias), Estudios Geolo´gicos, 38, 15–25.

Tanguy, J.C., Le Goff, M., Principe, C., Arrighi, S., Paiotti, A., Chillemi, V., La Delfa, S., Patanè, G., 2003: Acheomagnetic dating of mediterranean volcanics from the last 2,100 years: validity and limits. Earth Planetary Sciences Letters, 211, 111–124.

Kolzenburg, S., Giordano, D., Cimarelli, C., Dingwell, D. B., 2016. In situ thermal characterization of cooling/crystallizing lavas during rheology measurements and implications for lava flow emplacement. Geochimica et Cosmochimica Acta, 195, 244–258.

Kolzenburg, S., Giordano, D., Thordarson, T., Höskuldsson, A., Dingwell, D. B., 2017. The rheological evolution of the 2014/2015 eruption at Holuhraun, Central Iceland. Bulletin of Volcanology, 79, 45

Kolzenburg S., Giordano D., Hess K.U., Dingwell D.B., 2018. Shear rate-dependent Disequilibrium Rheology and Dynamics of Basalt Solidification. Geophys. Res. Lett. 10.1029/2018GL07779;

Villasante-Marcos V., Pavòn-Carrasco F.J., 2014. Palaeomagnetic constraints on the age of Lomo Negro volcanic eruption (El Hierro, Canary Islands). Geophys. J. Int. 199, 1497–1514.

Session 4. Petrology, geochemistry and characteristic times of magmatic processes at monogenetic volcanism

Petrology and geochemistry of the volcanic objects are the surface representation of the deep underground processes, which are controlled by regional and local tectonic conditions. Among other volcanic objects, monogenetic volcanism, including large monogenetic fields, flank areal volcanism, diatremes and phreatomagmatism, with its abundance of mafic lavas produces the least contaminated rocks and therefore is informative to study the primary mantle sources and processes. Due to high source-to-surface ascent rates, the composition of zoned minerals from the monogenetic events often keeps information about times of such processes as magma ascent, magma mixing, magma chamber replenishment, fractional crystallization and crustal assimilation. Correlation of these times with geophysical and observed parameters and events improve the understanding of eruption mechanisms and its forecasting. We invited contributions that include field observations, petrological, geochemical, and isotopic data, as well as diffusion timescales records based on the distributions of the chemical compositions in minerals.

Clinopyroxene compositions from monogenic volcanoes and maars of Karymsky volcanic center

Ivan Belousov[1], Alexander Belousov[2], Leonid Danyushevsky[1]

[1]*CODES, University of Tasmania, Australia*
ivanb@utas.edu.au
[2]*Institute of volcanology and seismology FEB RAS, Petropavlovsk-Kamchatsky 683006*

Keywords: Karymsky, clinopyroxene, LA ICPMS

Karymsky volcano, which is part of Karymsky volcanic center, is one of the most currently active volcanoes in Kamchatka. It is characterized by contrasting basaltic and andesitic volcanism, as during the 1996 eruption, which initially proceeded at two interrelated centers (Karymskoe Lake and Karymsky volcano) (e.g. Belousov, Belousova, 2001). Based on the geochemistry of the rocks and the composition of their minerals and melt inclusions in them (e.g. Portnyagin et al., 2011), it has been demonstrated that the basalts and andesites of the Karymsky center are closely interrelated by the fractional crystallization of a single basaltic magma, whose injection into a crustal andesitic chamber likely triggered the eruption of Karymsky stratovolcano.

Here we present trace element compositions of clinopyroxenes measured by LA ICPMS. Samples analyzed represent 3 eruptions in Karymsky lake (2 eruptions of ~4600 BC and eruption of 1996) as well as eruption that formed Lagerny cone and Valentina maar (Fig.1). Clinopyroxene contains highest abundances of REE and is one of the earliest minerals to crystallize. Therefore, difference in compositions of Cpx could indicate differences in melt generation of different batches erupting along the same fault system with time and their subsequent fractionation. Comparison with clinopyroxene compositions from other island arc basalts as well as boninites and low Ti basalts from Hunter Ridge and Tonga highlights differences in sources and conditions of melting.

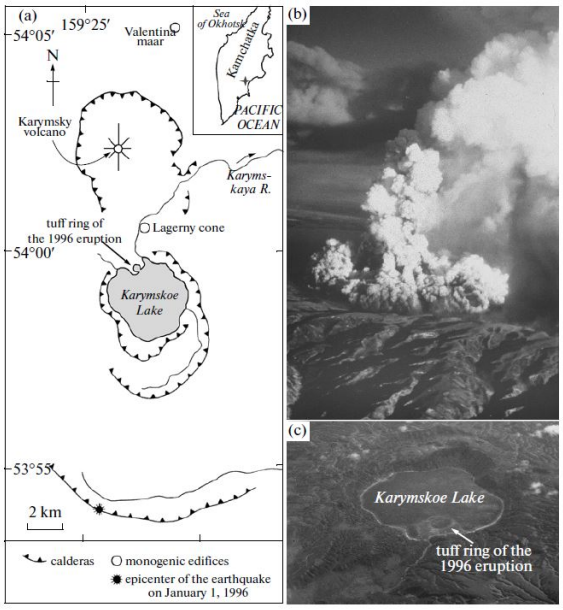

Fig. 1 – Geological setting of the 1996 eruption in the Akademii Nauk caldera. (a) Schematic geological map of the Karymsky volcanic center. The inset shows the location of Karymsky volcano in Kamchatka as well as monogenic volcanoes studied here. (b) Eruption on January 2, 1996 (photo: Ya.D. Murav'ev). (c) Karymskoe Lake as can be seen nowadays (photo: A.B. Belousov).

References

Portnyagin M.V, Naumov V.B, Mironov N.L, Belousov I. A., Kononkova N.N., 2011. Composition and Evolution of the Melts Erupted in 1996 at Karymskoe Lake, Eastern Kamchatka: Evidence from Inclusions in Minerals. Geochemistry International Vol. 49, No. 11: 1085–1110.

Belousov A., Belousova M., 2001. Effects and Deposits of the 1996 and the Ancient Basaltic Phreatomagmatic Eruptions in Karymskoye Lake, Kamchatka, Russia. Spec. Publ. Int. Ass. Sediment 30: 35–60.

Petrography and geochemistry of post-caldera monogenetic volcanism in Acoculco Caldera complex, Mexico.

Mario Boijseauneau-López[1-2], Xavier de Bolós[1], Giovanni Sosa-Ceballos[1], José Luis Macías[1]

[1] *1 Institute of Geophysics, UNAM, Campus Morelia, 58190 Morelia, Michoacán, Mexico boijseauneau@comunidad.unam.mx*
[2]*Graduate School in Earth Sciences, UNAM, Campus Morelia, 58190 Morelia, Michoacán, Mexico.*

Keywords: Acoculco Caldera Complex, Monogenetic Volcanism

The Acoculco Caldera (ACC) is a volcanic complex that represent Plio-Quaternary volcanism of the eastern part of Trans-Mexican Volcanic Belt (TMVB), subduction related magmatic arc (Fig.1a). Magmatism in this region has ~2.7 Ma and persists until 0.06 Ma (Avellán et al., 2017). Largest volcanic eruptions of ACC are ~2.7 Ma andesitic ignimbrite, Piedras Encimadas rhyolitic ignimbrite and Tecoloquillo rhyolitic ignimbrite ~0.09 Ma (Sosa-Ceballos et al., 2018). Monogenetic volcanism is present in the region before and after the caldera eruption with ages of ~3.0 Ma (Terrerillos lava dome) to ≤ 0.06 Ma (Tulimán lava cone). These monogenetic products show chemical and mineralogical variations through the time (Sosa-Ceballos et al., 2018). In this paper, we focus on the post-caldera monogenetic volcanism and the changes of its chemistry variations in time.

Early post-caldera (Epc) volcanism (~2.7–2.0 Ma) was restricted to the inner part of the caldera (Avellán et al., 2019). A period of dome extrusion emplaced during the late post-caldera (Lpc) produced rhyolitic domes and mafic products along the caldera rim, between 2 and 1 Ma (Avellán et al., 2019). Extra-caldera volcanism of the Apan-Tezontepec Volcanic Field (~3.00 to ~0.19Ma) emplaced basaltic scoria cones, associated lava flows, and a few half-shield volcanoes. These mafic products were contemporary with the felsic calc-alkaline volcanism in the Acoculco region (Sosa-Ceballos et al., 2018).

The ACC rocks are deformed by three main fault systems: the NE-striking Tenochtitlán-Apan fault system, and the NW-striking Tulancingo-Tlaxco fault system (Avellán et al. 2018). Locally, the Tenochtitlán-Apan fault system is represented by the Apan-Tlaloc and Chignahuapan faults, and the Tulancingo-Tlaxco structural system is represented by the Manzanito fault (Fig.1b). Extensional processes evidenced by normal faulting in ACC could be promoted by geometry and kinematic situation of oblique subduction of the Cocos plate beneath the North American plate (Kostoglodov and Bandy, 1995, De Mets and Stein, 1990). This structural setting produces tilted horst blocks that allowed the extrusion of magmas in ACC region (García-Palomo et al., 2018).

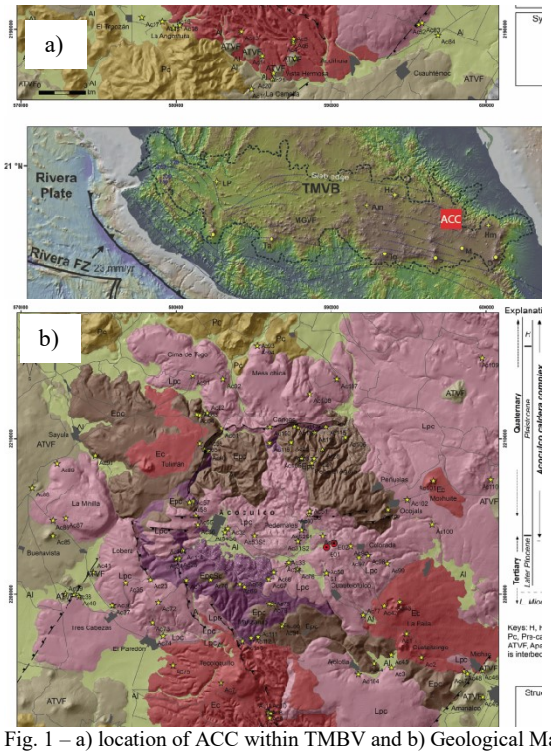

Fig. 1 – a) location of ACC within TMBV and b) Geological Map of ACC Modified of Sosa-Ceballos et al., 2018.

The local stress field of ACC was changed several times after explosive eruptions and collapses, such as is evidenced by chemical changes in magmas of the ACC. Chemical variations are associated with the ascent of peralkaline magmas that genetically are unrelated to calc-alkaline melts dominated by the pre-caldera activity and the post-collapse deformation. These processes promoted a swarm of dykes and sills above the collapsed reservoir (Sosa-Ceballos et al., 2018).

Here we present new bulk rock data, petrography analysis, and mineral chemistry analysis of three representative monogenetic volcanoes of the Epc and Lpc. Samples were collected for each volcano on three different stratigraphic levels. Data analyzed allows us to detect chemical inter-eruptive variations and petrography changes across the Epc and Lpc deposits. Our chemical results show that silica and alkalis trend to increase at the end of Epc eruptions. However, not all samples follow this behavior, some Lpc samples show changes without a defined trend (Fig. 2a). Epc and Lpc deposits have calc-alkaline behavior with Pb, Nb and Ta anomalies (Fig. 2b). Petrography of Epc and Lpc samples shows holohyaline matrix with microlites, paragenesis of Px+ Pl ± Ol ± Fe-Ti Oxides and disequilibrium

textures in some mineral phases. Different size populations in phenocrystals and micro-phenocrystals of feldspar minerals are presents. Phenocrystals sizes phases have most of disequilibrium textures like rounded rims, patchy cores and sieve textures (Fig. 3). These textures could reflect processes such as magma mixing, assimilation, or over heating that impact the last stages of crystal growth (i.e. Sosa-Ceballos, 2014).

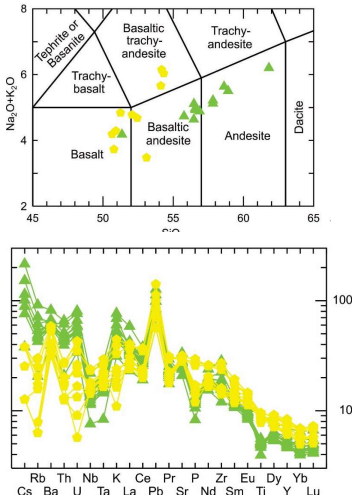

Fig. 2 – a) Total Alkali vs Silica diagram (TAS, LeBass, 1986) yellow symbols represents Lpc samples, green symbols represents Epc samples. b) AFM diagram of Epc and Lpc monogenetic products.

The data presented show that monogenetic volcanism of Epc and Lpc eruptions reflects different calc-alkaline pulses in ACC. The magmas studied of Lpc are less evolved than the Epc volcanic deposits (Fig. 2) and occurs in different structural trend. Epc deposits show a NW-SE alignment whereas Lpc deposits present a NE-SW direction. Moreover, we suggest that the inter-eruptive chemical and mineralogical variations are produced by different magmatic pulses and/or as result of complex magmatic processes during the single eruption.

Fig. 3 – Disequilibrium texture of plagioclase phenocrystal.

The chemical and mineral texture show evidences of mixed magmatic process that could be promoted by new magma injections, and storage periods associated with changes in the regional stress field.

The total volumes of monogenetic volcanism in the whole ACC have been greatly underestimated, taking into account that this type of volcanism persists from the pre- and post-caldera stages producing an important number of cinder cones, and eruptive fissures.

Acknowledgements

Funding for this research was provided to José Luis Macías by the WP4.4 of GEMEX.

References

Avellán, D. R., Macías, J. L., Layer, P. W., Cisneros, G., Sánchez-Núñez, J. M., Gómez-Vasconcelos, M. G., ... & Osorio-Ocampo, S., 2019. Geology of the late Pliocene–Pleistocene Acoculco caldera complex, eastern Trans-Mexican Volcanic Belt (México). Journal of Maps 15(2): 8–18.

DeMets, C., Stein, S., 1990. Present‐day kinematics of the Rivera plate and implications for tectonics in southwestern Mexico. Journal of Geophysical Research: Solid Earth 95(B13): 21931–21948.

García-Palomo, A., Macías, J. L., Jiménez, A., Tolson, G., Mena, M., Sánchez-Núñez, J. M., ... & Lermo-Samaniego, J., 2018. NW-SE Pliocene-Quaternary extension in the Apan-Acoculco region, eastern Trans-Mexican Volcanic Belt. Journal of Volcanology and Geothermal Research 349: 240–255.

Kostoglodov, V., Bandy, W., 1995. Seismotectonic constraints on the convergence rate between the Rivera and North American plates. Journal of Geophysical Research: Solid Earth 100(B9): 17977–17989.

Bas, M. L., Maitre, R. L., Streckeisen, A., Zanettin, B., & IUGS Subcommission on the Systematics of Igneous Rocks, 1986. A chemical classification of volcanic rocks based on the total alkali-silica diagram. Journal of petrology 27(3): 745–750.

Sosa-Ceballos, G., Gardner, J. E., Lassiter, J. C., 2014. Intermittent mixing processes occurring before Plinian eruptions of Popocatepetl volcano, Mexico: insights from textural–compositional variations in plagioclase and Sr–Nd–Pb isotopes. Contributions to Mineralogy and Petrology 167(2): 966.

McDonough, W. F., Sun, S. S., 1995. The composition of the Earth. Chemical geology 120(3-4): 223–253.

Sosa-Ceballos, G., Macías, J. L., Avellán, D. R., Salazar-Hermenegildo, N., Boijseauneau-López, M. E., Pérez-Orozco, J. D., 2018. The Acoculco Caldera Complex magmas: Genesis, evolution and relation with the Acoculco geothermal system. Journal of Volcanology and Geothermal Research 358: 288–306.

Magma ascent and residence times in monogenetic volcanism of Kamchatka

Tatiana Churikova[1,2], Boris Gordeychik[2,3], Gerhard Wörner[2], Andreas Kronz[2], Maria Pevzner[4], Yaroslav Muravyev[1], Alexander Belousov[1], Oleg Dirksen[1]

[1] *Institute of Volcanology and seismology FEB RAS, Petropavlovsk-Kamchatsky 683006, Russia.tchurikova@mail.ru*
[2] *Geowissenschaftliches Zentrum Göttingen, Abteilung Geochemie, Universität Göttingen, Göttingen 37077, Germany.*
[3] *Institute of Experimental Mineralogy RAS, Chernogolovka 142432, Russia.*
[4] *Geological Institute RAS, Moscow 119017, Russia*

Keywords: Kamchatka, olivine, diffusion.

Introduction

We present the geochemical profiles across the olivine phenocrysts in four different magmatic regimes at Kamchatka: (a) maars and tuff rings, (b) monogenetic cones, (c) dikes formation, and (d) lavas of stratovolcanoes. Each volcanic-magmatic regime is characterized by their specific olivine zoning history, size and shape of the crystals, ascending and residence times. Time scales were estimated by Ni-Mg/Fe diffusion modeling of zoning in olivine crystal cores and outer rims by quantitative geochemical profiles. Modeling is based on the analytical solution of diffusion equation to approximate measured geochemical profiles and estimates for P and T from Al-in-olivine thermometry and Cpx-melt barometry.

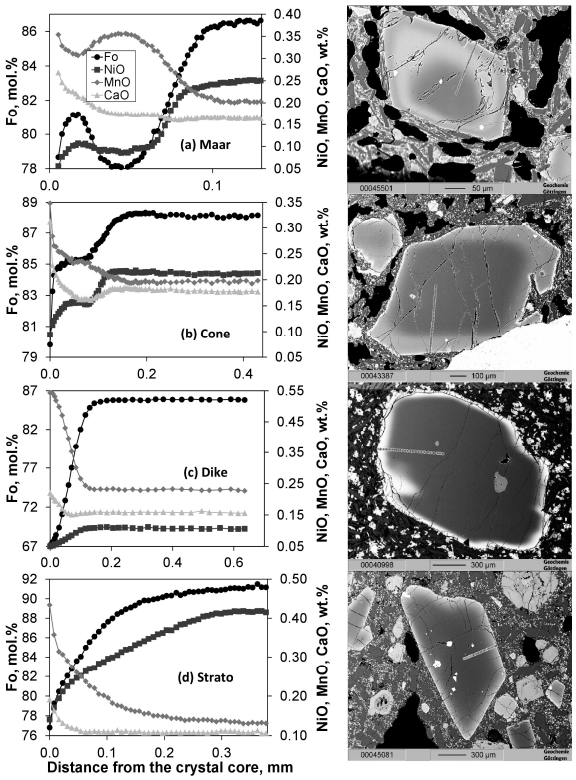

Fig. 1 – Fo, NiO, MnO and CaO in representative Kamchatka olivine crystals from different magmatic regimes.

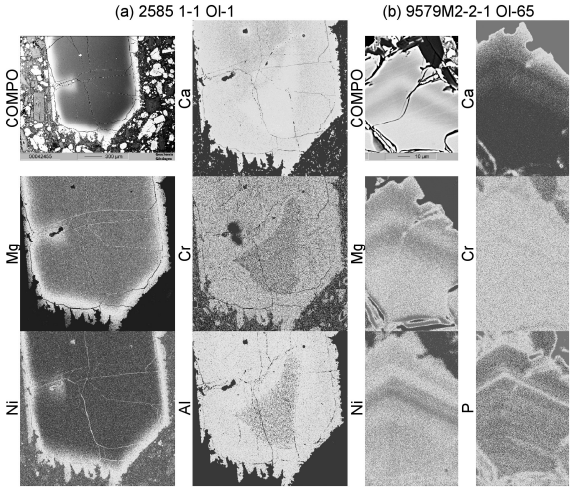

Fig. 2 – Mg-, Ni-, Ca-, Cr-, Al-, and P-distribution maps in the olivine crystals from Kamchatka. (a) element maps showing Ca-Cr-Al enriched core in olivine phenocryst from stratovolcano where diffusion has partially erased Mg/Fe and Ni zoning patterns; (b) olivine rim from maar, showing distinct growth zones, which due to fast magma ascend rate can be still recognized even in elements with high diffusivity such as Mg and Ni.

Results

Olivine crystals in basalts erupted from of maars preserved the most diverse types of compositional zonation – normal, inverse, and even oscillatory in Fo78 to Fo92 olivine crystals (Fig. 1 a; Fig. 2 b). In lavas erupted at monogenic cones, oscillatory zonation in olivine is absent, but normal and inverse zoning are found in all samples, with sharp gradients between the cores and outer parts of crystals (Fig. 1 b). The majority of crystals from dikes and stratovolcanoes show normal zoning. Compositional gradients in Fo and Ni between the olivine cores and outer parts are smoother, indicating longer diffusion times. Also, olivine with reverse zoning and compositional gradients in their cores are rare in samples from stratovolcanoes. Diffusion therefore probably erased earlier zonation gradients (Fig. 1 c, d; Fig. 2a).

The size of olivine crystals in maar eruptions is small (<0.3 mm) compared to olivine crystals from other eruptive regimes, which indicates short crystal growth times. The size of the crystals in monogenic cones is larger than for maar lavas (<0.5 mm). The size of olivine crystals in dikes and stratovolcanoes are larger (0.8-1 mm), which indicates a relatively longer time of crystal growth in their feeding systems (Fig. 3).

Crystal residence times and time of magma ascent for maars and tuff rings are estimated at 100-

2000 and 1-10 days, respectively. Magmas erupted in maars thus move most rapidly to the surface. The time of magma ascent for monogenetic volcanoes varies from 10 to 60 days (Fig. 4). Residence time, estimated for few crystals lasted up to 300 days.

Conclusions

Maar eruptions are fed from rapidly ascending magmas that do not reside, cool and fractionate during ascent fast from their mantle reservoirs.

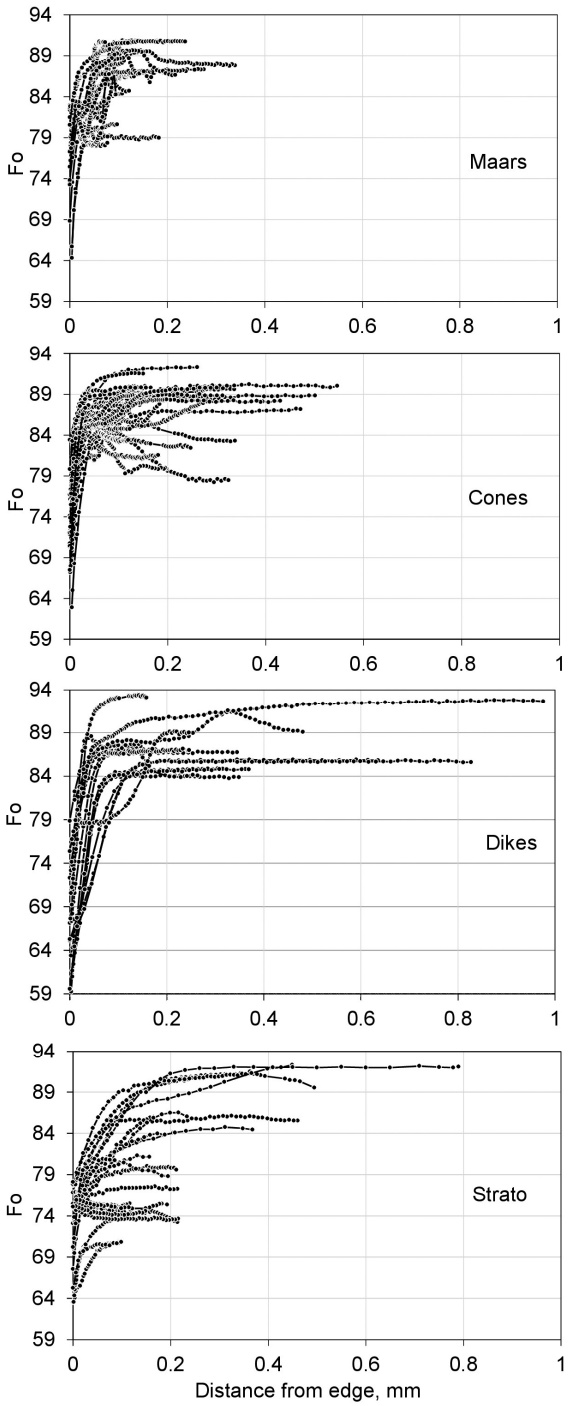

Fig. 3 – Fo zonation in Kamchatka olivine crystals from different magmatic regimes.

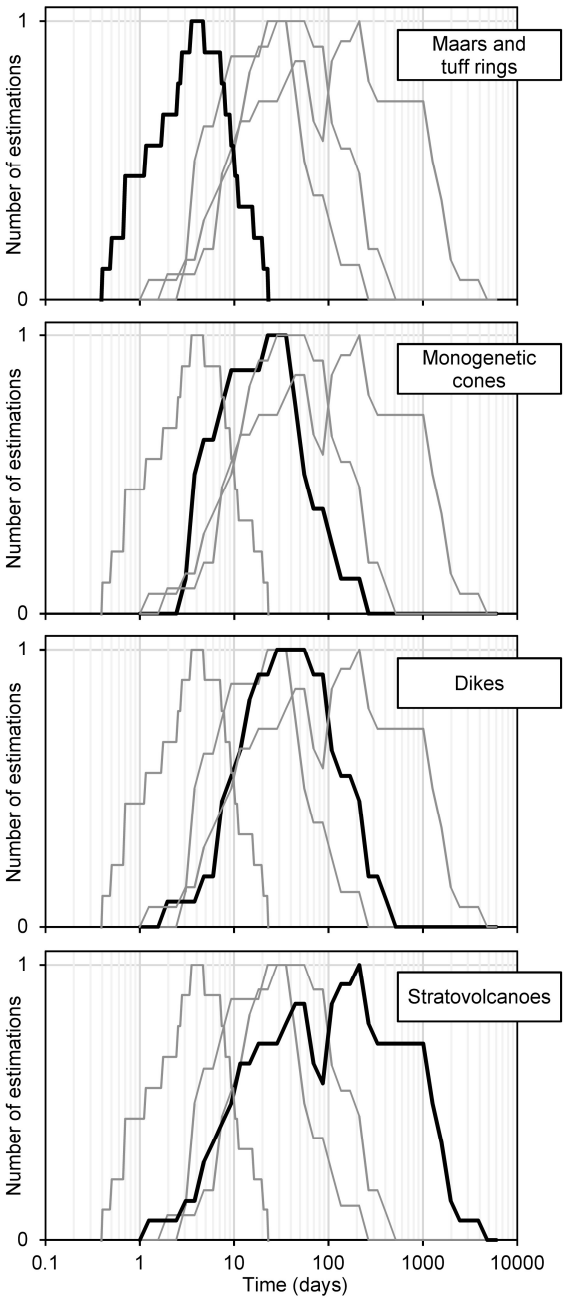

Fig. 4 – Results of ascending time calculations for different magmatic regimes.

Monogenetic cones are similarly sourced from magmas that ascended relatively fast.

By contrast, lavas erupted in stratovolcanoes and those that ascended through their feeder dikes have longer residence times in crustal magma systems, where crystallization and mixing occurs.

Acknowledgements

This research was supported by DFG grant No. Wo 362/51-1, RFBR-DFG-grant No. 16-55-12040, and RFBR-JSPS-grant No. 17-55-50005.

Monogenetic cones of Klyuchevskaya group of volcanoes (Kamchatka, Russia)

Olga Girina[1], Vladimir Ladygin[2]

[1] *Institute of Volcanology and Seismology FEB RAS, Petropavlovsk-Kamchatsky 683006, Russia.girina@kscnet.ru*
[2]*Lomonosov Moscow State University, Faculty ofGeology, Moscow, 119991, Russia.*

Keywords: monogenetic cones, Klyuchevskaya volcanic group, Kamchatka

The Klyuchevskaya group of volcanoes (KGV) is the center of the most active volcanism not only in Kamchatka, but also in the world, due to the location this group in the subduction zone at the intersection of the Aleutian and Kuril-Kamchatka volcanic arcs. The evolution of volcanic arcs, the unevenness of subduction processes led to the formation of the block structure of the KGV, the revival of faults in certain directions at different eras, the contiguity of fault zones, and the long-term volcanic activity of the region (The deep structure…, 1976; Ivanov et al., 2001). Of the 13 volcanoes of the group, four are active; on the slopes of three volcanoes (Klyuchevskoy, Tolbachik and Tolbachinsky Dol, Ushkovsky) monogenic cones are widespread.

The hypothesis of the existence of a common magma chamber for all KGV, as well as independent magma cameras for each of these volcanoes, was first presented in the works of G.S. Gorshkov (1956) and B.I. Piip (1956). Magma chambers and cameras of the KGV volcanoes continue to be studied by geophysical and geological methods.

A generalized schematic tectonic map of the KGV is shown in the work (Girina, 2016). This scheme of principal fault zones in the area of the KGV was created on the basis of the analysis of a set of various published materials and numerous satellite data of middle and high resolution (MODIS, SRTM, Aster, Landsat, Meteor-M, Kanopus-B and the others), as well as on the author's studies of the volcanoes of the Klyuchevskaya group. It is shown that the faults ever formed here are long-lived and their activisation is associated with certain stages of the evolution of the KGV. The formation of all stratovolcanoes of KGV mainly happens owing to deep faults (1-3 on Fig. 2 from (Girina, 2016)) of the northwest, northeast and west-northwest directions. Regional zones of monogenic cones of the KGV, identified by B.I. Piip (1956), in the area of Ushkovsky, Tolbachik, and Klyuchevskoy volcanoes, are associated with the deep fault zones of the northwestern and northeastern directions. For example, one of these zones (6 on Fig. 2 from (Girina, 2016)) extends to the southeast and east slopes of Klyuchevskoy; according to B.I. Piip (1956), this fault zone was the reason for the beginning of the formation of Plosky Tolbachik volcano and the existence of a lava lake in its crater. It is characteristic, that the monogenic cones associated with this fault zone, break through the deposits of the andesitic volcanoes Zimina and Bezymianny. The fissure zone of north-north-eastern direction in the central part of the KGV is well expressed on the Tolbachinsky Dol and on the south-western slope of Ushkovsky volcano (7 on Fig. 2 from (Girina, 2016)). For example, on such of a fault the breakthrough of 50th anniversary of the IVS FEB RAS was formed on Tolbachinsky Dol in 2012-2013 (Girina, 2016). Another fissure zone (8 on Fig. 2 from (Girina, 2016)), on which young monogenic cones are planted, is well manifested on the Tolbachinsky Dol. For example, the Severny Proryv of 1975 was formed on such fissure. Probably, the activisation of faults 7 and 8 on the Tolbachinsky Dol affected the fault zone 6 (Girina, 2016), which more than once led to the disappearance of the lava lake after the formation of the collapse caldera at the top of Plosky Tolbachik volcano (Piip, 1956).

Rocks erupted by volcanoes and their monogenic cones of the KGV refer to the basalt-andesite-basalt formation (Ermakov, 1977), associated with extension zones and magma sources confined to the upper and middle mantle (Ivanov et al., 2001; Large Tolbachik…, 1984).

According to the petrochemical characteristics, the rocks of monogenic cones are divided into the following subtypes: magnesian basalts (Ushkovsky, Klyuchevskoy, Tolbachinsky Dol); high aluminous basalts (Klyuchevskoy, Tolbachinsky Dol); aluminous basaltic andesite, magnesian basaltic andesites (Klyuchevskoy) (Large Tolbachik…, 1984; Popolitov, Volynets, 1981; Volynets et al., 1976). The rocks of monogenic cones of Ushkovsky volcano are the most ancient rocks (pre-Holocene), and the cones of Klyuchevskoy and Tolbachinsky Dol - Holocene (Ponomareva et al., 2007).

The magnetic properties of the lavas of monogenic cones of Tolbachinsky Dol and Klyuchevskoy volcano were studied using the Kappameter (KT-6) field device (SatisGeo) (Girina, Bagenov, 2014, 2015). On Tolbachinsky Dol was studied a value of the magnetic susceptibility of lavas eruptions on 1975, 1941, 1000-1500 years ago (Kleshnya cone), and 1500-2000 years ago (lavas Maguskin field) (age of old lavas according of "Large Tolbachik…", 1984). On Klyuchevskoy volcano was studied a value of the magnetic susceptibility of lavas eruptions on 1945 (Zavaritsky), 1946 (Apakhonchich), 1956 (Kryzhanovsky). Lavas of Tolbachinsky Dol are

magnesian basalts (eruptions on 1941, and 1975), and aluminous basalts (eruptions of Kleshnya, and Maguskin field); lavas of Klyuchevskoy volcano are aluminous basalts (Girina, Bagenov, 2014, 2015; Large Tolbachik…, 1984).

The range of changes of the magnetic susceptibility value of the studied basalts of Tolbachinsky Dol is from 3 to 38 · 10^{-3} SI units (Fig. 1).

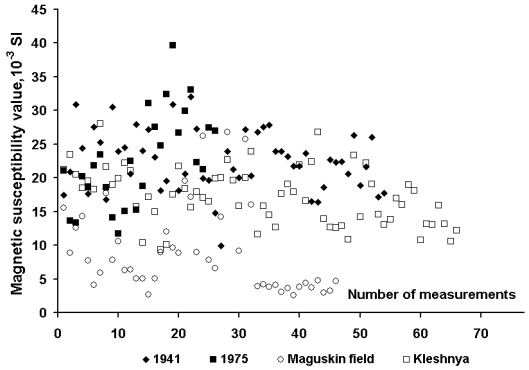

Fig. 1 – The value of magnetic susceptibility of the studied lavas of Tolbachinsky Dol.

The range of changes of the magnetic susceptibility value of the studied basalts of Klyuchevskoy volcano varies from 10 to 52 · 10^{-3} SI units (Fig. 2).

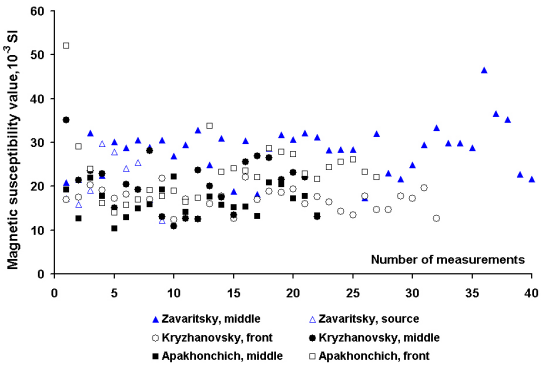

Fig. 2 – The value of magnetic susceptibility of the studied lavas of Klyuchevskoy volcano.

Magnesian basalts have higher magnetic susceptibility parameters compared to aluminous (the higher the MgO content in the rock, the higher the magnetic susceptibility of the rocks). Lavas of the Tolbachinsky Dol of eruptions on 1941 and 1975 have the highest average values of magnetic susceptibility, lavas of the Maguskin field - the lowest.

Although lavas are similar in petrographic characteristics, the magnetic susceptibility values of basalts of lava flows of the Zavaritsky cone is somewhat higher relative to other studied rocks due to their larger quantity of phenocrysts of dark-colored minerals.

References

Ivanov B.V., Popruzhenko S.V., Aprelkov S.E., 2001. The deep structure of the Central Kamchatka Depression and the structural position of volcanoes. Geodynamics and volcanism of the Kuril-Kamchatka Island arc system. Petropavlovsk-Kamchatsky: IVGG FEB RAS. 45–57.

Ermakov V.A., 1977. Formational dissection of Quaternary volcanic rocks. Moscow: Nedra, 224.

Girina O.A., 2016. Satellite high-resolution data to clarify the position of fault zones within Klyuchevskaya volcanic group of Kamchatka. Sovremennye problemy distantsionnogo zondirovaniya Zemli iz kosmosa 13/6: 148–156. doi: 10.21046/2070-7401-2016-13-6-148-156

Girina O.A., Bagenov E.V., 2014. About magnetic properties of Tolbachinsky Dol basalts, Kamchatka. Educatio, 3/7: 52-54. https://edu-science.ru/wp-content/uploads/2016/03/edu_3_p7_4-63.pdf

Girina O.A., Bagenov E.V., 2015. Magnetic properties of Klyuchevskoy volcano basalts. Evraziiskoe nauchnoe ob'edinenie 2/5(5): 175–177. https://elibrary.ru/item.asp?id=23527972

Gorshkov G.S., 1956. On the depth of the magma chamber of Klyuchevskoy volcano. Doklady AN SSSR 106/ 4: 703–705.

Large Tolbachik Fissure Eruption (1975–1976, Kamchatka) / Ed. S.A. Fedotov. 1984. Moscow: Nauka, 637.

Piip B.I., 1956. Klyuchevskaya sopka and its eruptions in 1944-1945, and last. Moscow: AN SSSR, 312.

Ponomareva V., Kyle P., Pevzner M. et al., 2007. Holocene eruptive history of Shiveluch Volcano, Kamchatka Peninsula, Russia. Volcanism and Subduction: the Kamchatka Region. Washington: AGU: 263–282.

Popolitov E.I., Volynets O.N., 1981. Geochemical features of Quaternary volcanism of the Kuril-Kamchatka Island arc and some issues of petrogenesis. Moscow: Nauka, 182 p.

The deep structure, seismicity and modern activities of the Klyuchevskaya group of volcanoes / Ed. B.V. Ivanov, S.T. Balesta, 1976. Vladivostok: FESC AN SSSR, 148.

Volynets O.N., Ermakov V.A., Kirsanov I.T., Dubik Yu.M., 1976. Petrochemical types of Quaternary basalts of Kamchatka and their geological position. Bulletin of Volcanological station 52: 115–126.

The lava field in the center of Dzendzur-Zhupanovsky volcanic group, Eastern Kamchatka

Natalia Gorbach[1] and Anastasiya Plechova[2]

[1]Institute of volcanology and seismology FEB RAS, Petropavlovsk-Kamchatsky 683006, Russia. n_gorbach@mail.ru
[2]Institute Vernadsky Institute of Geochemistry and Analytical Chemistry, Russian Academy of Sciences, Kosygina st., 19, Moscow, 11933, Russia.

Keywords: andesitic lava field

Dzendzur–Zhupanovsky volcanic group (Fig. 1) is situated 70 km north of Petropavlovsk-Kamchatsky in the Eastern Volcanic Belt, Kamchatka. The eastern sector of the volcanic group is occupied by four cones of Late Pleistocene-Holocene Zhupanovsky volcano including Priemysh cone, active from 2013 to 2017. The older eroded edifices of Yur'evskii, Sirenevyi and Dzendzur volcanoes composed the western sector of the volcanic group. The extensive lava field (see Fig. 1) flooded ancient volcanic edifices in the center of volcanic group. The area and volume of Dzendzur-Zhupanovsky lava field are significant compared to other known objects in Kamchatka. For example, its scale is comparable to the biggest object of monogenetic volcanism in Sredinny Range represented by the lava flows from Southern and Nortern Cherpuk cones near the Ichinsky volcano (Pevzner et al., 1999).

The Dzendzur-Zhupanovsky lava field as well as other volcanoes of this group remain poorly studied with respect to the geochemical evolution, age and eruptive history. The chronology of eruptive activity and data on rock composition were described only for the active Priemysh cone (Bazanova et al., 2009; Puzankov et al., 2016; Gorbach et al., 2018). The previous studies of lava field report the geological observation and a few whole rock composition data (e. g., Ermakov et al., 1973; Litvinov and Burmakov, 1993). We present the first geochemical data characterizing andesite and rare basaltic andesite lava from Dzendzur-Zhupanovsky lava field. We compare the obtained geochemical characteristics with the similar data for rocks of the recently erupted Priemysh cone to test the hypothesis of their genetic commonality.

The Dzendzur–Zhupanovsky lava field covered an area about 100 km^2. At least five eruptive centers (e.g., scoria and lava cones) are clearly visible in the aerial photographs. The most of eruptive centers were formed by a single eruption. The exception is Tetyaev crater, which produced multiple lava flows (Ermakov et al., 1973). The longest lava flows extend for 13-15 km from the eruptive centers. The average thickness of lava flows is about 30 m, but for the several lava lobes the thickness increases up to 80-100 m. The most of the flows have well expressed, prominent lava levees along the edges (see Fig. 1). Closer to the eruptive centers, the pressure ridges and huge sharp-angle lava blocks are observed on the surface of lava flows. Based on geological observation, Ermakov et al. (1973) suggested that the lava field has Middle-to-Late Holocene age.

The lavas sampled from the central part of lava field and from Tetyaev crater are mainly of andesitic composition (SiO_2~59-61 wt. %). Basaltic andesite lavas (SiO_2~56 wt. %) compose several flows in the vicinity of Dzendzur volcano edifice.

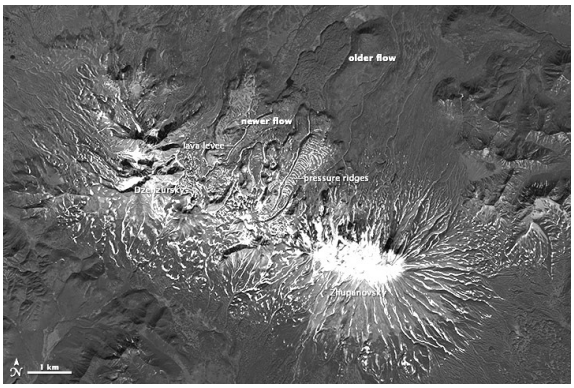

Fig. 1 – The Dzendzur-Zhupanovsky volcanic group with extensive lava field in the center.
Airphoto taken from https://earthobservatory.nasa.gov/

All lavas are crystal-rich with modal abundance of phenocrysts of ~30-35 %. The dominant lava type is plagioclase-two pyroxene andesite with sporadic hornblende and olivine phenocrysts. In lower-SiO_2 rock varieties the amount of olivine increases and hornblende occurs very rarely. The rocks commonly have the complex texture including resorbed phenocrysts and clots of plagioclase and pyroxenes, xenogenic quartz grains, and microxenoliths of plutonic rock.

The basaltic andesite and andesite lavas have calc-alkaline affinity (FeO*/MgO~1.20-1.76) and moderate potassium contents (K_2O~0.97-1.32 wt.%). The basaltic andesites are characterized by elevated Mg-number (Mg/Mg+Fe^{2+} up to ~0.60). With MgO decrease, the compositions of all rocks form narrow, but common evolutional trends suggesting the fractional crystallization processes.

The preliminary comparison of obtained petrographical and geochemical data for the lava field rocks with the known data for the active Priemysh cone (Bazanova et al., 2009; Puzankov et al., 2016; Gorbach et al., 2018) indicates their similarity. Both lava field and Priemysh cone rocks are characterized by the identical patterns of the

rare-earth elements and similar enrichment in the large-ion lithophile elements (e.g., Rb~15-25, Sr~369-437, Ba~285-438 ppm) and in the high field strength elements (e.g., Zr~100-149, Nb~2.4-3.4, Ta~0.19-0.26 ppm). The geochemical similarity and approximately simultaneous Middle-to-Late Holocene eruptive period (e.g., Ermakov et al., 1973; Bazanova et al., 2009) may imply that the rocks of lava field and Priemysh cone are genetically related and originated from a common parental magma. On the contrary, a comparison of the geochemical data for lava field and Priemysh cone rocks with the data reported by Plechova et al. (2011) for primary magma of Zhupanovsky volcano indicates the difference in many petrogenetic indicators (e.g., Mg-number, Zr/Y, Nb/Y, Zr/Nb, Th/La, Ba/Nb, Ba/Th).

The obtained data highlights the complex petrogenetic history of Dzendzur-Zhupanovsky lava field as a part of long-lived and large volcanic system. As has been shown by Smith and Németh (2017) such volcanic setting is transient between polygenetic and monogenetic volcanism and commonly associated with internally complicated plumbing systems. Further studies of Dzendzur-Zhupanovsky lava field may target on mineral composition and zoning patterns for improving of our understanding of processes of magma storage and evolution in the transitional condition between polygenetic and monogenetic volcanoes.

Our preliminary data also may be important for the assessment of the volcanic hazard in Dzendzur-Zhupanovsky volcanic group. The similarity of the composition and the approximately simultaneous past eruptions from lava field and Priemysh cone allow us to suggest a possibility of such a scenario for the future. On resuming of activity in the lava field, long lava flows may spread mainly to the north and the south of the axial part of the Dzendzur-Zhupanovsky volcanic group. In this case, the lava flows and potentially associated lahars may threaten the Zhupanova River valley.

References

Bazanova, L.I., Dirksen, O.V., Kulish, R.V. and Kartasheva E.V., 2009. Evolution of recent volcanism of Zhupanov ridge (Kamchatka) // In Gordeev E.I. (eds), Proceedings of the IV All-Russian Symposium of Volcanology and Paleovolcanology, Petropavlovsk-Kamchatsky: 265–268.

Gorbach, N.V., Plechova, A.A., Manevich, T.M., Portnyagin, M.V., Philosofova, T.M., Samoilenko, S.B., 2018. Composition of vocanic ash and the dynamics of the 2013-2013 Zhupanovsky volcano eruption //Journal of Volcanology and Seismology 12 (3): 155–171. DOI: 10.1134/S0742046318030028

Masurenkov Yu. P., Florensky I.V., Melekestsev I.V., 1991. Zhupanovsky volcano In: Fedotov SA, Masurenkov YP (eds) Active volcanoes of Kamchatka, vol 1. Nauka Press, Moscow: 84–103.

Ermakov, V.A., Volynets, O.N., and Sapozhnikov, E.A., 1973. The Dzenzur–Zhupanovsky volcanic cluster. Byull. Vulkanol. St. 49: 36–41.

Litvinov, A.F. and Burmakov, Yu.A., 1993. The geological struc-ture and Quaternary volcanism of the Zhupanov mountain range, eastern Kamchatka. Vulkanol. Seismol 2, 16–26.

Pevzner, M.M., Melekestsev, I.V., Volynets, O.N., Melkiy, V.A. 1999. South Cherpuk and North Cherpuk - the Largest Holocene Monogenetic Volcanoes on the Sredinnyi Range of Kamchatka. Journal of Volcanology and Seismology 6: 22–32.

Plechova, A.A., Portnyagin, M.V., and Bazanova, L.I., 2011. The origin and evolution of primary magmas in frontal volcanoes of Kamchatka based on a study of magmatic inclusions in the olivine of Zhupanovsky Volcano. Geokhimiya 8: 787–812.

Puzankov, M.Yu., Bazanova, L.I., Dirksen, O.V., et al., 2016. Hybrid lavas of Priemysh cone: The Zhupanovsky Vol-canic Cluster, Kamchatka. In Proceeding of regional conference Volcanism and Associated Processes Devoted to Volcanologist's Day, March 29–30, 2016, Petropavlovsk-Kamchatskii: IViS DVO RAN: 139–145.

Smith, I. E. M., Németh, K., 2017. Source to surface model of monogenetic volcanism: a critical review. Geological Society, London, Special Publications 446: 1−28.

Olivine phenocrysts from Kamchatka show Fo and Ni relative diffusivities

Boris Gordeychik[1, 2], Tatiana Churikova[2, 3], Andreas Krontz[2], Gerhard Worner[2]

[1]*Institute of Experimental Mineralogy RAS, Chernogolovka 142432, Russia. gordei@mail.ru*
[2] *Geowissenschaftliches Zentrum Göttingen, Abteilung Geochemie, Universität Göttingen, Göttingen, 37077, Germany.*
[3]*Institute of Volcanology and Seismology FEB RAS, Petropavlovsk-Kamchatsky 683006, Russia.*

Keywords: Kamchatka, olivine, diffusion.

Diffusion coefficients for Fo and Ni in olivine (D_{Fo} and D_{Ni}) are available for temperatures from 750 to 1400 °C, experiments were carried out on high-Fo olivine close to Fo_{90}, from 1 bar to 120 kbar pressure, and an oxygen fugacity between 10^{-10} and 10^{-4} Pa, see review in (Chakraborty, 2010). Chakraborty (2010) built a set of formulas that quantitatively describe the dependency of D_{Ni} and D_{Fo} on olivine composition, P-T-fO_2 conditions, and crystal orientation. Dohmen et al. (2007) and Chakraborty (2010) noted D_{Ni} may be "*slightly slower*" or "*slightly smaller*" compared to D_{Fo}. At the same time, other authors found D_{Ni} might be slightly higher than D_{Fo} under some conditions (e.g. Fig. 1 from Lynn et al., 2018). Given these uncertainties, we evaluate existing information about the relative diffusivities of Fo and Ni, which is crucial for the analysis of the Fo-Ni relationships.

If zoning in a natural olivine crystal can be attributed to diffusion, then Fo and Ni variations can be used to assess the relative values of diffusivities. The classical analytical solution of diffusion in a semi-infinite media (Crank, 1975) allows to fined relations between diffusion coefficients and the widths of diffusion zones δ_{Fo} and δ_{Ni}:

$$\delta_{Fo,Ni} = 2 \cdot \sqrt{D_{Fo,Ni} t}, \qquad \frac{D_{Ni}}{D_{Fo}} = \left(\frac{\delta_{Ni}}{\delta_{Fo}}\right)^2. \qquad (1)$$

Combined measurements of Fo and Ni in olivine has been documented in several studies (e.g. Costa and Dungan, 2005; Qian et al., 2010; Lynn et al., 2017a, 2017b, 2018; Gordeychik et al., 2018). The data make it possible to evaluate the D_{Ni}/D_{Fo} by two ways: (1) through the widths of diffusion zones, using Eq. 1; and (2) using formulas in (Chakraborty, 2010).

(1) Olivine compositions measured along some profiles from above publications with distinct Fo and Ni zoning were used to determine the widths of diffusion zones. The ratios D_{Ni}/D_{Fo} were extracted from the ratios δ_{Fo}/δ_{Ni} using Eq. 1 for three natural examples (Costa and Dungan, 2005; Qian et al., 2010; Lynn et al., 2017a, 2017b, 2018) and belong to the vertical axis in Fig. 1. The effective temperatures of the diffusion profiles formation were specified by the above authors and belong to the horizontal axis. All results show that the D_{Ni}/D_{Fo} ratios calculated from the relative diffusion zone widths are always less than unity.

The zoning patterns used in this approach were all made on the rims of olivine crystals. In this case a variety of edge phenomena can influence the zoning pattern. Better information should be gained from diffusion zones from inside crystals.

Complexly zoned olivine phenocrysts from the 7600 BP Shiveluch eruption preserve distinct Fo and Ni concentration gradients at the boundary between low-Fo low-Ni cores and high-Fo high-Ni overgrowths (Fig. 2a). A simple diffusion model of a semi-infinite space (Crank, 1975) can be used to describe symmetrical Fo and Ni profiles across the core/overgrowth boundary. Fo and Ni diffusion zones widths are shown in Fig. 2a and their ratio of δ_{Ni}/δ_{Fo} is about 0.4.

Newly collected Fo and Ni data in olivine crystals from the 3600 BP Shiveluch eruption (Fig. 2b) and from the Bulochka and Novograblenov cones of Klyuchevskoy volcano (Fig. 2c) give similar relationships. Despite their different provenance, these olivine phenocrysts show the diffusion zones that are both narrower in Ni compared to Fo (Figs. 2b, c) with calculated diffusivity ratios of D_{Ni}/D_{Fo}=0.45 for Shiveluch 3600 BP eruption and D_{Ni}/D_{Fo}=0.51 for Klyuchevskoy

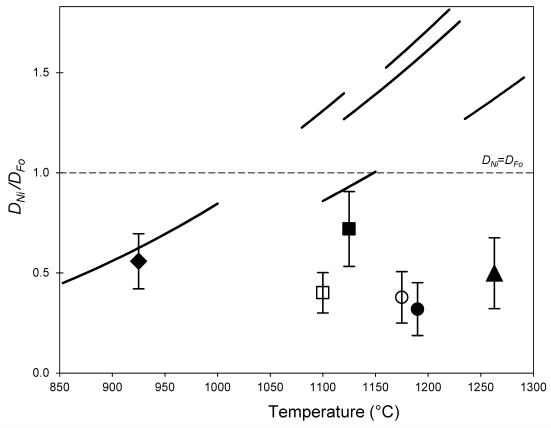

Volcano studied	D_{Ni}/D_{Fo} through δ_{Ni}/δ_{Fo}	Compositional and thermodynamic conditions: Fo (mol%)	Temperature interval (°C)	Pressure (bar)	Fugacity buffer
Tatara-San Pedro (Costa & Dungan, 2005)	■	82	1 100 - 1 150	3 000	NNO
Handan-Xingtai (Qian *et al.*, 2010)	◆	91	850 - 1 000	4 000	QFM+0.75
Kllauea (Lynn *et al.*, 2017a; 2017b; 2018)	▲	85	1 235 - 1 291	850	QFM
Shiveluch 7600 BP (Gordeychik *et al.*, 2018)	●	90	1 160 - 1 220	8 000	QFM+1
Shiveluch 3600 BP (this study)	□	86	1 080 - 1 020	8 000	QFM+2.1
Klyuchevskoy, high-Mg basalt (this study)	○	87	1 120 - 1 230	7 500	QFM+1.3

Fig. 1 – Relative values of diffusion coefficients for Fo and Ni in olivine expressed as D_{Ni}/D_{Fo} for different conditions. Each symbol represents an average value of D_{Ni}/D_{Fo} ratio calculated by Eq. 1 for several profiles from nature examples found in the corresponding literature reference. The error bars reflect the average of absolute deviation for several considered profiles from each example. Solid curves show the D_{Ni}/D_{Fo} ratio calculated by formulas from (Chakraborty, 2010) under the compositional and thermodynamic conditions from the legend.

high-Mg basalts.

2) Curves in Fig. 1 show D_{Ni}/D_{Fo} ratios calculated by formulas for Fo and Ni (Chakraborty, 2010) under compositional and thermodynamic conditions documented in the corresponding references. The thermodynamic conditions for the 3600 BP Shiveluch eruption were based on (Gorbach and Portnyagin, 2011; Nekrylov et al., 2018), and for Bulochka and Novograblenov cones on (Mironov et al., 2015; Nekrylov et al., 2018). The ratios D_{Ni}/D_{Fo} calculated by (Chakraborty, 2010) are in good agreement with those obtained by δ_{Fo}/δ_{Ni} ratios at the temperatures of 850-1000 °C, but differs at temperatures over 1100°C up to 5 times and exceeds unity.

Such discrepancies between estimates leads us to conclude that Fo and Ni diffusion coefficients from formulas (Chakraborty, 2010) may not be applicable in all cases and these formulas should be used with some caution. We should assume that for a reasonable range of pressures, temperatures, and oxygen fugacity, the D_{Ni} should always be lower than D_{Fo}.

Apparently, D_{Ni} and D_{Fo} are similar within experimental uncertainties, and D_{Ni}/D_{Fo} ratios are poorly constrained by formulas and allow for $D_{Ni}/D_{Fo}>1$ that we, however, do not observed in natural samples. This discrepancy may also be due to the fact that natural olivine crystals may reflect conditions different from experiments. Another reason may be the fact that the compositional and/or thermodynamic conditions for the natural samples are outside the permissible limits of the validity of the formulas (Chakraborty, 2010).

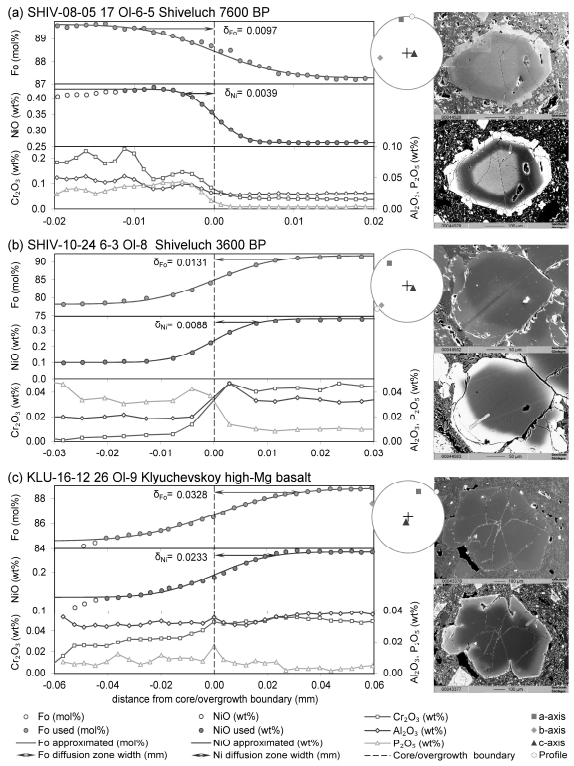

Fig. 2 – Comparison of the diffusion zone widths for Fo and Ni in representative core-overgrowth profiles inside the olivine phenocrysts from Kamchatka rocks: (a) – Shiveluch eruption 7600 BP; (b) – Shiveluch eruption 3600 BP; (c) – Bulochka and Novograblenov monogenetic cones of Klyuchevskoy volcano. Zero point at x-axis and dashed line are the boundary between core on the right and overgrowth on the left. The projections of a-, b-, and c-axes of crystals as well as profile orientation shown at stereographic lower hemisphere plot. SEI picture shows the common view of olivine phenocryst in thin section with position of measured profile relatively the crystal boundaries. COMPO picture shows the position of profile relatively the core/overgrowth boundary. Filled and open circles are EPMA measured data, used and not used in the calculations, respectively. The solid lines show the analytical solutions for diffusion in a semi-infinite media. Arrows with values mark Fo and Ni diffusion zone widths, which give D_{Ni}/D_{Fo}=0.16 for (a), 0.45 for (b), and 0.51 for (c) using Eq. 1. Cr-Al-P plot show variations in olivine composition through the core/overgrowth boundary.

Acknowledgements

This research was supported by DFG grant No. Wo 362/51-1, RFBR-DFG grant No. 16-55-12040.

References

Chakraborty, S., 2010. Diffusion coefficients in olivine, wadsleyite and ringwoodite. Rev. Min. Geochem. 72 (1): 603–639.

Costa, F., Dungan, M., 2005. Short time scales of magmatic assimilation from diffusion modeling of multiple elements in olivine. Geology 33(10): 837–840.

Crank, J., 1975. The Mathematics of Diffusion. Oxford.

Dohmen, R., Becker, H.-W., Chakraborty, S., 2007. Fe–Mg diffusion in olivine I: experimental determination between 700 and 1,200°C as a function of composition, crystal orientation and oxygen fugacity. Phys. Chem. Minerals 34(6): 389–407.

Gorbach, N.V., Portnyagin, M.V., 2011. Geology and petrology of the lava complex of Young Shiveluch Volcano, Kamchatka. Petrol. 19(2): 134–166.

Gordeychik, B., Churikova, T., Kronz, A. et al., 2018. Growth of, and diffusion in, olivine in ultra-fast ascending basalt magmas from Shiveluch volcano. Sci. Rep. 8(11775): 1–15.

Lynn, K.J., Garcia, M.O., Shea, T. et al., 2017a. Timescales of mixing and storage for Keanakāko‘i Tephra magmas (1500–1820 C.E.), Kīlauea Volcano, Hawai‘i. Contrib. Mineral. Petrol. 172(9): 76(1–20).

Lynn, K.J., Shea, T., Garcia, M.O. et al., 2018. Lithium diffusion in olivine records magmatic priming of explosive basaltic eruptions. Earth Planet. Sci. Let. 500: 127–135.

Lynn, K.J., Shea, T., Garcia, M.O., 2017b. Nickel variability in Hawaiian olivine: Evaluating the relative contributions from mantle and crustal processes. Amer. Mineral. 102(3): 507–518.

Mironov, N., Portnyagin, M., Botcharnikov, R. et al., 2015. Quantification of the CO_2 budget and H_2O–CO_2 systematics in subduction-zone magmas through the experimental hydration of melt inclusions in olivine at high H_2O pressure. Earth Planet. Sci. Let. 425: 1–11.

Nekrylov, N., Portnyagin, M.V., Kamenetsky, V.S. et al., 2018. Chromium spinel in Late Quaternary volcanic rocks from Kamchatka: Implications for spatial compositional variability of subarc mantle and its oxidation state. Lithos 322: 212–224.

Qian, Q., O'Neill, H.S.C., Hermann, J., 2010. Comparative diffusion coefficients of major and trace elements in olivine at ~950 °C from a xenocryst included in dioritic magma. Geology 38(4): 331–334.

Diverse origins of high-Nb basalts in volcanic arcs

Pavel Kepezhinskas[1] and Nikita Kepezhinskas[2]

[1] *PNK GeoScience, Tampa, Florida, USA.pavel_k7@yahoo.com*
[2]*Earth and AtmosphericSciences, University of Alberta, Edmonton, Alberta, Canada*

Keywords: high-Nb basalt, adakite-peridotite interaction, OIB.

High-Nb basalts (HNBs) are small-volume, high field strength (HFS) element-enriched melts in volcanic arcs otherwise dominated by HFSE-depleted volcanic rocks. They typically form monogenetic volcanoes, dikes and cinder cones and are frequently associated with adakites (Defant and Kepezhinskas, 2001). HNBs are aphyric to weakly porphyritic rocks with olivine, Ti-augite, plagioclase and minor amphibole phenocrysts. They display high TiO_2 (> 1 wt.%) and Nb (> 20 ppm) contents along with elevated total alkalinity (mostly Na_2O) in comparison to typical calc-alkaline arc basalts (Kepezhinskas et al., 1996). Differentiated variaties with somewhat lower Nb contents (10-20 ppm) were termed Nb-enriched arc basalts and basaltic andesites (NEABs) or Nb-enriched basalts (NEBs).

Trace element compositions of HNBs, especially their enrichment in large-ion lithophile and HFS elements, are remarkably similar to the ocean island basalts (OIB), especially of EM-I and EM-II types, as well as low-degree E-MORB melts (Fig. 1). Other

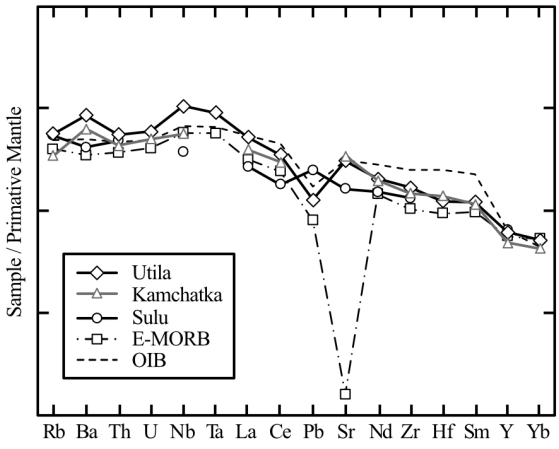

Fig. 1 – Trace element compositions of HNBs from Honduras (Kepezhinskas et al., 2020), Kamchatka (Kepezhinskas et al., 1997) and Sulu arc (Macpherson et al., 2010) compared to low-degree E-MORB melt (Kamenetsky et al., 2000) and OIB (Sun and McDonough, 1989).

distinct geochemical features of the HNB clan include high Nb/U (> 10), Nb/La (> 1), Zr/Sm (> 25) and low Ba/Nb and Ba/La ratios (Kepezhinskas et al., 1996; 2020).These HFSE-enriched trace element patterns have been interpreted as evidence for involvement of enriched, OIB-type mantle sources in arc petrogenesis (Macpherson et al., 2010). This is, however, contradicted by Sr, Nd and Pb isotope co-variations in HNBs (Fig. 2), which suggest diversity of mantle sources and petrogenetic processes involved in their generation (Kepezhinskas et al., 2020). HNBs with highest Nb contents (30 ppm and higher) and Nb/LREE or Nb/LILE ratios, such as Kamchatka and Honduras, also display the most depleted Sr and Nd isotopic compositions (Fig. 2), similar to the Pacific MORB, and usually somewhat even more depleted than the associated "normal" arc lavas (Kepezhinskas et al., 1997). Pb isotopes in these isotopically depleted HNBs also point to MORB-type mantle sources, although a minor (1-3%) involvement of subducted sediment (comparable to EM-I and EM-II Pb-isotope signature) was also detected in both Kamchatka and Honduras (Kepezhinskas et al., 1997; 2020).

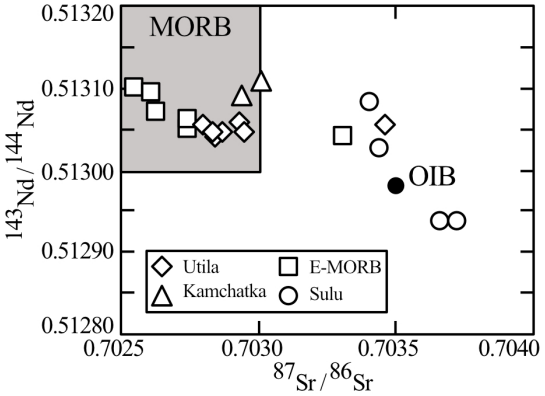

Fig. 2 – Sr and Nd isotopes in HNBs from Honduras (Kepezhinskas et al., 2020), Kamchatka (Kepezhinskas et al., 1997) and Sulu arc (Macpherson et al., 2010) compared to low-degree E-MORB melts (Kamenetsky et al., 2000).

HNBs with enriched Sr-Nd-Pb isotope signature (Sulu arc, Baja California) plot into OIB fields and most probably reflect involvement of an enriched mantle component (Fig. 2; Macpherson et al., 2010).

Frequent (but not universal) association of HNBs with adakites allowed us to propose that slab melt hybdridization of the depleted sub-arc mantle may produce mantle sources with metasomatic mineral assemblages that can carry substantial HFSE (Kepezhinskas et al., 1996). HFSE-enriched minerals, such as amphibole, titanite and rutile have been produced in experiments (Proteau et al., 2001) and observed in subduction-related accretionary complexes (Zhang et al., 2015). Presence of adakitic glasses (Kepezhinskas et al., 1996) and veins (Shimizu et al., 2004) rimmed by amphibole and other metasomatic phases in subduction-related mantle peridotites suggest that slab melt-peridotite interaction is an important petrogenetic process responsible for HFSE recycling in volcanic arcs.

Accreted terranes of the Routan Island in Honduras contain ultramafic rocks impregnated (Fig.

3A) by veins (cm) and dikes (up to 1 m) of adakitic affinity (Sr/Y=40-288). Rutile and titanite developed along the ultramafic/felsic contacts (Fig. 3B) exhibit clear enrichment in Nb and Ta (Fig. 3C-D). Melting of such slab melt-hybridized mantle source will inevitably generate arc basalts enriched in HFSE (Nb) in respect to LILE and LREE.

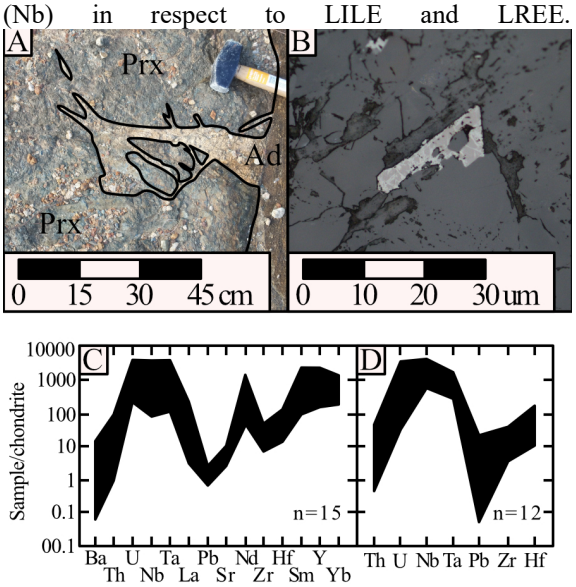

Fig. 3 – Interaction between adakite (Ad) and ultramafic rock (Prx) in Honduras (A), hybrid rutile-titanite(B) and trace element compositions (LA-ICPMS) of hybrid titanite (C) and rutile (D).

We propose three principal models for high-Nb basalts formation in arcs on the basis of their geologic and geochemical characteristics (Kepezhinskas et al., 2020). Type 1 HNBs are found in both back-arc (Honduras), behind-the-front (Kamchatka) and arc front (Kamchatka, Jamaica, Grenada) environments with or without contemporary adakites. They display MORB-like Sr-Nd-Pb isotope signatures together with highest alkalinity and OIB-like trace element geochemistry. Type 1 HNBs are believed to be generated via melting of slab melt-hybridized sub-arc peridotite mantle. Type 2 HNBs essentially have OIB-like Sr-Nd-Pb isotopes and are believed to derive from enriched OIB-like mantle sources isolated, one way or another, among the depleted mantle wedge lithologies (Castillo et al., 2007). This is achieved either through influx of asthenospheric mantle through slab windows after cessation of active subduction (Baja California) or mixing between enriched and depleted components within a compositionally heterogeneous mantle wedge (Sulu). Third potential mechanism of HNB formation involves low degrees of melting of enriched MORB mantle, possibly in a leaky transform environment (Kamenetsky et al., 2000; Kepezhinskas et al., 2020). However, this model requires a very specific set of geologic conditions, which so far were not documented in volcanic arcs. In conclusion, HNBs are rare lavas produced under unique petrogenetic conditions in volcanic arcs, where they are frequently associated with giant epithermal gold and copper porphyry deposits (Philippines, Lihir, Indonesia, Papua New Guinea).

References

Castillo, P.R., Rigby, S.J., Solidum, R.U., 2007. Origin of high field strength element enrichment in volcanic arcs: geochemical evidence from the Sulu Arc, southern Philippines. Lithos 97: 271–288.

Defant, M.J., Kepezhinskas, P.K. 2001. Evidence suggests slab melting in arc magmas. EOS, 82: 65–69.

Kamenetsky, V.S., Everard, J.L., Crawford, A.J., Varne, R., Eggins, S.M., Lanyon, R., 2000. Enriched end-member of primitive MORB melts: petrology and geochemistry of glasses from Macquarie Island (SW Pacific). Journal of Petrology 41: 411–430.

Kepezhinskas, P., Defant, M.J., Drummond, M.S., 1996. Progressive enrichment of island arc mantle by melt-peridotite interaction inferred from Kamchatka xenoliths. Geochimica et Cosmochimica Acta 60: 1217–1229.

Kepezhinskas, P., McDermott, F., Defant, M.J., Hochstaedter, A., Drummond, M.S., Hawkesworth, C.J., Koloskov, A.V., Maury, R.C., Bellon, H., 1997. Trace element and Sr-Nd-Pb isotopic constraints on a three-component model of Kamchatka Arc petrogenesis. Geochimica et Cosmochimica Acta 61: 577–600.

Kepezhinskas, N., Kamenov, G.D., Foster, D.A., Kepezhinskas, P., 2020. Petrology and geochemistry of alkaline basalts and gabbroic xenoltihsfrom Utila Island (Bay Islands, Honduras): insights into back-arc processes in the Central American Volcanic Arc. Lithos 352–353:105306.

Macpherson, C.G., Chiang, K.K., Hall, R., Nowell, G.M., Castillo, P.R., Thirlwall, M.F., 2010. Plio-Pleistocene intra-plate magmatism from the southern Sulu Arc, Semporna peninsula, Sabah, Borneo: implications for high-Nb basalt in subduction zones. Journal of Volcanology and Geothermal Research 190: 25–38.

Proteau, G., Scaillet, B., Pichavant, M., Maury, R.C., 2001. Evidence for mantle metasomatism of hydrous silicic melts derived from subducted oceanic crust. Nature 410: 197–200.

Shimizu, Y., Arai, S., Morishita, T., Yurimoto, H., 2004. Petrochemical characteristics of felsic veins in mantle xenoliths from Tallante (SE Spain): an insight into activity of silicic melt within the mantle wedge. Transactions of Royal Society Edinburgh 95: 265–276.

Sun, S.-s., McDonough, W.F., 1989. Chemical and isotopic systematics of oceanic basalts: implications for mantle composition and processes. Geological Society of London Special Publication 42: 313–345.

Zhang, G., Niu, Y., Song, Sh., Zhang, L., Tian, Z., Christy, A.G., Han, L., 2015. Trace element behavior and *P-T*-t evolution during partial melting of exhumed eclogite in the North Qaidam UHPM belt (NW China): implications for adakite genesis. Lithos 226: 65–80.

Metals, melts and fluids in island-arc mantle: new evidence from Avachinsky xenoliths (Kamchatka)

Pavel Kepezhinskas[1], Nikolai Berdnikov[2] and Nikita Kepezhinskas[3]

[1] *PNK GeoScience, Tampa, Florida, USA. pavel_k7@yahoo.com*
[2]*Institute of Tectonics and Geophysics, Khabarovsk, Russia*
[3]*Earth and AtmosphericSciences, University of Alberta, Edmonton, Canada*

Keywords: Metal-rich melts, slab fluids, mantle metasomatism.

Previous studies of Avachinsky xenoliths established their origin in the convecting mantle wedge beneath the Kamchatka arc at equilibration temperatures of 890-1100^{0}C and pressures of 1 to 1.8 GPa (Kepezhinskas et al., 2002; Benard and Ionov, 2012). They exhibit numerous modal (Opx- and Cpx-rich veins, replacement of Ol with Opx, interstitial glass and amphibole, Cr-poor, Al-rich spinel, fluid inclusions) and cryptic (Ba, Rb, Sr, U, LREE enrichment of bulk-rock and silicate minerals) metasomatic features previously linked to a) hydrous, Cl-rich slab-derived fluid (Ishimari et al., 2009); b) carbonate-rich melt from the old Pacific slab (Kepezhinskas and Defant, 1996; Widom et al., 2003); c) hydrous melt of adakitic affinity (Ishimari et al., 2009); d) melt of low-Caboninitic affinity (Benard and Ionov, 2012).

Our samples are vein-free spinel harzburgites composed of olivine (Fo_{90-93}), Opx (Mg#=90.8-91.7), spinel (Cr#=61-81) with minor amounts of modal Cpx (Mg#=92-94), pargasitic amphibole (Al_2O_3=8-12 wt.%) and typical, arc-related depleted bulk chemistry (Al_2O_3=0.14-2.34 wt.%; CaO=0.25-1.94 wt.%). Avachinsky peridotites contain texturally and compositionally exotic mineral phases recording a complex mantle refertilization history beneath the southern Kamchatka arc.

Porphyroclastic olivine and orthopyroxene in Avachinsky samples include euhedral to sub-hedral native metals such as platinum, iron, copper, silver, lead and zinc (Fig. 1) as well as Cu-Ag alloys and Fe-carbides. Native Ni, Fe and Fe-silicides were reported earlier by Ishimari et al. (2009). Occurrence of native metals along with carbides and silicides in Avachinsky nodules suggests existence of locally reduced conditions within otherwise oxidized mantle wedge beneath Kamchatka.

Avachinsky harzburgites contain several exotic metasomatic phases either as inclusions in orthopyroxene or discrete grains associated with pyroxene-amphibole-chlorite mineral aggregates (Fig. 2). Orthopyroxene porphyroclasts contain armalcolite with variable minor concentrations of Ce,Nd, Y and Th (Fig. 2A-B). One Opx grain includes La-Ce-bearing barite (Fig. 2C), while an Opx-Cpx-chlorite aggregate carries native silver and unnamed La-Ce-bearing Ti-silicate (Fig. 2D).

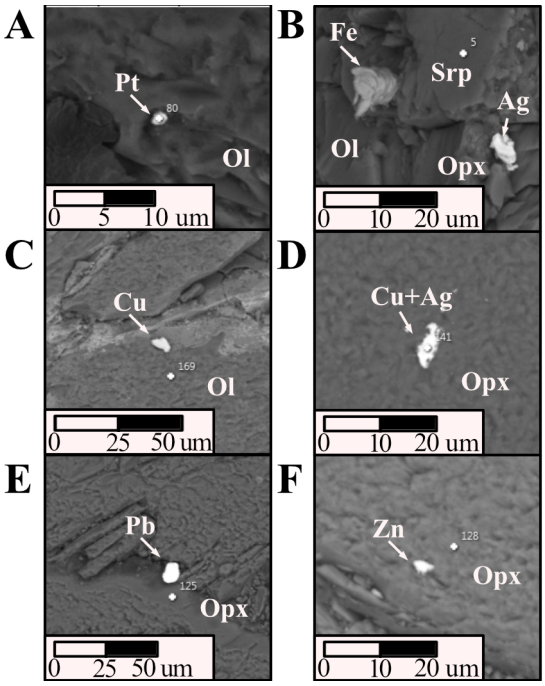

Fig. 1 – Native metals: platinum (A), iron and silver (B), copper (C), cupriferous silver (D), lead (E) and zinc (F). Ol - olivine, Opx - orthopyroxene, Srp - serpentine.

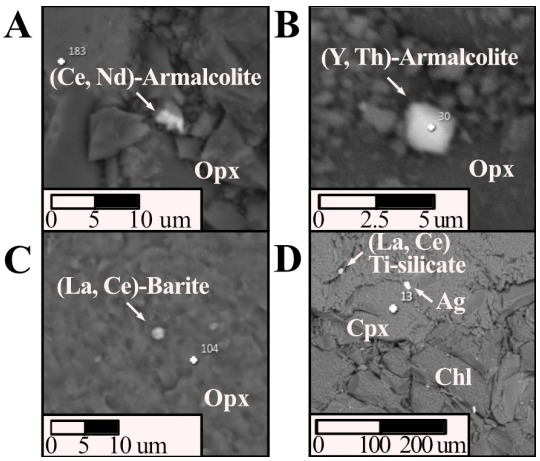

Fig. 2 – Metasomatic phases: (Ce,Nd) (A) and (Y,Th) (B) armalcolites, (La,Ce) barite (C) and (La,Ce) Ti-silicate (D). Opx - orthopyroxene, Cpx - clinopyroxene, Chl - chlorite, Ag - native silver.

Besides the native metals and LREE/HFSE-bearing metasomatic phases, Avachinsky xenoliths contain additional textural and compositional evidence for intense percolation of various melts and fluids through the sub-Kamchatkan mantle wedge. Halogen-bearing slab fluids are represented by cyrargyrite(Fig. 3A). In addition to discrete euhedral

to anhedral Cu-Fe-S grains, droplets of Ni-Fe-S composition (Fig. 3B) are entrapped in olivine representing sulfide melt "frozen" in sub-arc mantle.

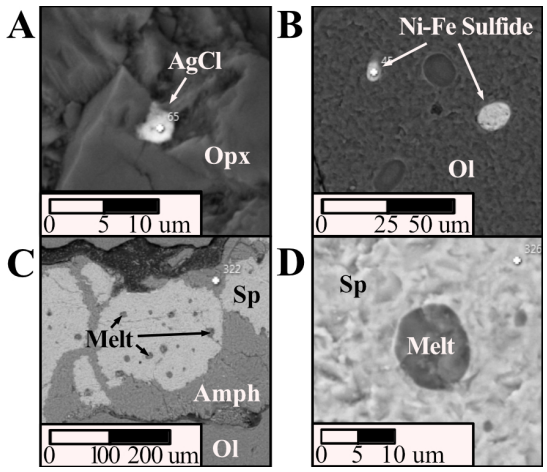

Fig. 3 – "Frozen" fluids and melts. A – cerargyrite (AgCl) inclusion. B - droplets of sulfide melt. C-D - droplets of high-Na-Al felsic melt. Ol - olivine, Opx - orthopyroxene, Amph - pargasitic amphibole, Sp - Cr-Al-Fe-Mg spinel.

Cr-Al-Fe-Mg spinels in some Avacha peridotites contain numerous droplet-shaped inclusions, which reflect chemical mixture of feldspar and amphibole (Fig. 3 C–D) and which compositionally resemble Na-Al-rich felsic melts in other sub-arc peridotite xenoliths (Wang et al, 2007).

These mineral assemblages reflect multi-stage metasomatism of island-arc mantle by melts and fluids. REE/HFSE-bearing minerals (armalcolite, barite, Ti-silicate, baddeleyite) suggest involvement of carbonated alkaline melt, possibly similar to the slab-derived, carbonate- and sulfate-rich phonolite (McInnes and Cameron, 1994). This is consistent with Os-isotope systematics of Kamchatka mantle xenoliths (Widom et al., 2003). Silver salts reflect percolation of slab-derived, chlorine-rich fluids, which might or might not be associated with the carbonated slab melt. This is supported by elevated halogen content (mostly F and Cl, with minor I and Br) of our Avachinsky peridotite samples as indicated by detailed SEM mapping. Sulfide droplets suggest presence of immiscible sulfide melt similar to primitive Tolbachik basalt (Zelenski et al., 2018), while Na-Al-rich felsic inclusions in spinel from Avachinsky xenoliths most probably record percolation of slab-derived melts with possible adakitic affinity. Occurrence of native metals, alloys and carbides suggests existence of localized highly-reduced conditions in the Kamchatka mantle. Formation of metallic phases may be related to serpentinization-deserpentinization reactions in the water-peridotite system related to slab devolatilization and release of aqueous fluids into the mantle wedge. It is important to emphasize that melting of organic-rich sediment on top of subducted basalt is capable of producing low fO_2 conditions in the overlying mantle wedge (Wang et al., 2007). Kamchatka trench-fill sediments are rich in organic matter (Romankevich and Artemiev, 1969) and Sr-Nd isotopic signature of Avachinsky peridotites allows possible sediment involvement. We suggest that mantle wedge beneath Kamchatka records prolonged history of metasomatism by a wide range of subduction components reflecting compositional heterogeneity of downgoing oceanic slab, highly variable conditions of its devolatilization and melting, as well as complex melt extraction-refertilization history of the island-arc mantle under a wide range of redox conditions.

References

Benard, A., Ionov, D.A., 2012. Melt- and fluid-rock interaction in supra-subduction lithospheric mantle: evidence from andesite-hosted veined perdiotite xenoliths. Journal of Petrology 54: 2339–2378.

Ishimari, S., Arai, S., Shukuno, H., 2009. Metal-saturated peridotite in the mantle wedge inferred from metal-bearing peridotite xenoliths from Avacha volcano, Kamchatka. Earth and Planetary Science Letters 284: 352–360.

Kepezhinskas, P., Defant, M.J., 1996. Contrasting styles of mantle metasomatism above subduction zones: constraints from ultramafic xenoliths in Kamchatka. Subduction: Top to Bottom, AGU Geophysical Monograph 86: 307–314.

Kepezhinskas, P., Defant, M.J., Widom, E., 2002. Abundance and distribution of PGE and Au in the island-arc mantle: implications for sub-arc metasomatism. Lithos 60: 113–128.

McInnes, B.I.A., Cameron, E.M., 1994. Carbonated, alkaline hybridizing melts from a sub-arc environment: mantle wedge samples from the TLTF arc, Papua New Guinea. Earth and Planetary Science Letters 122: 125–141.

Romankevich, E.A., Artemiev, V.E., 1969. Composition of organic matter in bottom sediments from the Kuril-Kamchatka Trench. Oceanology 9: 644–653.

Wang, J., Hattori, K., Kilian, R., Stern, C.R., 2007. Metasomatism of sub-arc mantle peridotites below southernmost South America: reduction of fO_2 by slab-melt. Contributions to Mineralogy and Petrology 153: 607–624.

Widom, E., Kepezhinskas, P., Defant, M., 2003. The nature of metasomatism in the sub-arc mantle wedge: evidence from Re-Os isotopes in Kamchatka peridotite xenoliths. Chemical Geology 196: 283–306.

Zelenski, M., Kamenetsky, V.S., Mavrogenes, J.A., Gurenko, A.A., Danyushevsky, L.V., 2018. Silicate-sulfide liquid immiscibility in modern arc basalt (Tolbachik volcano, Kamchatka): Part I. Occurrence and composition of sulfide melts. Chemical Geology 478: 102–111.

Petrology of the Takikawa monogenetic volcano group and surrounding shield volcanoes, in central Hokkaido, Japan: Magma generation and evolution of the episodic volcanism from late Miocene to early Pleistocene at the arc-arc junction

Mistuhiro Nakagawa and Ryunosuke Enoeda

[1] *Department of Earth and Planetary System Science, Hokkaido University, Sapporo 0600810, Japan.*
mnakagawa@sci.hokudai.ac.jp

Keywords: arc-arc junction, monogenetic volcano, shield volcano.

Unique and episodic volcanism occurred from late Miocene to early Pleistocene in the Takikawa region of the Central Hokkaido, which is located at the junction of Kuril and NE Japan arcs. Based on eruptive age, mode of activity, and magma type, the volcanism can be divided into three, monogenetic volcano group (MVG), basaltic shield volcanoes (BSV) and andesitic shield volcanoes (ASV) stages. The activity of MVG began around 10 Ma, and formed basaltic, monogenetic volcanoes, such as cinder cones, lava flows and dykes. Magma production late had largely increased since ca. 3 Ma, resulting to the formation of basaltic shield volcanoes (BSV). Then, magma type changed to be andesitic, forming large shield volcanoes (ASV) until 2 Ma. Although several basaltic, monogenetic volcanoes had been active, volcanic activity of the region terminated since 1.7 Ma.

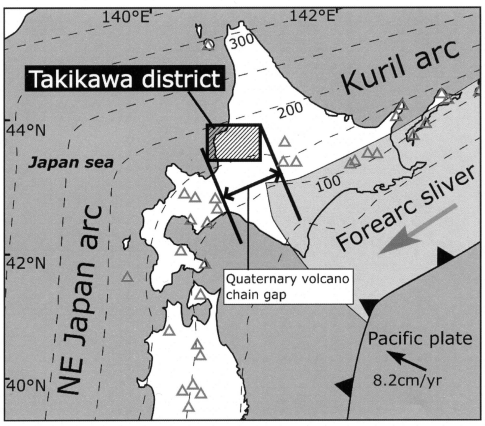

Fig. 1 – Locality of the Takikawa district and related tectonic setting. The Kuril fore-arc sliver has moved since late Miocene due to the oblique subduction of the Pacific plate (Kimura, 1986).Triangles are Quatenary volcanoes. Dotted lines show the depth of slab.

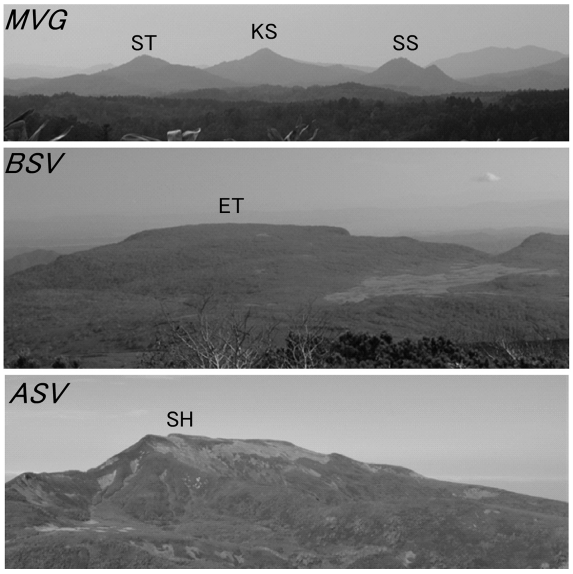

Fig. 2 – Representative volcanoes in the Takikawa district. MVG, BSV and ASV are described in the text. Abbreviations in photos are indicated in Fig. 3.

Although SiO_2 contents of the rocks of MVG range from 49 to 58 %, basaltic rocks are dominant. Many of these rocks are classified as medium-K and sub-alkaline, whereas some rocks are high-K and alkaline rock types. The rocks of BSV are mostly basaltic, ranging from SiO_2=50 to 56 %. These locks are sub-alkaline type, and show transitional compositions between medium-K and high-K. The rocks of ASV are calc-alkaline andesite, ranging from SiO_2=54 to 65 %. Considering SiO_2 – Nb/Zr, Rb/Zr and $^{87}Sr/^{86}Sr$ diagrams, it can be concluded that differentiated rocks of each stage can be produced not by fractional crystallization but by effect of crustal materials. Disequilibrium petrographical features, such as disequilibrium phenocryst assemblages, heterogeneous matrix and the occurrence of mafic inclusions, suggest that the differentiated rocks from each stage were formed by magma mixing between mafic and the silicic magmas, which were derived from crustal melting.

Both of MVG and BSV basalts are arc-type, characterized by Nb and Ta anomaly in spidergrams. In addition, Sr-Nd isotopes suggest that these basaltic rocks are derived from depleted mantle. The basaltic rocks of the two stages respectively show possible variations in the ratios of incompatible elements and isotope ratios, suggesting that primary magmas of each stage are various. Compared with these basaltic rocks, Nb/Zr ratios of MVG basalts are slightly higher than those of the BSV one, indicating that the source mantle of the MVG basalts was fertile compared with that of the BSV. On the other hand, Ba/Nb ratios of the basaltic rocks of BSV are higher than those of MVG, suggesting that the source of the BSV basalts were more affected by

slab components and/or crustal materials. These difference in the source mantle of the two types of basalts correspond to the difference in the depth of the source. According to Tb/Lu – Nb/Yb diagram, the basaltic rocks of MVG are generated in deeper level and by lower degree of melting. This is also consistent with the normative plots for estimated primary melts of these basaltic rocks.

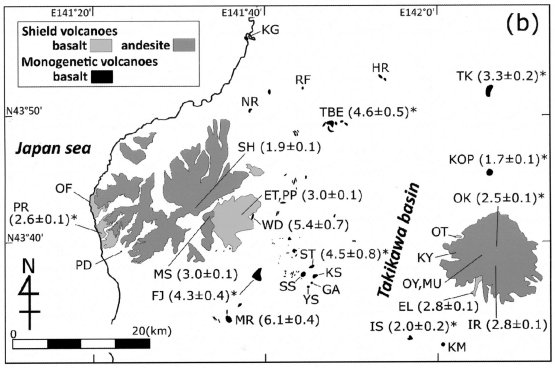

Fig. 3 – Distribution of late Miocene and early Pleistocene volcanoes in the Takikawa district (Nakagawa et al., 1993). The activity can be divided into three stages, MVG (monogenetic volcano group), BSV (basaltic shield volcano) and ASV (andesitic shield volcano) ones. K-Ar ages of representative samples are indicated.

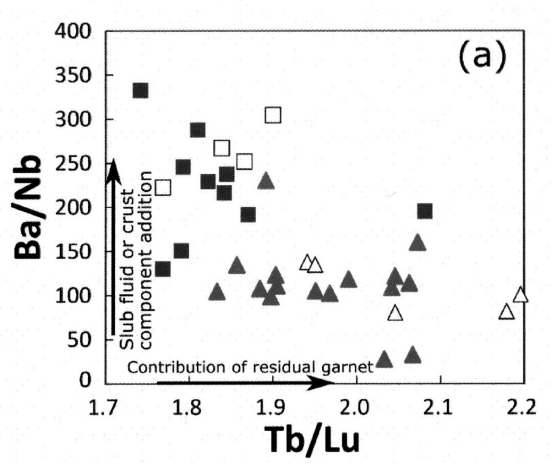

Fig. 4 – Tb/Lu – Ba/Nb diagram for basalts of MVG and BSV stages. Triangle and square symbols are MVG and BSV, respectively. Closed and open symbols show western and eastern volcanoes, respectively.

Based on temporal change of magma type and style of volcanism since late Miocene, magmatism of the Takikawa district could be summarized as follows. In late Miocene, upwelling of asthenospheric mantle began beneath the region, resulting to the generation of MVG basalts at deeper source with lower degree of melting. The upwelling had continued in early Pleistocene to form voluminous BSV magma at shallower level of mantle with higher degree of melting. With increasing of volume of basaltic magma, shield volcanoes were constructed. Due to the formation of the BSV magma, partial melting of lower crust occurred. Mixing of mafic magma and crustal melt formed ASV magma. The activity of BSV and ASV from 3 to 2 Ma was maximum. Since then, volcanic activity of Takikawa region has terminated since 1.7 Ma. Thus, the activity of the region can be explained by upwelling of asthenospheric mantle since late Miocene, whereas the termination of the activity was due to cooling of the source.

In summary, the volcanic activity of the Takikawa region was episodic and unique at NE Japan and southern Kuril arcs. The presence of monogenetic and shield volcanoes strongly suggests that the stress field of the region was tensional during late Miocene and early Pleistocene. This period corresponded to the timing, in which Kuril fore-arc sliver had collided to NE Japan arc. The collision could migrate the sliver to south, resulting to the formation of a tensional stress field at the Takikawa region. This tensile stress could force the upwelling of deeper asthenothpheric mantle. In conclusion, the volcanic activity of the Takikawa region would be important to understand tectonic events at the arc-arc junction.

References

Enoeda, R. 2019. Petrology of late Miocene to early Pleistiocene volcanic rocks in Takikawa-Shokanbetsu area, central Hokkaido: The origin of the episodic volcanism in the arc-arc junction. Mster Thesis of Hokkaido Univ., p. 70 (in Japanese).

Kimura, G. 1986. Oblique subduction and collision: Forearc tectonics of the Kuril arc. Geology 14: 404–407.

Nakagawa, M., Goto, Y., Arai, K., Wada, K. and Itaya, T. 1993. K-Ar ages and major element chemical compositions of Late Miocene and Pliocene basalts from Takikawa district, central Hokkaido: Basaltic monogenetic volcano group at the junction of the northeastern Japan and Kuril arcs. Journal of Mineralogy, Petrology and Economic Geology 88: 390–401 (in Japanese with English abstract).

Sources of Volcanism in the Itasy Volcanic Field, Madagascar

Christine Rasoazanamparany[1], Elisabeth Widom[1], David Kuentz[1], Tsilavo Raharimahefa[2], Kanto Rakotondravelo[3], A.F. Michel Rakotondrazafy[3]

[1] *Department of Geology and Environmental Earth Science, Miami University, Oxford, Ohio, USA.*
widome@MiamiOH.edu
[2]*Department of Geology, University of Regina, Regina, Canada.*
[3]*Departement des Sciences de la Terre, Universite d'Antananarivo, Antananarivo, Madagascar.*

Keywords: Madagascar, Itasy, volcanism.

The Itasy Volcanic Field is the youngest known volcanism in Madagascar, and comprises scoria cones and associated lava flows, as well as domes and maars. Prior ^{14}C dating has revealed eruptive activity as recent as ~8.5 Ka (Vogel, 1970), establishing it as an active volcanic field. Nevertheless, relatively little has been documented regarding the number of vents, eruptive ages, or eruptive frequency; and the cause and source of volcanism in this region remain poorly understood. We have sampled a suite of mafic lavas from volcanic centers across the Itasy Volcanic Field to better constrain the age range, eruptive recurrence interval, and magma sources.

Ar-Ar ages for the sample suite range from ~31 to 104 Ka, contemporaneous with Pleistocene volcanism in the neighboring Ankaratra Volcanic Field (Rufer et al., 2014).The lavas are generally alkaline, ranging from foidite to tephra-phonolite (MgO ~3-10 wt%), with OIB-type trace element patterns. Ratios of Nb/U and Ce/Pb are within the MORB-OIB range, and do not correlate with indices of differentiation, indicating minimal influence of crustal assimilation on incompatible trace elements. The lavas exhibit Sr-Nd-Pb isotope signatures similar to enriched Indian Ocean MORB, particularly the SW Indian Ridge (SWIR).

In Pb-Pb and Hf-Nd isotope plots, the samples fall along or close to the mantle arrays, inconsistent with a significant contribution from *in situ* SLCM. Rather, the Itasy data are consistent with a heterogeneous mantle source derived through a two-stage, three-component mixing scenario similar to that proposed previously for the SWIR (e.g. Douglass & Schilling, 2000; Mahoney et al., 1992). In this model, depleted MORB mantle was polluted by ancient SCLM that was eroded and incorporated into the asthenosphere during the breakup of Madagascar and India (Storey et al., 1997; Mahoney et al., 1992), followed by mixing with a plume component similar in composition to "C" (Hanan and Graham, 1996) and related to past Indian Ocean Plumes (Marion, Reunion, Crozet and Amsterdam/St. Paul; Douglass & Schilling, 2000). Isotope modeling results suggest that the Itasy magmas may be derived from a mantle source produced by a mixture of ~80% DMM and 20% SCLM, which subsequently mixed with ~30–50% of the common plume component. Anomalously thin lithosphere in the region (Rindraharisaona et al., 2013; Pratt et al.,2017) may focus asthenospheric flow and lead to decompression melting of this mixed source beneath the Itasy Volcanic Field.

Acknowledgements

This study has been supported by NSF EAR grant #1523442 (awarded to E. Widom), which partially funded a Postdoctoral position at Miami University for C. Rasoazanamparany. Supplementary support for the Postdoctoral position was provided by Miami University.

References

Douglass, J., Schilling, J.G., 2000. Systematics of three-component, pseudo-binary mixing lines in 2D isotope ratio space representations and implications for mantle plume-ridge interaction. Chemical Geology 163: 1–23.

Hanan, B.B., Graham, 1996. Lead and helium isotope evidence from oceanic basalts for a common deep source of mantle plumes. Science 272: 991–995.

Mahoney, J.J., le Roex, A.P., Peng, Z.X., Fisher, R.L., Natland, J.H., 1992. Southwestern limits of Indian ocean ridge mantle and the origin of low 206Pb/204Pb mid-ocean ridge basalt: isotope systematics of the central Southwest Indian Ridge (17-50E). Journal of Geophysical Research 97: 19,771–19,790.

Pratt, M.J., Wysession, M.E., Aleqabi, G., Wiens, D.A., Nyblade, A.A., Shore, P., Rabolamanana, G., Andriampenomanana, F., Rakotondraibe, T., Tucker., R.D., Barruol, G., Rindraharisaona, E., 2017. Shear velocity structure of the crust and upper mantle of Madagascar derived from surface wave tomography. Earth Planetary Science Letters 458: 405–417.

Rindraharisaona, E.J., Guidarelli, M., Aoudia, P. and Rambolamanana, G., 2013. Earth structure and instrumental seismicity of Madagascar. Implications on the seismotectonics. Tectonophysics 594: 165–181.

Rufer, D., Preusser, F., Schreurs, G., Gnos, E., Berger, A., 2014. Late Quaternary history of the Vakinankaratra volcanic field (central Madagascar): insights from luminescence dating of phreatomagmatic eruption deposits. Bulletin of Volcanology, DOI: 10.1007/s00445-014-0817-7.

Storey, M., Mahoney, J.J., Saunders, A.D., 1997. Cretaceous basalts in Madagascar and the transition between plume and continental lithospheric mantle sources. Mahoney, J.J., Coffin, M.F. eds., Geophysical Monograph Series, Large Igneous Provinces: Continental, Oceanic, and Planetary Flood Volcanism. v. 100: 95–122.

Vogel, J.C., 1970. Groningen radiocarbon dates IX. Radiocarbon 12: 444–471.

Session 5. Volcanic hazard and risk assessment in monogenetic volcanic fields

A volcanic field is produced by distributed basaltic to rhyolitic volcanism of a variety of explosive and effusive eruption styles, which is often termed monogenetic. These types of eruption are often episodic and characterized by short periods of intense activity (e.g. days to years). Moreover, each new eruption occurs in a distinct location, rather than repeatedly from the same site, such as at polygenetic volcanoes. This apparent evolution pattern and overall behavior make eruption forecast and volcanic hazard assessment of monogenetic volcanic fields extremely complex. In contrast, many monogenetic volcanic fields are situated near critical infrastructure, transport routes and large populations, requiring continuous development and refinement of the current practice of volcanic hazard assessment. This session invited submissions to further our understanding of volcanic hazards within active monogenetic volcanic fields, including but not limited to field-based, remote sensing, numerical modelling, geophysical and statistical approaches.

Conjectures regarding the fluid-magmatic feeding system's architecture of the Uzon caldera (Kamchatka): some methodological aspects of the geomorphological, geological and geophysical data interpretation

Ivan Delemen

Institute of volcanology and seismology FEB RAS, Petropavlovsk-Kamchatsky 683006, Russia. delemen@kscnet.r

Keywords: caldera, fluid-magmatic feeding system, maar

For the 75 years since the publication of L.C. Graton of his "Conjectures regarding volcanic Heat", the volcanology has advanced far ahead. However, even now volcanologists continue to hunt after answers to the question that Louis Carol Graton considered the most important for a researcher studying volcanic processes: "how did this happen?".

The contemplation of the processes occurring at the depths and on the territory of the Uzon caldera (Kamchatka) is of great applied and fundamental importance. However, to date, all models of the deep structure of the caldera, based on the interpretation of geological, geophysical, petrological and geochemical data, are hypothetical, i.e. conceptual models. Such models usually do not take into account the inhomogeneity and heterogeneity of the geological environment, multi-stage and hierarchical objects and processes that appear in the structure and development of the Uzon caldera.

The report examined some important aspects of comparing such (compiled by various researchers) conceptual models. The technology for creating refined conceptual schemes based on the use of formal logic and standard big data algorithms is also briefly described. The solution to this problem allows one to perform the formalization of the available geological and geophysical data, which is adequate for the real conditions and the required accuracy, necessary for setting the initial and boundary conditions necessary for the numerical simulation of objects and / or processes.

Unfortunately, authors of conceptual models do not always take into account the fact that any geological interpretations of quantitative data obtained in geophysical, petrological, geochemical, and even morphostructural studies are inverse problems.

The solution of any inverse problem (even when a priori information is included in the interpretation) leads to errors.

When studying the deep structure of calderas and other types of volcanoes, their magmatic feeding systems, fluid supply and fluid unloading zones, the false identification of the desired object or the omission of an event (error of the first kind) leads to excessive expenditure of resources aimed at identifying the nature of erroneously recognized objects, phenomena or events. When studying the deep structure of calderas and other types of volcanoes, their magmatic feeding systems, fluid supply and fluid unloading zones, the false identification of the desired object or the omission of an event (error of the first kind) leads to excessive expenditure of resources aimed at identifying the nature of erroneously recognized objects, phenomena or events. Errors of the second kind (missed goal) are dangerous because the features of the processes most important for the researcher, objects, or, for example, forecasted events, may not be revealed.

Errors of the second kind (missed goal) are dangerous because the most important for the researcher features of processes, objects, or, for example, forecasted events, may not be revealed. So, all three catastrophic processes of spontaneous destruction of slopes on the Valley of Geysers (Kamchatka) that suddenly occurred in 1981, 2007 and in 2014 were not predicted - the parameters of the monitoring system assumed mainly only geysers, but were not configured to prevent errors; the studies were configured to prevent errors in skipping the target for such processes.

Obviously, in developing the existing infrastructure on the Uzon-Geyser cluster of the Kronotsky State Biosphere Reserve, it will be necessary to consider volcanic hazards from flank instability, landslides, hazardous gas emissions, and monogenetic eruption within Uzon-Geyser cluster.

An analysis of the citation and publication activity of the authors shows that a common methodological error is that alternative concepts are not always considered, and moreover, work is not done to compare them and justify the most plausible selection. This trend is also noticeable when reading publications devoted to the study of the Uzon caldera.

In addition to the results of the author's personal investigations, the completeness of the bibliographic database used by him is of great importance for the formation of a source database for creating a conceptual model substantiated by these data.

It should be borne in mind that when searching for publications by descriptors and keywords in available on-line bibliographic databases, an error of the first kind (detection by search query of

publications that do not correspond to the research subject) is from 10 to 20%. The probability of an error of the second type increases significantly during full-text search, when the texts of all documents stored in the database are analyzed for the search for matches, the logical statements in the given search are not clearly defined. When conducting instrumental measurements, as well as accounting for errors in the quantitative interpretation of the results, in Russia are regulated by industry (in the areas of research) regulatory.

At the instrumental stage of research, such errors are minimized, however, at the stage of geological interpretation, the chance of occurrence of errors of both kinds appears due to the phenomenon of the convergence of signs in various processes occurring in the calderas, including Uzon. With the convergence of signs, the same values of the parameters describing the system under study can have a different nature.

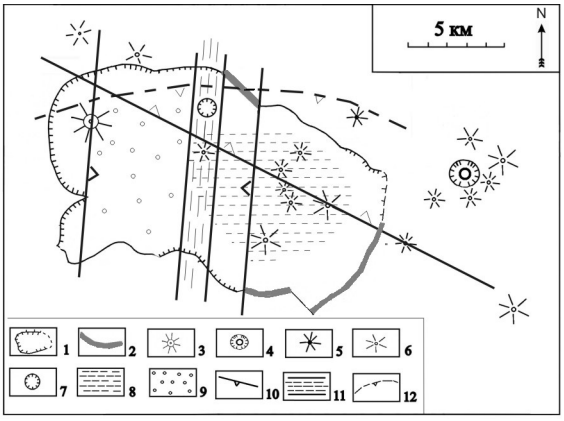

Fig. 1 – The structural position of Dal'nee Lake Maar in the linear caldera disjunctive pattern. 1 – caldera rims; 2 – extrusions located on caldera rim; 3 – supposed vent of the Uzon Mid Pleistocene stratovolcano, overlain by hydrothermally altered landslide (Western thermal field of the caldera); 4 – Crater of the Holocene volcano Joung Kikhpinych; 5 – Holocene cinder cones on the Arc hill (sopka Duga); 6 – other Holocene centers of volcanic eruptions in the caldera and in its framing; 7 – crater of the Dal'nee lake maar; 8 – area of intracaldera centers of monogenic volcanism located above the East consolidating apical ledge of the large long-living magma chamber in bottom of caldera; 9 – area of intracaldera centers of gas hydrothermal activity located above the West unconsolidating apical ledge of this magma chamber; 10 – the centerline of the assume precalder major dyke in the basement feeding the magma chamber of the caldera; 11 – the centerline of the assume precalder major dyke in the basement feeding the magma chamber of the caldera; submeridional zone of increased permeability in the axial part of the transverse graben of the caldera; 12 – the northern edge of the sub-latitudinal arcuate zone of gravitational descending above the northern flank of the magma chamber of the caldera.

The report presents the results of an analysis of existing concepts of a feeding magmatic system published by various authors. The most probable 3-D concept is presented, which made it possible to take into account a priori data to reduce the probability of errors of the first and second kind.

In a vertical section, the magmatic, gas, and thermal water flows cyclically in time to the surface at the pre-caldera, caldera, and post-caldera stages occur due to the nucleation and development of several sources of endogenous matter and thermal energy of different depths. The caldera is located above the apical dome-shaped part of the lenticular magma chamber, which formed in the middle Pleistocene due to the northwest strike through an extended magma dike, into a weakened shallow zone of interformational disruption at the boundary of the crystalline basement and overlying sedimentary rocks.

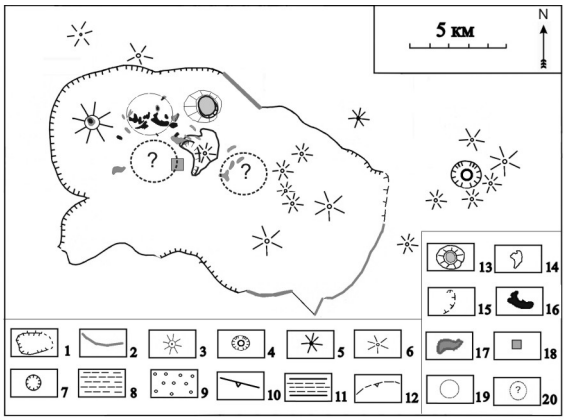

Fig. 2 –The location of the centers of the newest and modern fluid-magmatic and fluid-hydrothermal activity above the edging of the magmatic feeding system of the White hill (Belaya sopka) Late Pleistocene extrusion and around of younger resurgent uplift on the same place. Conventions 1 – 12 are shown in Figure 1.
13 – the edifice of the Dal'nee lake maar; 14 – the borders of the base of the White hill (Belaya sopka); 15 – erosion circus in the southwestern weakened slope of the White hill (Belaya Sopka); 16 – Thermal fields, pools and other thermal sites;); 17 – fields of hydrothermally altered rocks18 – Groundwater discharge sites with high concentrations of dissolved carbon dioxide; 19 - the range of development of modern hydrothermal explosion processes; 20 - suppose ranges of availability conditions for the formation of maars and hydrothermal explosion craters in the future.

The architecture features of the permeable zones that control the discharge sites of the fluid-magmatic feeding system of the caldera are shown in Figure 1.

Figure 2 shows the structural position of the Dal'nee lake maar. In the future, the most probable places for the forming of new places for the formation of maars and hydrothermal explosions are such areas edged by a resurgent uplift, where the base of an impenetrable primary or secondary caprock overlaps or intersects with vertical permeable ruptures.

Lava flow dynamics for volcanic risk assessment in the Negros de Aras monogenetic volcanic field (northern Chile)

Matías Vilches[1,4], Gabriel Ureta[2,3,4], Károly Németh[5], Felipe Aguilera[1,2,4]and Mauricio Aguilera[1,4]

[1] *Departamento en Ciencias Geológicas, Facultad de Ingeniería y Ciencias Geológicas, Universidad Católica del Norte, Av. Angamos 0610, Antofagasta, Chile.mvilchesapablaza@gmail.com*
[2] *Centro Nacional de Investigación para la Gestión Integrada del Riesgo de Desastres (CIGIDEN), Av. Vicuña Mackenna 4860, Santiago, Chile.*
[3] *Programa de Doctorado en Ciencias Mención Geología, Universidad Católica del Norte, Av. Angamos 0610, Antofagasta, Chile.*
[4] *Núcleo de Investigación en Riesgo Volcánico - CKELAR volcanes, Universidad Católica del Norte, Av. Angamos 0610, Antofagasta, Chile.*
[5] *Volcanic Risk Solutions, School of Agriculture and Environment, Massey University, Palmerston North, New Zealand.*

Keywords: monogenetic volcanism, effusion rate, Q-LAVHA.

Negros de Aras (also called as El Negrillar; Fig. 1) is a monogenetic volcanic field located between Socompa volcano and Salar de Atacama basin, northern Chile. This work is to define the various lava flow surface textures, lava flow structures, emplacement systems, effusion rates, emplacement times and volumes of the lava flows from Negros de Aras monogenetic volcanic field. Negros de Aras lava flows correspond mainly to a'a and blocky lava flows of basaltic andesite (55.58 wt.% for SiO_2) and andesite (60.89 wt.% for SiO_2) composition that show a wide diversity of volcanic structure such as levees, lobes, channels and ogives, which were identified through DEM-based slope maps (e.g. Fig. 2) and field observations. The recognized diversity of volcanic structures can be explained by magmatic processes and pre-eruptive surface morphology of the lava flows, characterizing a lava flow morphotype from platy-a'a to blocky (e.g. Murcia et al., 2014).

In this work, we have selected one of the several lava flows from Negros de Aras monogenetic volcanic field, with which we run four lava flow simulations whose vent are located at 7,334,309.07 mN – 582,030.40 mE extending toward NW-W (Fig. 2). Three of this simulations correspond to three lava flow that we identified as LF1, LF2 and LF3, respectively (Fig. 2), while the fourth simulations correspond to erupted total volume (LFt = LF1+LF2+LF3). As a consequence of the flow emplacement simulations we were able to compare the effusion time and effusion rate of each individual lava flows simulated (LF1, LF2 and LF3), and use these values to define the effusion time and effusion rate of the total lava flow (LFt).

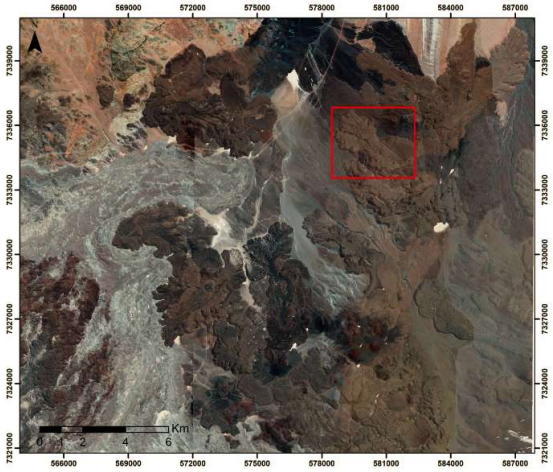

Fig. 1 – Map of Negros de Aras monogenetic volcanic field. Outlined red box shows the position of the lava flows in study.

The simulations were employed the Q-LAVHA tool extension (Mossoux et al., 2016) of the Q-GIS software. The parameters required for this software correspond to maximum lava flow length, initial viscosity of the lava flow, water content of the whole rock, cooling temperature, initial ratio of phenocrystals, lava flow channel ratio and pre-eruptive surface topography.

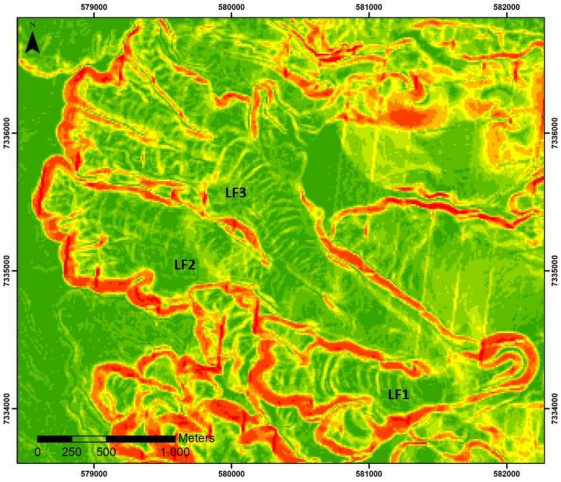

Fig. 2 – Slope map of lava flows of the Negros de Aras monogenetic field and the position of LF1, LF2 and LF3

We used a composition of 60.89 wt.% for SiO_2, while the viscosity (3.83 Pa*s) was estimated from the major elements content according to Giordano et al. (2008).

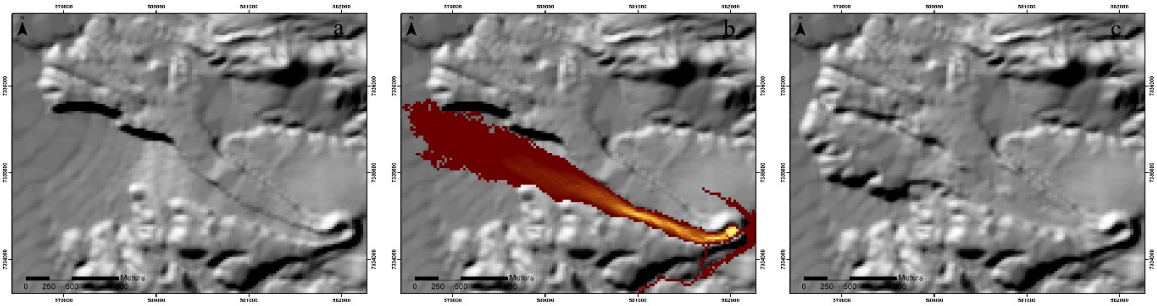

Fig. 3 – Simulation of a lava flow of Negros de Aras monogenetic volcanic field: (a) pre-eruptive topography, (b) lava flow modeled by Q-LAVHA in Q-GIS under specific parameters to determine the effusion rate, (c) real topography of lava flow.

For its part, cooling temperature was estimated from the Mg content according to Putirka (2008), obtaining an average temperature of 1066 ° C. The water content (0.09 wt.% for H_2O) was obtained by calculating the LOI of the whole rock at 105°C for 2 hours. On the other hand, the initial ratio of phenocrysts (6%) was estimated by the analysis of thin section images using the ImageJ software (Schneider et al., 2012). Crystal size was defined following González (2008), where phenocrystals are > 0.50 mm, microphenocrysts range between 0.05 to 0.50 mm, and microlites are < 0.05 mm, which are part of the groundmass. Through of TanDEM-X images of 12 m resolution was estimated an erupted total volume of 0.17 km^3 (LFt), while for each individual lava flow the erupted volume is 0.05 km^3 to LF1, 0.06 km^3 to LF2, and 0.05 km^3 to LF3. Which reach lengths of 2.00 km, 3.74 km and 3.97 km; and covering areas of 0.92 km^2, 1.49 km^2, and 2.22 km^2, respectively. On the other hand, we obtained the pre-eruptive surface (Fig. 3a) for each individual lava flow, as well as the simulation of the pre-eruptive surface for the total lava flow. This process was carried out by generating of a point mesh distanced 1 m x 1 m outside of each lava flow. Subsequently, a TIN model was created by the Delaunay criteria to finally to generate a Raster image from the TIN image (e.g. Kereszturi et al., 2016). The Fig. 3 shows the modeling for the LF2, where the results indicate the eruptive event was prolonged over time of 35days and 12.24 hours with an effusion rate of 18.42 m^3/s. On the other hand, the evolution process for this lava flow was modeled obtaining the same length that the lava flow formed originally (Fig. 3b and Fig. 3c). Based on our result we concluded that Q-LAVHA tool extension could deliver a simulation and consistent data for the evolution model of the lava flows and assessing the volcanic risk. The variability of these results is strictly linked to three essential aspects such as whole rock chemical composition, whole rock water content, and the pre-eruptive surface. In addition, the understanding of the formation and development of the lava flow structures permit to determine the behavior that future emissions of lava flows would have, and the duration of the volcanic activity. This knowledge would permit to have an approximation of the volcanic hazard associated to lava flows at south of the Salar de Atacama basin, facilitating the mitigation of volcanic hazard in case of future eruptions near of Tilomonte and Peinevillages, water wells of Zaldivar and Escondida mines, the Socompa border crossing (Chile-Argentina), and the power lines installations between Chile-Argentina.

Acknowledgements

To Pablo Grosse, CONICET researcher and Fundación Miguel Lillo academic, for facilitating and allowing to use the TanDEM-X 12 m.

References

Giordano, D., Russell, J. K., & Dingwell, D. B.,2008. Viscosity of magmatic liquids: a model. Earth and Planetary Science Letters *271*(1-4): 123-134.

González, P., 2008. Texturas de los cuerpos ígneos. Asociación Geológica Argentina: 172–196.

Kereszturi, G., Nemeth, K., Moufti, M.R., Cappello, A., Murcia, H., Ganci, G., Negro, C., Procter, J., Zahran, H., 2016. Emplacement conditions of the 1256 AD Al-Madinah lava flow field in Harrat Rahat, Kingdom of Saudi Arabia – Insights from surface morphology and lava flow simulations. Journal of Volcanology and Geothermal Research 309: 14–30.

Mossoux, S., Mathijs, S., Bartolini, S., Poppe, S., Canters, F., Kervyn, M., 2016. Q-LAVHA: A flexible GIS plugin to simulate lava flows. Computers & Geosciences: 97.

Murcia, H., Németh, K., Moufti, M.R., Lindsay, J.M., El-Masry, N., Cronin, S.J., Qaddah, A., Smith, I.E.M., 2014. Late Holocene lava flow morphotypes of northern Harrat Rahat, Kingdom of Saudi Arabia: implications for the description of continental lava fields. J. Asian Earth Sci. 84: 131–145.

Putirka, K., 2008. Thermometers and Barometers for Volcanic Systems. Reviews in Mineralogy & Geochemistry - Rev Mineral Geochem 69: 61-120.

Schneider, C., Rasband, W., Eliceiri, K., 2012. "NIH Image to ImageJ: 25 years of image analysis", Nature methods 9(7): 671-675, PMID 229308341.

Session 6. Maar lakes and environment

Most volcanic lakes on Earth are maar lakes. Many maar craters are occupied by a lake. These two strong statements require major attention in future research. On the one hand, the presence of water intrinsically inhibits the study of the geological record, as a large portion of volcanic deposits is submerged by the lake. On the other hand, the deep anoxic water enables to preserve volcanogenic as well as allochthonous sediments. As such, the investigation of the well preserved sediment cores permits to (1) reconstruct the past volcanic activity, in time (100-1000s of years) and space (crater vs field), (2) detail the genetic process of the maar crater, (3) detect inter-eruptive periods, limnic gas bursts and possible climate change events that alternated with volcanic activity in the area. Thorough insights into the architecture of aquifers surrounding maar lakes and their relation with the lake itself helps to assess future hazardous scenarios (e.g. phreatomagmatic activity) for monogenetic or polygenetic maar fields. Moreover, the limnology of the lake water permits to trace back on the year to decade time scale. How stable is the lake water stratification throughout the seasons and years? Are there any signs of active volcanic input (e.g. sublacustrine hot springs or degassing vents)? Is CO_2 accumulated in the deep lake strata, up to critical conditions to cause a "Nyos-type" gas burst? What is the relation between the lake's thermal regime and the tectonic environment (e.g. geothermal heated deep rift lakes)? This session seeks for studies on (1) the sedimentology of lake core sections and its relation to the reconstruction of the genetic processes of the lake basin, (2) physical and biological limnology of the lake water, (3) geochemistry of water and dissolved gases of maar lakes.

Maar Lakes in Myanmar and high resolution paleoclimatic records in varved sediment

Guoqiang Chu[1], Qing Sun[2], Zhaoyan Gu[1], Qingzen Zhu[1], Youliang Su[3], Manman Xie[2], Kyaing Sein[4]

[1] *Key Laboratory of Cenozoic Geology and Environment, Institute of Geology and Geophysics, Chinese Academy of Sciences,Beijing, China; chuguoqiang@mail.igcas.ac.cn*
[2]*National Research Center of Geoanalysis, Beijing 100037, China.*
[3]*Institute of Geophysics, China Earthquake Administration, Beijing 100081, China.*
[4]*Myanmar Geosciences Society, Yangon, Myanmar.*

Keywords: Myanmar, Paleoclimate, drought.

The tropical Asian regions are particularly prone to catastrophic droughts due to high temperature and evaporation and their sensitivity to variable oceanic-atmospheric circulation. The extent to which future global warming may intensify droughts in this populous region is a matter of utmost concern. Palaeoclimatic data can help inform scientists learn more about the temporal patterns and drivers of monsoon change over geological timescales.

Maar lakes are recognized as ideal sites for the preservation of high-resolution sediment archives because they are closed basins with a relatively simple hydrological system and they provide continuous sedimentary sequences for paleoclimatic changes. There are five Maar Lakes (Nyaunggan, Twintaung, Taungbyauk, Twinma and Lashe) in the northwestern region of the Indo-China Peninsula, Myanmar (Fig. 1). The lakes have maximum water depth ranging from 50 meter to 1meter.

In Maar Lake Twintaung, calcareous varves are well preserved in the sediment. The light-colored layers were composed mainly of calcite crystals with thicknesses ranging from 50 μm to 400 μm, and the dark-colored layers consisted of organic and siliceous matter (Fig. 2).

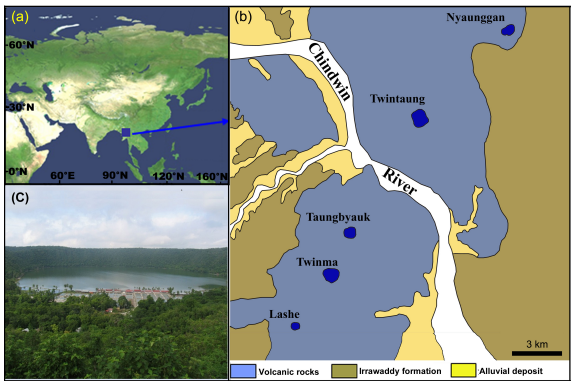

Fig. 1 – Location of Maar Lakesin Myanmar.
(a) Location of Maar Lakesin Myanmar Maar Lake; (b) Five maar lakes in the region;(c) Maar Lake Twintaung.

The calcite crystals deposit due to strong evaporation and Spirulina blooms in the dry season, whereas clastic and organic matter are deposited during the wet season. In the dry season, calcite crystals form due to less precipitation and strong evaporation. In addition, algal blooms could intensify the endogenic precipitation of carbonate crystals due to photosynthetic activity. In the wet season, summer precipitation causes floods that transport more minerogenic detritus into the lake. The varved sediments are almost continuous from 0-315 cm depth, except for a few intervals that have either poorly-developed or no laminations. The varve chronology roughly corresponds to radiometric age control (within error bars). Two AMS^{14}C ages at 182 cm and 211 cm are slightly older than the varve chronology.

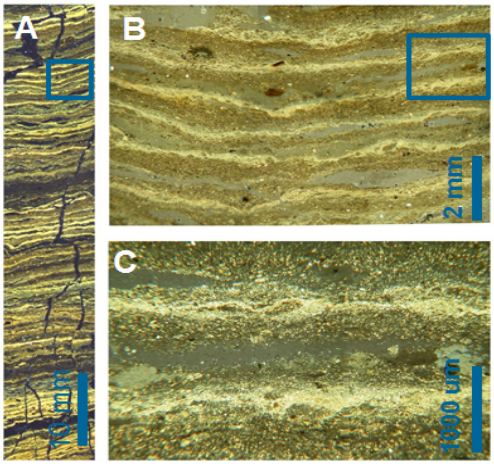

Fig. 2 – Photomicrographs of carbonate varves.
(a) Microphotographsunder a stereoscopic microscope (with polarized and transmitted light); (b) detail of laminations from a marked area in figure 2a under a Leitzlight microscope; (c) Detail of laminations from a marked area in figure 2b.

In order to obtain a multi-proxy record from Maar Lake Twintaung high-resolution elemental data by using in situ synchrotron radiation X-ray fluorescence (SRXRF), *n*-alkanes and compound-specific carbonisotopic value were used for studying paleoclimate change over past 8200 years. Based on the comparing with instrumental data and modern process, we interpret the elemental data in terms of climate variables such as precipitation and temperature. The first component includes lithogenic elements such as K, Ti, Fe, Cu, Zn, Rb and Zr, and might be controlled by various factors such as physical and chemical weathering processes and rainfall. The second component, calcium and strontium, might be principally regulated by the balance between evaporation and precipitation. During drought periods, the calcium ion might supersaturate, causing carbonate calcite precipitation from the water column. In this forest (C3 plants)

dominant region, the compound-specific carbonisotopic value from long chain alkanes is mainly regulated by plant physiological and biochemical responses to drought stress; and as such, can be used as a proxy of past changes in moisture.

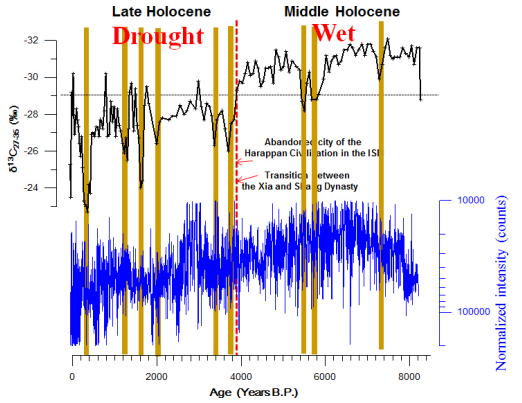

Fig. 3 – Paleoclimatic changes over past 8200 years.
Black line: the weighted $\delta^{13}C_{27\text{-}35}$ values of the n-C27-C35 alkanes; Blue line: normalized intensity of Ca. Brown bars show drought period.

The elemental variations show distinct interannual and decadal variabilities. On interannual time scales, spectral analysis of the Ca and Sr time series indicates stronger El Niño–Southern Oscillation (ENSO)-like (Indian Ocean Dipole(IOD)-like) variability at periods of 2–7 years (Fig.3). The compound-specific carbon isotopic of long chain alkanes reveals distinct decadal-to-centennial scale droughts superimposed on a trend of gradually decreasing summer monsoon intensity from the mid-Holocene to late Holocene (Fig.3). Within the limits of the dating uncertainties, these decadal-to-centennial scale droughts are found to be well-correlated with the southward shift of the ITCZ. It highlights the importance of the ITCZ shift (tropical monsoon trough) in regulating monsoon rainfall in the region. In addition, most of the droughts are likely to be linked with active volcanism and solar minima, and suggest a coupled process between external drivers and internal climate dynamics.

References

Chu, G., Sun, Q., Zhu, Q., Shan, Y., Shang, W., Ling, Y., Su, Y., Xie, M., Wang, X., Liu, J., 2017. The role of the Asian winter monsoon in the rapid propagation of abrupt climate changes during the last deglaciation. Quaternary Science Reviews 177: 120–129.

Kalugin, I., Daryin, D., Smolyaninova, L., Andreev, A., Diekmann, B., Khlystov, O., 2007. 800-yr-long records of annual air temperature and precipitation over southern Siberia inferred from Teletskoye Lake sediments. Quaternary Research 67: 400–410.

Ojala, A.E.K., Francus, P., Zolitschka, B., Besonen, M., Lamoureux, S.F., 2012. Characteristics of sedimentary varve chronologies—A review. Quaternary Science Reviews 43: 45–60.

Sun, Q., Shan, Y. B., Sein, K., Su, Y., Zhu, Q., Chu, G., 2015. Carbonate varves and minor element variations during the past 100 years in Maar Lake Twintaung, Myanmar. Chinese Science Bulletin 60: 1038–1047.

Sun, Q., Shan, Y., Sein, K., Su, Y., Zhu, Q., et al., 2016. A 530 year long record of the Indian Summer Monsoon from carbonate varves in Maar Lake Twintaung, Myanmar. Journal of Geophysical Research 121: 5620–5630.

Zolitschka, B., P. Francus, A. E. J. Ojala, and A. Schimmelmann, 2015. Varves in lake sediments—A review. Quaternary Science Reviews 117: 1–41.

Maar lake Sihailongwan (northeastern China): varve chronology and climate reconstruction

Guoqiang Chu[1], Qing Sun[2], Andrey Darin[3]

[1]*Key Laboratory of Cenozoic Geology and Environment, Institute of Geology and Geophysics, Chinese Academy of Sciences, China; chuguoqiang@mail.igcas.ac.cn*
[2]*National Research Center of Geoanalysis, Chinese Academy of Geological Sciences, China.*
[3]*Institute of Geology and Mineralogy SB RAS. Novosibirsk, 630090, Russia.*

Keywords: maar lakes, varve chronology, climate reconstruction.

Reconstructing temperature variations during the last millennium are important to better understand natural climatic variability, evaluate the relative contributions of anthropogenic forcing, and predict future climate (Jones et al., 2009; Mann et al., 2009).

Seasonal temperature variability over longer timescales could offer new insights into understanding different forcing factors and response processes in the climate system. Here we report a climate reconstruction over the past 1600 years from the varved sediment in Lake Sihailongwan, northeastern China.

Lake Sihailongwan, a closed maar lake, is located in northeastern China (Fig. 1).

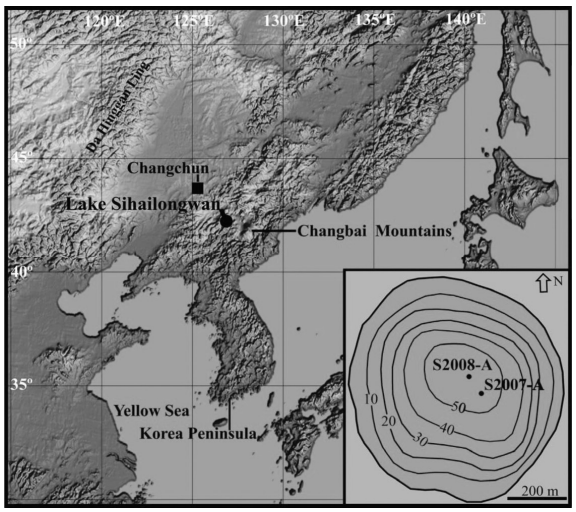

Fig. 1 – Location of Lake Sihailongwan. Inset bathymetric map showing the coring sites (the interval of the isobathic curve is 10 m).

The lake is a dimictic lake with a surface area of 0.4 km2, a maximum depth of 50 m, and a catchment area of 0.7 km.

Annually laminated sediments have been reported in earlier studies and provide a reliable timescale for paleoclimatic research in this data-sparse area (Chu et al., 2005, 2009; Jiang et al., 2008; Mingram et al., 2004; Schettler et al., 2006).

A series of cores (freeze-cores, gravity cores and piston cores) were retrieved from Lake Sihailongwan since 1999. The cores were split in half longitudinally, and one half of the core was used for making thin sections and solid samples for scanning micro-XRF, whilst the other half was used for Long chain alkenone analyses (Chu et al., 2012).

Thin-sections were examined at different magnifications under a Leitz polarizing microscope for counting varves. Varves appear as rhythmic units of a diatom-rich layer (autumn), followed by a lightcolored siliciclastic layer (spring), and a subsequent mixed layer (summer) (Chu et al., 2005). Varves were counted for each centimeter. Sample ages were calculated in the middle of each sample.

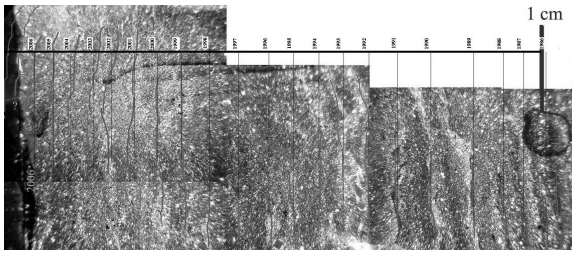

Fig. 2 – An example of the annual layers calculation in samples of Lake Sihailongwan bottom sediments.

For Long chain alkenone analyses the cores were sampled at 0.5 cm interval and analyzed according to the procedure (Chu et al., 2012).The obtained Long chain alkenone time series were used for climatic reconstructions (fig.3).

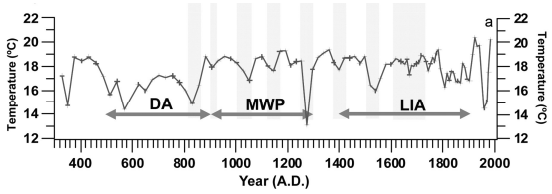

Fig. 3 – Alkenone-derived temperatures during the growing season.

Solid samples impregnated with epoxy resin were used for high-resolution micro-XRF using synchrotron radiation beams (Darin et al., 2013). Time series of concentrations changes more than 25 rock-forming and microelements were obtained (K, Ca, Ti, V, Cr, Mn, Fe, Ni, Cu, Zn, Ga, Ge, As, Se, Br, Rb, Sr, Y, Zr, Nb, Mo, Pb, Th, U).

Micro-XRF was performed with high spatial resolution (scanning step is equal to the average sediment accumulation rate). Therefore, the statistical processing of the obtained time series made it possible to find and evaluate the frequency of natural climatic cycles.

Figure 4 shows an example of finding the natural cyclic zirconium content in the bottom sediments of the Lake Sihailongwan.

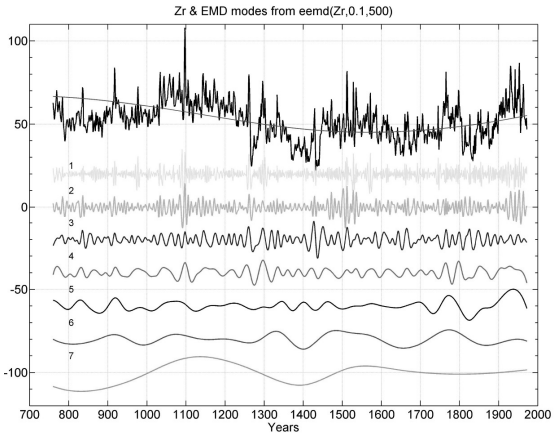

Fig. 4 – An example of finding the natural cyclic zirconium content.

Acknowledgements

This research was jointly supported by the Strategic Priority Research Program of the Chinese Academy of Sciences (XDB03020000), the National Natural Science Foundation of China under grants 41371219 and 41272198 and Russian Project RFBR 19-05-50046.

Supported by the Strategic Priority Research Program of Chinese Academy of Sciences, Grant No. XDB26000000.

References

Chu, G.Q., Liu, J.Q., Schettler, G. et al., 2005. Sediment fluxes and varve formationin Sihailongwan, a maar lake from northeastern China. Journal of Paleolimnology 34: 311–324.

Chu, G.Q., Sun, Q., Gu, Z. et al., 2009. Dust records from varved lacustrine sediments of two neighbouring lakes in northeastern China over the last1400 years. Quaternary International 194: 108–118.

Darin, A.V., Kalugin, I.A., Rakshun, Ya.V., 2013. Scanning x-ray microanalysis of bottom sediments using synchrotron radiation from the BINP VEPP-3 storage ring. Bulletin of the Russian Academy of Sciences: Physics. Vol. 77, № 2: 182–184.

Mann, M.E., Zhang, Z., Rutherford, S. et al., 2009. Global signatures and dynamic alorigins of the Little Ice Age and Medieval Climate Anomaly. Science 326: 1256–1260.

Mingram, J., Allen, J.R.M., Bruchmann, C. et al., 2004. Maar- and crater lakes of the Long Gang Volcanic Field (N.E. China) – Overview, laminated sediments, and vegetation history of the last 900 years. Quaternary International 123–125: 135–147.

Jiang, W.Y., Leroy, S.A.G., Ogle, N. et al., 2008. Natural and anthropogenic forest fires recorded in the Holocene pollen record from a Jinchuan peat bog, northeastern China. Palaeogeography Palaeoclimatology Palaeoecology 261: 47–57.

Jones, P.D., Briffa, K.P., Osborn, T.J. et al., 2009. High-resolution palaeoclimatologyof the last millennium: A review of current status and future prospects. The Holocene 19: 3–49.

Schettler, G., Liu, Q., Mingram, J. et al., 2006. Palaeo variations in the East-Asianmonsoon regime geochemically recorded in varved sediments of Lake Sihailongwan (Northeast China, Jilin province). Part 1: Hydrological conditions and dust flux. Journal of Paleolimnology 35: 239–270.

How many maar lakes are there on Earth? A preliminary catalog

Dmitri Rouwet[1], Karoly Németh[2], Giancarlo Tamburello[1]

[1] *Istituto Nazionale di Geofisica e Vulcanologia, Sezione di Bologna, Bologna, Italy.*dmitri.rouwet@ingv.it
[2] *Institute of Agriculture and Environment, Massey University, Palmerston North, New Zealand.*

Keywords: maar lakes, preliminary global catalog, conceptual models

This compilation of volcanic lakes in the world, VOLADA2.0, has recently been picked up where the previous version VOLADA was left (Rouwet et al., 2014). The original VOLADA data base contained 474 volcanic lakes that were only classified for the physical and chemical characteristics, but not for the type of lake basin they fill (i.e. genetic classification, introduced by Christenson et al., 2015).

The scopes of this new catalog are: (1) present an arguably complete compilation of all volcanic lakes in the world, (2) classify the lakes for their physical-chemical properties, and the genetic process behind the lake basin formation, (3) quantify how many volcanic lakes are actually maar lakes, (4) investigate the lake basin morphology based on the indicative ratios introduced and applied to maar *craters* by Graettinger (2018), (5) apply a statistical analyses that can support conceptual models on the genetic processes and geographical distribution of maar lakes (work-in-progress).

VOLADA2.0 contains 823 volcanic lakes (Table 1): 220 lakes in Africa, 142 in America, 311 in Asia, 107 in Europe, and 43 in Oceania. The African data base is, at the day of writing, the most complete on the global level: 81 lakes in Uganda, 37 in Kenya, 33 in Cameroon, 28 in Madagascar, 19 in Ethiopia, 6 in Tanzania, 2 in Rwanda, 2 in Sudan, 2 in D.R. Congo, 1 in Libya, and 9 on the minor islands around Africa. In Africa 78.2% of the volcanic lakes are maar lakes (Table 1). The predominant rift-related volcanism in Africa favors basaltic eruptive products, leading to volcanoes with highly permeable edifices, and hence less-developed hydrothermal systems. Basal aquifers accumulate under large volcanoes and in rift depressions providing a potential scenario for phreatomagmatic volcanism. This hypothesis explains the predominance of maar lakes in large monogenetic fields in Africa (e.g. Uganda, Cameroon, Ethiopia), and the complete absence of peak- or high-activity crater lakes, generally found in arc-volcanoes. Considering the large number of maar lakes in Africa (172), with similar geotectonic settings and meteoric conditions, it is somewhat surprising that "only" Lake Monoun and Lake Nyos fatally exsolved CO_2 from the deep lake strata. Explaining why other maars did *not* erupt is a question that can only be answered by enhancing insights into physical limnology and fluid geochemistry of the so far poorly studied lakes.

For the Americas, maar lakes dot the monogenetic volcanic fields in Mexico (Michoacán volcanic field), Serdán Oriental (N-Puebla), Los Tuxtlas Volcanic Field (Veracruz). Most renowned volcanic lakes in Central America, host to the most dense volcanic arc in the world, are often crater lakes on top of (active) stratovolcanoes (e.g. Poás, Rincón de la Vieja, Irazú in Costa Rica; Santa Ana in El Salvador, Cosigüina, Nicaragua). Maar lakes are located on volcano flanks (e.g. Río Cuarto, Laguna Hule in Costa Rica), rather than in monogenetic volcanic fields. Caldera lakes are more common than maar lakes (e.g. Apoyo in Nicaragua; Coatepeque, Ilopango in El Salvador). South America manifests relatively few volcanic lakes, despite the elongated volcanic arc. The high altitude and desert climate does probably not provide a sufficient source of water for lakes to form. The Palei Aike Volcanic Field in Patagonia, Argentina, is the only notorious area where maar lakes dominate.

Asia is the continent with most volcanic lakes on Earth (311, Table 1): 95 in Russia, 79 in Mongolia, 59 in Japan, 21 in China, 36 in Indonesia, 7 in S-Korea, 6 in the Philippines (prior to the 12 January 20202 Taal eruptions), 1 in Saudi Arabia, 1 in Yemen, 1 in Taiwan, 1 in N-Korea (Chinese border). 54.0% of volcanic lakes in Asia are maar lakes (Table 1), most of them are concentrated in Eastern Russia and Mongolia: Eravninskij and Transbajkalia Volcanic Fields in Russia, and Mongol Daur, Tased Khulstai, Yahi Nuur, Dariganga, Khanuy Gol, and Taryatu-Chulutu Volcanic Fields in Mongolia. Indonesia, country with the most active volcanoes in the world, hosts famous crater lakes (e.g. Kawah Ijen, Dempo, Kelimutu, Rinjani); maar lakes are often elongated reflecting the regional tectonic structures (e.g. along the Sumatra-Mentawai fault system).

The European country with most volcanic lakes is Portugal, with 35 out of the total European 107 lakes in the Azores archipelago; 31 of those are maar lakes. The Auvergne Puy de Dôme Volcanic Field in central France hosts 14 maar lakes, with Lac Pavin as its most famous lake, because of its dissolved CO_2 and CH_4 in deep lake strata. As well in Germany, 14 maar lakes spot the Eiffel Volcanic Field. Laacher See manifests CO_2 degassing. Many ephemeral volcanic lakes appear during snow melt in summer in Iceland. Askja caldera lake and its neighboring Viti crater lake are renowned. Seven out of twelve volcanic lakes in Italy are maar lakes. Despite its dimension, and two nested craters, Lago

Albano is generally considered a maar lake. The Calatrava Volcanic Field in southern Spain shows many ephemeral maar lakes, nine are perennial lakes. Turkey (7), Hungary (2) and Romania (1); nine of those ten lakes are considered maar lakes.

Moving to Oceania, at least 27 volcanic lakes are located in New Zealand, 6 in Australia, 3 in Vanuatu, 2 in both Bougainville Island and Papua New Guinea, 1 in Tonga and 1 pertains to France on the Kerguelen Islands (Southern Indian Ocean). The southern Australian lakes are maar lakes, in the Newer Volcanics Province. Volcanic lakes in New Zealand on their turn are rather geothermal lakes (Okataina-Rotorua), or crater lakes topping actively degassing or erupting volcanoes (Ruapehu, White Island). Volcanic lakes on the minor islands are no maar lakes.

The first geomorphological analysis for Africa, following Graettinger (2018), fit well within the findings of maar lakes in the MaarVLS data base. Africa is particularly rich in maar lakes (78.2%, Table 1); subsequent analyses for the remaining continents might suggest a deviation from the typical maar morphologies, for having less maar lakes than Africa. Caldera lakes and crater lakes generally show an even more circular shape than maar lakes; on a statistical basis, this difference should be clearly notable.

Continent	VL	ML	%ML
Africa	220	172	78.2
America	142	39	27.5
Asia	311	168	54.0
Europe	107	84	78.5
Oceania	43	6	13.9
total	823	469	<57.0>

Table 1 – Preliminary compilation of volcanic lakes and maar lakes on Earth. VL = Volcanic Lakes, ML = Maar lakes, %ML = percentage of maar lakes.

A peculiar, but arguably not coincidental observation is that high-latitude lakes (Arctics and Patagonia) are extremely abundant, to the level to be practically unquantifiable, and hence not (yet) included in VOLADA2.0. A working hypothesis is that permafrost soils provide large volumes of water able to interact with magma during phreatomagmatic activity. All these high-latitude volcanic lakes are probably maar lakes. The morphometric-statistical approach (Graettinger, 2018) will be able to rule out the non-volcanic lakes from the numerous lakes observed.

In conclusion, the preliminary global compilation of 823 volcanic lakes reveals that 469 lakes (or 57%) are maar lakes (Table 1). The large difference of abundances in maar lakes between continents (Table 1) should find its explanation in the diverse geotectonic and volcanic settings. Further research will focus on fine-tuning the data base, followed by morphometric and statistical approaches, with the scope to reveal the genetic processes behind volcanic lake formation. Due to the abundance of maar lakes, this investigation could lead to novel insights regarding monogenetic volcanism worldwide.

Acknowledgements

VOLADA2.0 greatly enhanced due to the help of Veronica Chiarini, Virginia Micci, Sara Cafaggi, Silvia Albano-Notarnicola, Gaspare Averardi, Cesare Laquintana.

References

Christenson, B., Németh, K., Rouwet, D., Tassi, F., Vandemeulebrouck, J., Varekamp, J.C., 2015. Volcanic Lakes, Springer Advances in Volcanology: 1–20 .

Graettinger, A., 2018. Trend in maar crater size and shape using the global Maar Volcanic Location and Shape (MaarVLS) database. Journal of Volcanology and Geothermal Research 357: 1–13.

Rouwet, D., Tassi, F., Mora-Amador, R., Sandri, L., Chiarini, V., 2014. Past, present and future of volcanic lake monitoring. Journal of Volcanology and Geothermal Research 272: 78–97.

Holocene hydroclimatic change inferred from Jinchuan peat sequence: pyrolytic biomarker evidence

Qing Sun[1], Guoqiang Chu[2]

[1] *National Research Center for Geoanalysis, No.26 Baiwanzhuang Road, Xicheng District, Beijing 100037, China.* sunqing1616@yahoo.com
[2]*Institute of Geology and Geophysics Chinese Academy of Sciences, No. 19 Beitucheng West Road, Chaoyang District, Beijing 100029, China.*

Keywords: Holocene, Longgang volcanic field, peat, Py-GC/MS

Peatland consists of the partially remains of mosses and vascular plants in the region, according to McClymont et al. (2011); Stevenson and Abbott (2019) Py-GC/MS has proved a convenient method for rapid assessment of bulk samples from OM-dominated sediments. Studies of organic molecular proxies suggested n-alkane, n-alkene, alkenone-based ACL, Paq have promising prospect in reconstruction temperature and effective precipitation during Holocene. Here we present a characterization of changes in the molecular composition of sediment OM in Jinchuan peat bog throughout the Holocene and compare the changes with those recorded by conventional analyzed proxies, in order to interpret OM dynamics and climate changes.

The Jiinchuan peat bog (126.37 E, 42.35 N, 614 m above sea level) located in the western part of the Longgang Volcanic Field, the modern climate in NE China is controlled by the seasonal East Asian monsoon, combined with the cold-wet water vapor brought by the Okhotsk High. A 5.72 m length core was collected using disturbance-free gravity drill. Core sediments were recovered from the underlying floodplain deposits to the top of the peat surface. All sediments samples were freeze-dried before analysis. The age-depth model for Jinchuan peat bog has been established with AMS ^{14}C ages of plant remains and bulk samples.

Py–GC/MS was performed using CDS5200 Pyroprobe, and samples were pyrolysed at 650 °C for 20 s. Total 96 identified compounds were grouped into 8 organic compound groups, follow the order by normalized peak area: phenol (30.39%) > aromatic (24.87%) > lignin (16.38%) > carbohydrates (9.76%) > n-alkane (6.66%) > nitrogen compounds (5.89%) > n-alkene (5.44%) > n-ketone (0.60%).

1) n-alkane-based proxies obtained from pyrolytic method shows similar variations to P_{aq} and LPTP records of Xiaolongwan maar in the same monsoon area;

2) Phenols, lignin oligomers, carbohydrates, and n-ketones appeared positive correlation with P_{aq}; nitrogen compounds, and (poly)aromatics appeared negative correlation with compound-specific $\delta^{13}C_{27\text{-}31}$ record of Xiaolongwan (Fig. 1).

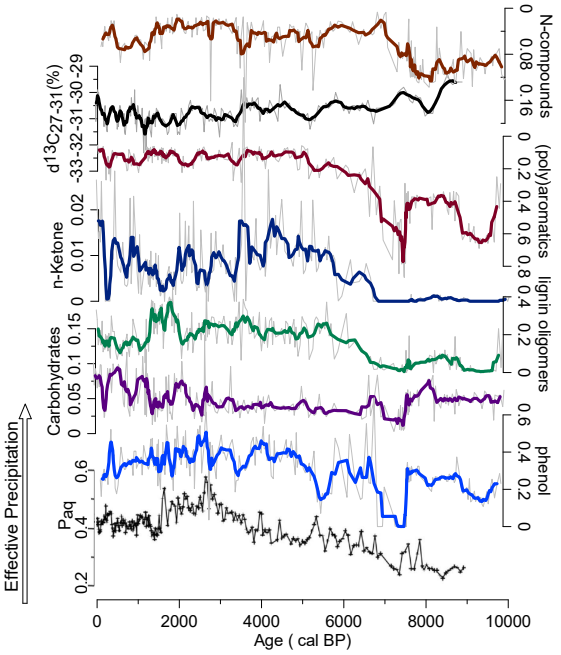

Fig.1 – Comparison of pyrolytic biomarkers with Paq and compound-specific $\delta^{13}C_{27\text{-}31}$ record of Xiaolongwan (Chu, 2014).

Base on the historical variation of pyrolytic biomarkers, we found in the early Holocene, a wide drought widely affect western and northern China could be observed around 10 ka to 8.5 ka, from 8.5 ka to the middle Holocene (4.0 ka) hydroclimatic condition was gradually getting more humid in northeast China, followed by several slight drought, and increased within last 300-500 years.

Acknowledgements

This work was supported by the NSFC (National Natural Science Foundation of China, 41877301 and 41402325).

References

Chu, Guoqiang, Qing Sun, Manman Xie, Yuan Lin, Wenyu Shang, Qingzen Zhu, Yabing Shan, Deke Xu, Patrick Rioual, Luo Wang, and Jiaqi Liu, 2014. Holocene cyclic climatic variations and the role of the Pacific Ocean as recorded in varved sediments from northeastern China. Quaternary Science Reviews, 102: 85–95.

Liu, Hanxiang, Xiaofei Yu, Chuanyu Gao, Zhenqing Zhang, Chunling Wang, Wei Xing, and Guoping Wang, 2017. A 4000-yr multi-proxy record of Holocene hydrology and

vegetation from a peatland in the Sanjiang Plain, Northeast China. Quaternary International, 436: 28–36.

McClymont, Erin L., Elizabeth M. Bingham, Chris J. Nott, Frank M. Chambers, Richard D. Pancost, and Richard P. Evershed, 2011. Pyrolysis GC–MS as a rapid screening tool for determination of peat-forming plant composition in cores from ombrotrophic peat. Organic geochemistry, 42: 1420–35.

Ninnes, Sofia, Julie Tolu, Carsten Meyer‐Jacob, Tim M Mighall, and Richard Bindler, 2017. Investigating molecular changes in organic matter composition in two Holocene lake‐sediment records from central Sweden using pyrolysis‐GC/MS. Journal of Geophysical Research: Biogeosciences, 122: 1423–38.

Schellekens, Judith, Jonathan A Bradley, Thomas W Kuyper, Isabel Fraga, Xabier Pontevedra-Pombal, Pablo Vidal-Torrado, Geoffrey D Abbott, and Peter Buurman, 2015. 'The use of plant-specific pyrolysis products as biomarkers in peat deposits. Quaternary Science Reviews, 123: 254-64.

Stebich, Martina, Kira Rehfeld, Frank Schluetz, Pavel E Tarasov, Jiaqi Liu, and Jens Mingram, 2015. Holocene vegetation and climate dynamics of NE China based on the pollen record from Sihailongwan Maar Lake. Quaternary Science Reviews, 124: 275–89.

Stevenson, Mark A, and Geoffrey D Abbott, 2019. Exploring the composition of macromolecular organic matter in Arctic Ocean sediments under a changing sea ice gradient. Journal of Analytical and Applied Pyrolysis.

Sun, Qing, ManmanXie, Liming Shi, Zhuyue Zhang, Yuan Lin, Wenyu Shang, Kaijun Wang, Wei Li, Jiaqi Liu, and Guoqiang Chu, 2013. Alkanes, compound-specific carbon isotope measures and climate variation during the last millennium from varved sediments of Lake Xiaolongwan, northeast China. Journal of paleolimnology, 50: 331–44.

Yamamoto, Shinya, Kimitaka Kawamura, Osamu Seki, Philip A. Meyers, Yanhong Zheng, and Weijian Zhou, 2010. Environmental influences over the last 16ka on compound-specific δ13C variations of leaf wax n-alkanes in the Hani peat deposit from northeast China. Chemical Geology, 277: 261–68.

Zhang, Mingming, Zhaojun Bu, Ming Jiang, Shengzhong Wang, Shasha Liu, Qing Jin, and Penghan Shi, 2019. Mid-late Holocene maar lake-mire transition in northeast China triggered by hydroclimatic variability. Quaternary Science Reviews, 220: 215–29.

Session 7. Maars and monogenetic volcanoes in geoheritage and geoconservation

Monogenetic volcanoes are commonly defined as erupting only once during their eruptive history through distinct eruptive phases. Systematically or randomly changing magma discharge rates, fluctuation of external versus internal influences on the eruption styles, and magmatic versus phreatomagmatic fragmentation can produce a great range of volcano types in terrestrial and subaqueous environments. In addition, monogenetic volcanic fields are the most common manifestation of volcanism on Earth hence they exist in every geotectonic settings and geoenvironments. As monogenetic volcanism played an important role in the global magmatism through the Earth history, there are monogenetic volcanic fields through the entire time of the evolution of Earth, hence we can come across with active, young or old eroded varieties of them. This extraordinary variety of monogenetic volcanism making it a very suitable subject to utilize them for geoeducation particularly for demonstrating of the variety of volcanic hazards. The small size, and the relatively simple volcano architecture that formed over short time making monogenetic volcanoes “human-scale” volcanic features hence perfect sites to promote volcanology to the general public. Monogenetic volcanic fields carry high geoheritage value especially if their eruptions influenced human society, they have high aesthetic value, or they are used as reference areas to describe unique volcanic processes. The complex geoheritage aspect of monogenetic volcanism has recently been recognized in geoconservation point of view and more and more monogenetic fields are in the frontline in various level of geopark establishments. In this session we called submissions that highlight this complex geoheritage aspects of monogenetic volcanism and its main volcanic landforms such as maars, tuff rings, tuff cones and scoria cones. Presentations that deal with various evaluation method to define the geoheritage values of monogenetic volcanic landforms as well as their link to human society, archaeology, indigenous world views and art were particularly welcomed in this session. Works that link modern and intact volcanic landforms to old eroded fields to utilize the geoeducation values of monogenetic volcanoes were also expected to be presented in this session. Works presenting new and advanced technologies applied in understanding the interaction of human societies with volcanic fields especially linking social studies, archaeology and volcano science were most welcome to this session.

How to lose volcanic geodiversity within a decade? The story of the neglected tuff rings in an ineffective bicultural geoheritage conservation strategy in Auckland, New Zealand

Boglárka Németh[1], Károly Németh[1], Ilmars Gravis[2], Boxin Li[1], April Foote[3] and Heather Handly[3]

[1] *School of Agriculture and Environment, Massey University, Palmerston North, New Zealand.* b.nemeth@massey.ac.nz
[2]*Ōpōtiki District Library, PO Box 44, 112 Church Street,Ōpōtiki, New Zealand.*
[3]*Department of. Earth and Environmental Sciences, Macquarie University, Sydney, Australia*

Keywords: maar, geodiversity, scoria.

Geoconservation strategies in New Zealand are guided by two of the most valued principles on national importance that shall be `recognized and provided for`; (1) the outstanding natural features and landscapes along with (2) the Māori culture, tradition, ancestral lands, water sites, waahi tapu (sacred sites) and other taonga (treasures) (Resource Management Act 1991, s 6). These principles call for a sound culturally infused geoheritage identification methodology that is rare in practice and nearly absent from the literature. Protection of Auckland`s geoheritage therefore raises issues of equity between science and culture as the geoscientific value of the remaining volcanic geosites has increased due to the effect of the overall loss of geodiversity of the volcanic field by the intense quarrying and urban expansion (Gravis et al. 2017, 2020). As the effects of the Resource Management Act (1991) and the Conservation Act (1987) Māori participation in resource management and conservation has become prominent enabling the enactment of a unique bicultural conservation management strategy. These acts included the right to have Crown land returned to traditional owners and the right of Māori to implement their cultural values into governance and resource management. The Te Uri o Hau Settlement Act 2002 transferred 14 areas of cultural significance in Auckland to the Māori tribal assets that are in geomorphologic terms, 14 scoria cones out of the currently recognized 55 small-volume, monogenetic volcanoes of the Quaternary Auckland Volcanic Fields (Hayward 2019). As Māori have a holistic view of their environment that links people and all living and non-living things. Māori are the kaitiaki (guardians) of both living and non-living that all possess spiritual qualities and have a responsibility to protect and enhance them hence the conservation of their areas is ensured from both biodiversity and geodiversity point of view. Earth Scientists of Auckland, however, recently expressed their concern on the unique diversity of the Auckland Volcanic Field and they extreme value for geoscience as research and teaching material. Important evidence of volcanic processes was exposed by intense quarrying activity of non-protected volcanoes with high international geoheritage value.

Fig. 1 – A typical Auckland scoria cone (Mt Victoria) as a recreational site has very small number of geologically valuable exposed sections while they are nice landscape elements.

The 14 volcanoes that are under the protection and management of the so called Maunga Authority are large and relatively well-preserved scoria cones with common lava spatter infill or short lava flows associated with them. They are mostly covered by vegetation and outcrops to examine their volcanic architecture are limited. They are however good lookout points and their cone shape clearly remind people to their volcanic origin. They are also located mostly in the elevated central part of the Auckland Urban areas and act as important urban recreational sites like regional parks or host spiritually significant locations commonly visited by Māori. In spite of these values, they are geologically scoria cones, that are the most common volcanic landform on Earth (Kereszturi and Németh 2016). The limited access to suitable outcrops for geological research is rare or their results are not overwhelmingly unique or different to any scoria cone sites elsewhere in the World. Volcanoes which are located mostly in the low-land coastal plains in the southern part of the Auckland urban region nearby Manukau however intensively researched in the past 50 years, and many of those sites form fundamental basic volcanological knowledge reservoir for the global science (e.g. Kereszturi et al. 2014; Agustin-Flores et al. 2014). The abundant tuff rings, shallow maars and associated scoria cones with their complex lava fields provided some key research results to understand the nature of monogenetic volcanism, phreatomagmatic explosive eruptions or the

variations of eruption style changes over the course of short-lived volcanic events (e.g. Kereszturi et al. 2017).

Fig. 2 – Tuff ring succession and magmatic infill contact exposed and still accessible in 21 December 2017.

Fig. 3 – The geosite shown on Fig. 2 blocked completely by 25 November 2019.

These volcanoes carry high geodiversity values that are completely out of any conservation policy sights. As many of these locations are tuff rings that host columnar jointed basalt infills in their crater and upper conduit sections, they are perfect aggregate sources and quarried in the past decades (e.g. Maungataketake, Wiri Mountain).

Fig. 4 – Tuff ring sequence exposing phreatomagmatic base surge and fallout deposits still preserved in an accessible wall in 21 December 2017.

Fig. 5 – The same wall shown on Fig. 4 removed by 25 November 2019.

As urbanization, airport expansion, logistical center development, railway and motorway constructions, and storage facility establishment are all occurred in this region, not only the demand for raw material for the constructions but also the physical space required to host these installations increased exponentially in these regions. As a result, an accelerated vanishing of these volcanic geoheritage sites can be clearly documented.

Without international obligation to a geoheritage convention it is very difficult to facilitate the protection of the geoscientific value of geoheritage and to get the narrative across on how geoscientific education along with cross-cultural fair-mindedness leads to more resilient citizens and strong communities that generate self-efficient conservation and sustainable geotourism.

Acknowledgements

BN and KN greatly appreciate the GNS-EQC00028 - Devora Sub Contract –"*GeoHeritage Values in Auckland*" support. Support from the Auckland City Council, Mangere Educational Center, DOC and Ōpōtiki District Library also acknowledged.

References

Agustin-Flores J., Németh K., Cronin S.J., Lindsay J.M., Kereszturi G., Brand B.D., Smith I.E.M., 2014. Phreatomagmatic eruptions through unconsolidated coastal plain sequences, Maungataketake, Auckland Volcanic Field (New Zealand). Journal of Volcanology and Geothermal Research 276: 46–63.

Gravis I., Németh K., Procter J.N., 2017. The Role of Cultural and Indigenous Values in Geosite Evaluations on a Quaternary Monogenetic Volcanic Landscape at IhumAtao, Auckland Volcanic Field, New Zealand. Geoheritage 9(3): 373–393.

Gravis I., Németh K., Twemlow C., Németh B., 2020. The case for community-led geoheritage and geoconservation ventures in Māngere, South Auckland; and Central Otago, New Zealand. Geoheritage, in press.

Hayward B.W., 2019. Volcanoes of Auckland: A field guide. Auckland University Press, Auckland, New Zealand, p. 335.

Kereszturi G., Bebbington M., Németh K., 2017. Forecasting transitions in monogenetic eruptions using the geologic record. Geology 45(3): 283–286.

Kereszturi G., Németh K., Cronin S.J., Procter J.N., Agustin-Flores J., 2014. Influences on the variability of eruption sequences and style transitions in the Auckland volcanic field, New Zealand. Journal of Volcanology and Geothermal Research 286: 101–111.

Resource Management Act, 1991. Resource Managment Act No 69 as at 29 October 2019. New Zealand Government, Wellington.

.